City University London

School of Mathematics, Computer Science and Engineering

PhD thesis

Study and suppression of vibrations in rotary-wing Unmanned Aerial Vehicles

Silvia Estellés Martínez

supervised by

Dr. M. Tomás-Rodríguez

October 2015

London

CITY UNIVERSITY LONDON

School of Mathematics, Computer Science and Engineering

City University London

Study and suppression of vibrations in rotary-wing Unmanned Aerial Vehicles

Silvia Estellés Martínez

1st Supervisor:

Dr. María Tomás-Rodríguez

2nd Supervisor:

Prof. George Halikias

Submitted as part of the requirements for
the degree of Doctor of Philosophy
in Aerospace Engineering
October 2015

Contents

City, University of London
Northampton Square
London
EC1V 0HB
United Kingdom

T +44 (0)20 7040 5060

THE FOLLOWING PARTS OF THIS THESIS HAVE BEEN REDACTED FOR COPYRIGHT REASONS:

Figure 1.1: Predator in military use

Figure 1.2: Left: Yamaha RMax UAV, conventional helicopter configuration Right: Draganflyer X6, multi-rotor configuration

Figure 1.3: High Altitude Airship, by Lockheed Martin [4]. Delfly flapping wing UAV, developed at the Micro Air Vehicle Lab of the Delft University of Technology

Figure 2.1: An artist depiction of the ying pigeon, the first documented UAV in history.

Figure 2.2: Typical Chinese top

Figure 2.8: Convertawings revived the concept tried in France by Oemichen and by G. de Bothezat in the United States, 1956

Figure 2.9: Image of the Curtiss-Wright VZ-7, a quadrotor configuration helicopter designed for the US army in the 1950's

List of Tables

List of Figures

Acknowledgements

I would like to dedicate these lines to all the people who has helped me to be here today. I want to acknowledge City University London, for providing the necessary fundings for my PhD studies and for giving me the chance to develop my potential as researcher.

I would specially like to thank my supervisor, Dr. M. Tomás-Rodríguez, who has helped me through all my years at the university, both academically and personally. I would also like to thank my study fellows, Salvador and Ciro, who welcomed me when I first arrived to London and who have always been eager to help me in whatever I needed from them. A especial mention for Pedro Albertos and people on *ai2*, who introduced me to the quadrotors world and encouraged me to follow the path of the academic research.

I would like to thank deeply to my family, specially my parents and siblings, who have always supported me on my crazy ideas and have always had a blind faith in me. They were the first to encourage me to undertake a new life in a different country, with a different culture. They have always been there for me, even when I did not know I needed them. Thanks to them, I am here today.

Papas, tetes, gracias por estar ahí para mí.

I can not forget my friends, the usual ones and the new I have acquired through my years here. Your trust is my strength.

Gràcies xics! Gracias chicos! Thank you guys!

Finally, I would like to thank my boyfriend, who has been my inspiration in the research world, who has been with me through thick and thin, who has always trusted me, even when I doubted myself and who helped me to find the path when I felt lost.

Julian, I could not have done this without you.

Abstract

This document contains the details of the thesis titled Study and suppression of vibrations in rotary-wing Uumanned Aerial Vehicles, which focuses on the study of vibrations of the so called quadrotors, which are formed by four rotors equispaced around a central structure.

Due to the morphological characteristics of the quadrotors, they present high manoeuvrability and better payload than other rotary-wing UAV configurations, reason why their use and study has increased in the last past years. Because quadrotors are unmanned vehicles, very often autonomous, they rely completely on the information they receive from the available sensors, and therefore, their performance should be improved as much as possible. It is then necessary to keep the undesirable vehicle's oscillations to the minimum as the measurement systems can obtain better readings, reducing the need for data processing, this is, reducing the energy consumption and increasing the vehicle's autonomy.

To reduce vibrations appearance and isolate their transmission, it is essential to deeply understand the mechanisms associated to the appearance and transmission of the oscillations in the vehicle, originated both from the external environment and from the vehicle itself. In order to do so, an extensive study of the vehicle's vibrational behaviour has been carried out here. The main sources of vibrations have been identified and effective solutions have been proposed for the reduction of the oscillations production and transmission, as an appropriate selection of materials and a predictor-corrector control methodology. Also the effect of rotor defects on the vehicle behaviour has been studied, and software and hardware modifications have been designed and implemented in the model in order to improve the vehicle performance, even in presence of rotor severe structural damage.

Abbreviations and symbols

List of abbreviations

Abbreviation	Description
AB-2	Adams-Basford 2^{nd} order
ABS	Acrylonitrile butadiene styrene
AM-2	Adams-Moulton 2^{nd} order
AM-3	Adams-Moulton 3^{rd} order
*ai*2	Instituto de Automática e Informática Industrial
BC	Before Christ
BRS	Body based reference system
CPU	Central Processing Unit
FAI	Fédération Aéronautique Internationale
ICD	Adams-Moulton 2^{nd} order
IMU	Inertial Measurement Unit
IRS	Inertial reference system
LQR	Linear quadratic regulator
MEMS	Micro-Electro-Mechanical Systems
ODE	Ordinary differential equations
PD	Proportional-Derivative
PD^2	Proportional-Derivative^2
PID	Proportional-Integral-Derivative
PVA	Proportional-Velocity-Acceleration

RK-2	Runge-Kutta 2nd order
UAV	Unmanned Aerial Vehicle
US	United States
VTOL	Vertical Take-off and Landing

List of symbols

Symbol	**Description**
α	Angle of attack
α_{in}	Incident angle of attack, measured between the chord of the airfoil and the incident airflow
$\alpha_{in_{ij}}$	Incident angle of attack of blade j, rotor i
α_n	Factor in beam nth natural frequency calculus
α_s	Structural angle of attack, measured between the rotor plane and the chord line
β	Flap angle
β_{ijk}	Flape angle of segment k, blade j, rotor i
γ_i	Angular position of the ith rotor's first blade in rotor plane
$\delta_l, l = 1...22$	Constant factors in controllability analysis
θ	Pitch, rotation of the quadrotor around its local Y axis
$\ddot{\theta}_C$	Pitch acceleration of the complete model
$\ddot{\theta}_{\texttt{CORR}}$	Corrected pitch acceleration
$\ddot{\theta}_S$	Pitch acceleration of the simple model
ξ	Damping ratio
ρ_∞	Air density
ϕ	Roll, rotation of the quadrotor around its local X axis
ψ	Yaw, rotation of the quadrotor around its local Z axis
$\omega_{1_{nr}}$	1st natural frequency for a rotating blade

$\omega_{2_{nr}}$	2^{nd} natural frequency for a rotating blade
ω_n	n^{th} natural frequency
Ω	Rotor rotational speed
$\mathbf{\Omega}$	Sumatory of the four rotors' rotational speeds
Ω_i	i^{th} rotor rotational speed
$\overline{\Omega}_i$	Intermediate variable for the controllability analysis, Ω_i-Ω_0
Ω_0	Rotors' rotational speed in hover conditions
AR	Blade's aspect ratio
a_1	Lift aerodynamic coefficient, available from $ai2$ data
a_2	Drag aerodynamic coefficient, available from $ai2$ data
b	Stiffness coefficient for one segment blade discretization
$b(n)$	Stiffness coefficient for n segments blade discretization
$b(n_f, n_t)$	Stiffness coefficient for n_f flexible segments and n_t total segments blade discretization
B_{ij}	Designation of blade j, rotor i
B_{ijk}	Designation of segment k, blade j, rotor i
C	Controllability distribution for the controllability analysis
c	Damping coefficient for one segment blade discretization
$c(n)$	Damping coefficient for n segments blade discretization
$c(n_f, n_t)$	Damping coefficient for n_f flexible and n_t total segments blade discretization
c_d	Profile Drag
C_D	Drag coefficient
C_{D_i}	Induced Drag coefficient
C_{dif}	Controllability distribution for a different mass blade
C_L	Lift Coefficient
C_{L_α}	Slope of the Lift Coefficient-Angle of Attack curve

C_{L_0}	Lift Coefficient at zero angle of attack
$C_{x,y}$	Damping constant on the Isolating Control Device, in the $\mathtt{X_{STR}}$ and $\mathtt{Y_{STR}}$ directions respectively
CDM	Counter Drag Moment
CDM_0	Counter Drag Moment value in hover conditions
CM	Control moment
CM_i	Control moment applied to rotor i
$(CM_i)_z$	Control moment applied to rotor, corresponding to variable z in this case
$CM_{max,min}$	Maximum torque given by the rotors
d	Longitudinal distance between the quadrotor centre and the rotors' centre
D	Drag force
$dL(r)$	Lift force distribution along the blade span
$D_{0_{ij}}$	Drag force acting on blade j, rotor i in hover conditions
D_{ijk}	Drag force acting on segment k, blade j, rotor i
DM	Drag Moment
DM_i	Drag moment acting at rotor i
e	Blade offset
	Span efficiency factor
E	Material Young modulus
$e_a(t)$	Acceleration error
$e_p(t)$	Position error
$e_v(t)$	Velocity error
$f_{0,1,2,3,4}$	Vector fields for the controllability analysis
$f_{0,1,2,3,4_{dif}}$	Vector fields for the controllability analysis of a different blade's mass system
$F_{c_{ij}}$	Centrifugal force acting on blade j, rotor i
g	Gravity constant

h	Vertical distance between the quadrotor centre and the rotors' centre
I	Second moment of inertia of the beam cross section
i	Subscript used to determine the rotor, i = 1...4
$I_{x_{STR}}$	Inertia of STR body around its local X azis
I_{y_b}	Second moment of inertia of the blade cross section
$I_{y_{STR}}$	Inertia of STR body around its local Y azis
$I_{z_{STR}}$	Inertia of STR body around its local Z azis
j	Subscript used to determine the blade on a rotor, j = 1,2
J_{r_i}	i^{th} rotor inertia around its local Z axis
k	Subscript used to determine the discretized segment on a blade, k=1...n Also used as parameter in the Prandtl's Lifting-Line Theory
k_a	Parameter for the calculus of the pitch's corrected acceleration
$K_{x,y}$	Spring constant on the Isolating Control Device, in the $\mathtt{X_{STR}}$ and $\mathtt{Y_{STR}}$ directions respectively
k_{TD}	Translational Drag coefficient
$k_{1,2,3}$	Control parameters proportional to position error, speed error and acceleration error respectively
$(k_{1,2,3})_{x,y,z,\theta,\phi,\psi}$	Control parameters for X, Y, Z, θ, ϕ and ψ variables respectively
L	Lift force
$L_{0_{ij}}$	Lift force for stationary conditions acting on blade j, rotor i
L_{ijk}	Lift force acting on segment k, blade j, rotor i
m	Beam mass in the natural frequencies calculus
m_{ij}	Mass of blade j, rotor i

M_b	Blade's mass
M_i	Moment acting on rotor i
$M_{r_{ijk}}$	Elastic restoring moment in segment k, blade j, rotor i
M_s	Rotor's mass
M_{STR}	STR body mass
M_t	Total quadrotor's mass
M_∞	Mach adimensional number
n	Number of segments in which the blade is discretized
$\mathtt{n_0}$	Inertial reference system origin
n_f	Number of flexible segments in which the blade is discretized
n_t	Total number of segments in which the blade is discretized, including rigid and flexible segments
P	Load applied for the blade calculus deflection
q_∞	Dynamic pressure
R	Blade radious
R_e	Reynolds adimensional nymber
r_1	Length of the segments in which the blade is discretized
r_{cp_0}	Pressure centre location in hover conditions
$r_{cp_{ijk}}$	Pressure centre location in segment k, blade j, rotor i
r_{cp_0}	Representative point location in hover conditions
$r_{cp_{ijk}}$	Representative point location in segment k, blade j, rotor i
RF	Aerodynamic resultant force
S	Representative blade surface for the aerodynamic forces calculus
S_i	Terminology used to refer to rotor i
STR	Terminology used to refer to the body composed by the two crossed arms and the measurement system

$\mathtt{STR_0}$	Origin of the body based reference system, situated in the two arms union
T	Torque force
T_{ijk}	Thrust force acting on segment k, blade j, rotor i
TD	Translational Drag force
$TD_{x,y,z}$	Translational Drag force in the X, Y or Z direction respectively
TQR	Torque to radious force, T/R
$TQR_{0_{ij}}$	Torque to radious force for stationary conditions acting on blade j, rotor i
TQR_{ijk}	Torque to radious force acting on segment k, blade j, rotor i
U	Control action
V_r	Rotational speed component to V_∞, due to the blade's rotation
V_t	Tranlational speed component to V_∞, due to the quadrotor's displacement
$V_{t_{ij}}$	Tranlational speed component of blade j, rotor i
V_∞	Airflow velocity relative to the blade
W	Weight force
w_{tip}	Blade's tip displacement due to blade's elasticity
X	Translation of the quadrotor along inertial X axis
$\overline{x}$	Intermediate states for the controllability analysis
$[\mathtt{X_n}, \mathtt{Y_n}, \mathtt{Z_n}]$	Axes defining the inertial reference system orientation
$[X_n^{ref}, Y_n^{ref}, Z_n^{ref}]$	Position references expressed in the inertial reference system
$[\mathtt{X_{STR}}, \mathtt{Y_{STR}}, \mathtt{Z_{STR}}]$	Axes defining the body based reference system orientation

$[X_{STR}^{ref}, Y_{STR}^{ref}, Z_{STR}^{ref}]$	Position references expressed in the body based reference system
Y	Translation of the quadrotor along the Y inertial axis
Z	Translation of the quadrotor along the Z inertial axis
$\overline{\ddot{Z}}$	Intermediate acceleration along Z axis for the controllability analysis
$\mathtt{Z}_{S_i}$	Local Z axis on rotor i

Chapter 1

Introduction

1.1 Unmanned Aerial Vehicles (UAVs)

Unmanned Aerial Vehicles (UAVs), also known as *drones*, are the latest generations of pilotless aircraft, usually defined as aircraft without the onboard presence of pilots.

During recent decades, significant efforts have been devoted to increase the flight endurance and payload of UAVs, resulting in various UAV configurations with different sizes, endurance levels, and capabilities. UAVs can be classified according to their structural configuration, typically falling into one of the following categories:

- Fixed-wing UAVs, which refer to unmanned airplanes with wings that require a runway to take-off and land, or catapult launching (Figure 1.1). These generally have long endurance and are able to fly at high cruising speeds.

- Rotary-wing UAVs, also called rotorcraft UAVs or vertical take-off and landing (VTOL) UAVs, which have the advantages of hovering capability

Figure 1.1: Predator in military use [1].

Figure 1.2: Left: Yamaha RMax UAV, conventional helicopter configuration [2]. Right: Draganflyer X6, multi-rotor configuration [3].

and high manoeuvrability. These capabilities are useful for many robotic missions, especially in civilian applications. A rotorcraft UAV may have different configurations, with main and tail rotors (conventional helicopter), coaxial rotors, tandem rotors, multi-rotors, etc (Figure 1.2).

- Blimps such as balloons and airships, which are lighter than air and have long endurance, fly at low speeds, and generally are large sized (Figure 1.3).

- Flapping-wing UAVs, which have flexible and/or morphing small wings inspired by birds and flying insects (Figure 1.3).

There are also some other hybrid configurations or convertible configurations, which can take-off vertically and tilt their rotors or body and fly like airplanes, such as the Bell Eagle Eye UAV.

Unmanned vehicles present numerous advantages when compared to conventional

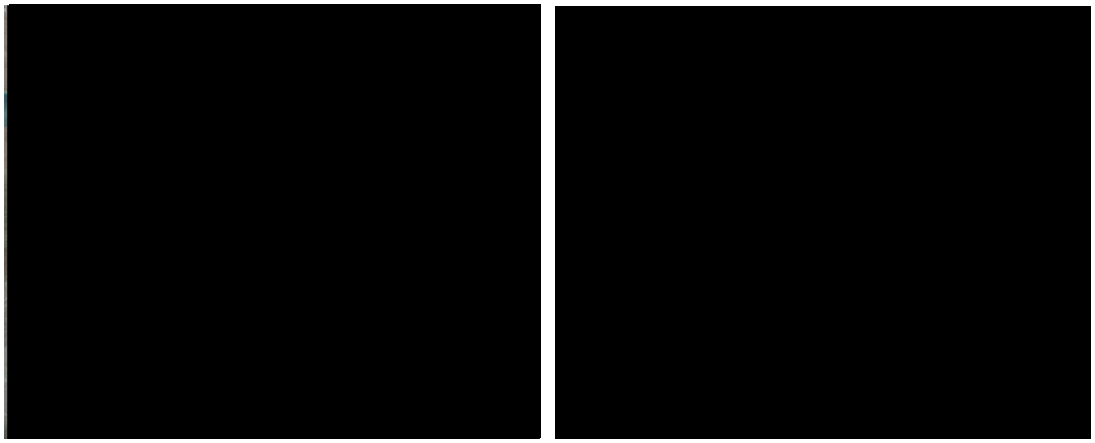

Figure 1.3: High Altitude Airship, by Lockheed Martin [4]. Delfly flapping wing UAV, developed at the Micro Air Vehicle Lab of the Delft University of Technology [5].

manned vehicles: due to their smaller size, they usually require a lower operational cost, both energetic and economic; besides, since they do not carry people on board they are better suited for dangerous or hazardous environments and risky missions for which the conventional vehicles could not be acceptable.

Currently the most relevant UAV applications are defense related and the major investments are driven by future military scenarios. Most military unmanned aircraft systems are primarily used for intelligence, surveillance and reconnaissance. Civilian markets for UAVs are still emerging, however, the expectations for the market growth of civil and commercial UAVs for the next decade are very high, starting first with government organizations requiring surveillance systems similar to military UAVs such as coast guards, border patrol organizations and similar national security organizations. Some other potential VTOL nonmilitary applications of UAVs are:

- Terrain inspection, pipelines, utilities, buildings, etc.
- Law enforcement and security applications.
- Surveillance of coastal borders, road traffic, etc.
- Disaster and crisis management, search and rescue.

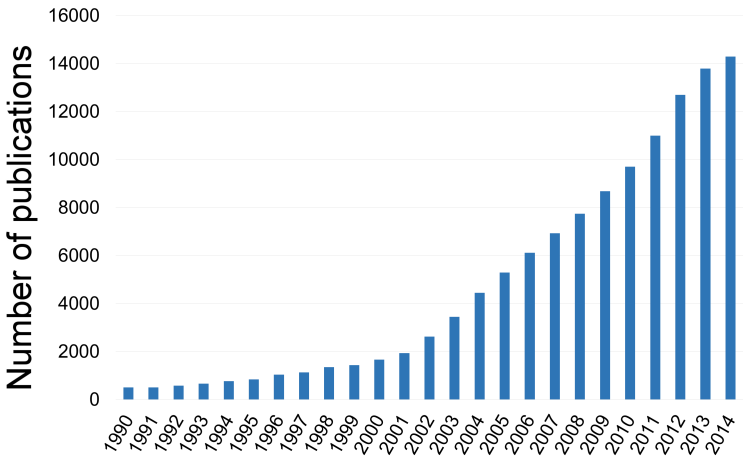

Figure 1.4: Number of UAV related publications per year. Source google scholar.

- Environmental monitoring.
- Agriculture and forestry (mostly in Japan).
- Fire fighting.
- Communications relay and remote sensing.
- Aerial mapping and meteorology.
- University/laboratories research.

The study of UAVs has increased in the last few years, as Figure 1.4 shows, and also have done the investments on these vehicles in US and to a lesser extent in Europe (Figures 1.5 and 1.6). Several market studies [6, 7] predict that the worldwide UAV market will expand significantly in the next decade. As stated in [7, 8], over the next 5-7 years, the UAV market in the US will reach $16 billion, followed by Europe, which will be spending about $3 billion.

Certainly, this introduction supports the idea that the future of UAVs is bright and this area will continue to grow. Therefore, it is important to concentrate in research and development of these vehicles, but also discuss challenges and limitations that need to be overcome in order to improve the functionality and use of unmanned aerial systems.

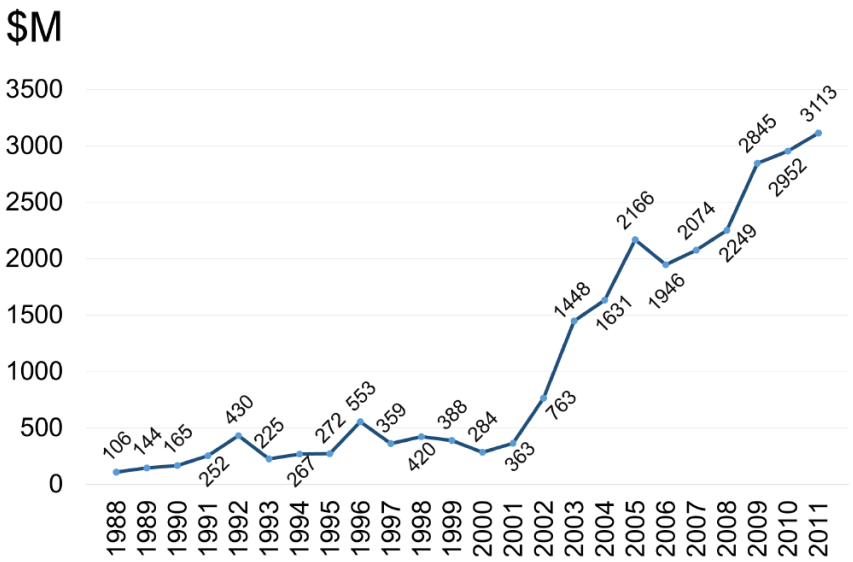

Figure 1.5: Annual funding profile of the US Department of Defense for UAVs. Data from [9].

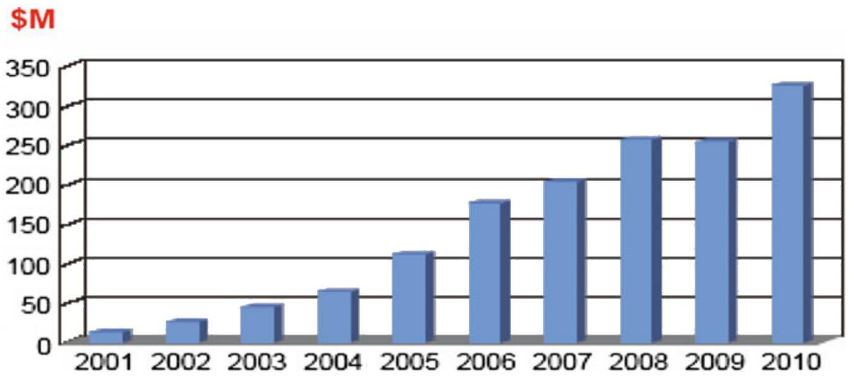

Figure 1.6: Annual funding profile in Europe for UAVs. Source [10].

1.2 Motivation and objectives

Unmanned aerial vehicles is a broad field that includes numerous types of devices. This thesis is focused on rotary-wing UAV, more specifically, on the so called quadrotors, that are formed by four rotors equispaced around a central structure.

Quadrotors present numerous advantages with respect to other conventional UAV configurations, specially vertical take-off and landing capabilities, and more important, hover capability. Therefore, this kind of vehicles is usually employed in reconnaissance and surveillance missions, in which it may be necessary to overfly a specific area. Due to the morphological characteristics of these vehicles, they present high manoeuvrability and better payload than other rotary-wing UAV configurations, reason why their use and study has increased in the last past years.

Since quadrotors are unmanned vehicles, very often completely autonomous, they need to perform in an exceptional manner, with good measurement and telemetry systems that allow the vehicle to manoeuvre in different environments, usually unknown ones. Unmanned aerial vehicles rely completely on the information they receive from the available sensors, and therefore their performance should be improved as much as possible. It is necessary to keep the undesirable vehicle's oscillations to the minimum as the measurement systems can obtain better readings, reducing the need for data processing, this is, reducing the energy consumption and increasing the vehicle's autonomy.

To reduce vibrations appearance and isolate their transmission, it is essential to deeply understand the mechanisms associated to the appearance and transmission of the oscillations in the vehicle, originated from both the external environment and from the vehicle itself. In order to do so, an extensive study of the vehicle's vibrational behaviour needs to be carried out, so that the main sources of vibrations are identified, the transmission mechanisms established and adequate and

effective solutions can be proposed.

The main motivation of this thesis is the study of the vibrations generation and transmission through the quadrotor's structure and their possible isolation and/or suppression from the sensitive parts of the vehicle, providing in this way a more suitable autonomous flying platform. In order to accomplish this task, a series of objectives need to be undertaken:

- The first step for the study of vibrations in quadrotors is the developing of a realistic and suitable simulation model. In order to obtain this simulation platform, the software VehicleSim will be used. This software allows the multibody modelling of dynamic systems, being possible to obtain the linear and nonlinear vehicle's equations of motion.

- In order to study the generation and transmission of the vibrations in quadrotor vehicles, it is necessary to study their performance in motion. Therefore a suitable control system will be designed and applied to the vehicle in order to obtain a stable simulation platform able to perform successful trajectory tracking without introducing extra vibrations.

- The aerodynamics involved in the quadrotors performance are a fundamental factor when considering the vibrations occurrence in the vehicle. Therefore a more detailed and realistic model than those used nowadays for the aerodynamic forces modelling will be considered for the study of vibrations generation.

- In rotary-wing vehicles, one of the main source of vibrations are the rotors. In order to consider all the possible contributions to the vibrations generation process, a detailed model of the rotor is needed. Therefore, the different bodies composing the rotor will be modelled and the elasticity of the lifting surfaces will be considered as a starting point of the vibrations generation study.

- Since quadrotors are occasionally used in hazardous, sometimes hostile, missions and environments, they may suffer from structural damage. This structural damage, which may be accidental or induced, could cause the vehicle's destabilization and in case of severe damage, it may produced the loss of the entire vehicle. In order to anticipate any eventuality that may arise during the development of a mission, it is necessary to fully understand the forces involved in the quadrotor's behaviour, not only in nominal conditions, but also when the vehicle is flying out of its normal expected performance. A likely situation that would take the vehicle out of its normal behaviour would be a faulty or missing actuator, which causes a rotating centrifugal acceleration at the affected rotor. Studying the effect of this centrifugal force on the vehicle's performance will allow the adoption of precautionary measures, making the quadrotor a more robust vehicle, being capable of flying even out of its expected normal safe flight conditions, preserving the basic integrity of the vehicle and any sensitive information it may carry as well.

1.3 Thesis outline

This thesis report has been divided in different chapters according to their content and the objectives mentioned:

- *Chapter 1: Introduction.* A brief introduction to the motivations and the intended objectives of the thesis is given, as well as an overall picture of the state of the UAVs market nowadays.
- *Chapter 2: Literature review.* A review of the first rotary-wing flying machines in the history and their evolution to the actual quadrotors is presented. Also a thorough review of the literature existing on quadrotors, their design, modelling and control is given highlighting their main features

and how the work here presented sits within the quadrotors vibrational study.

- *Chapter 3: Quadrotor modelling.* The quadrotor vehicle is introduced, pointing out the main forces and reference systems involved in the vehicle's motion. The basic rules of the modelling software used in this work are presented, giving details of the solving methods available. Also the different structural and aerodynamic models developed are detailed.

- *Chapter 4: Control system.* The equations of motion obtained from the modelling software are presented here, with an analysis of their controllability. The control system designed based on the PVA method and the smooth predefined trajectories are presented. The successful trajectory tracking of the vehicle is shown.

- *Chapter 5: Vibrations.* In this chapter the vibrational characterization of elastic blades made of different materials is shown. The effect of the elasticity is analysed on the overall vehicle's behaviour. Different approaches are presented in order to reduce the vibrations appearing in the structure, mainly produced by the aerodynamic forces and structural damage on the rotating blades.

- *Chapter 6: Conclusions and future work.* In this chapter a summary of the main conclusions of the thesis is given, pointing out the next steps to follow regarding the study and suppression of vibrations in rotary wing UAVs. Also the scientific contributions as a result of this thesis are listed.

1.4 Thesis contributions

This thesis presents some contributions to the vibrational study of rotary-wing UAVs. As a summary, here are some of them:

- Structural and aerodynamic quadrotor model developed in Lisp and VehicleSim. The structural model includes blades flexibility and the aerodynamic model considers variation of pressure centre.

- PVA control method applied to quadrotors that, together with smooth predefined trajectories, provides a controlled and stable simulation platform for the vibrational analysis.

- Vibrational analysis of the elastic blades for different materials. The analysis shows a good agreement between the natural frequencies of the blade and the obtained from the proposed discretization.

- Vibrational analysis of the full quadrotor behaviour when elastic blades and complex aerodynamics are considered.

- Design and study of an Isolating Control Device that isolates centrifugal forces produced on the blades and allows the safe flight of the quadrotor when it presents severe blade structural damage.

Chapter 2

Literature review

2.1 History of unmanned and rotary-wing vehicles

In modern times, manned aviation appeared in the late 1700s, and it took another century for heavier than air machines to take to the skies. Unmanned aircraft followed soon after the advent of the airplane, appearing around the time of the First World War (1916). However, the idea of building "flying machines" was first conceived close to 2,500 years ago, in ancient Greece and China.

The first known autonomous flying machine has been credited to Archytas from the city of Tarantas or Tarentum in South Italy, known as Archytas the Tarantine. In 425 BC Archytas built a mechanical bird, which he called "the pigeon", shown in Figure 2.1. According to Cornelius Gellius in his Noctes Atticae, the bird was made of wood, nicely balanced with weights, and flew using air (most likely steam) enclosed in its stomach [11]. It is alleged that Archytas' pigeon flew about 200m before falling to the ground, once all energy was used. The pigeon could not fly again, unless the mechanism was reset.

During the same era in a different part of the Ancient World - China - at about 400

Figure 2.1: An artist depiction of the flying pigeon, the first documented UAV in history. It is reported that it flew about 200 meters. Credits to [12].

Figure 2.2: Typical chinese top. Credits to [13].

BC, the Chinese were the first to document the idea of a vertical flight aircraft. The earliest version of the Chinese top consisted of feathers at the end of a stick. The stick was spun between the hands to generate enough lift before released into free flight.

Among da Vinci's work (late 15^{th} century) were sketches of a machine for vertical flight utilizing a screw-type propeller, but such a craft was never constructed. His theory for compressing the air and obtaining lift was substantially similar to that for today's helicopters. It was clearly far ahead of its time, but without adequate technology the ability to create such machines was virtually nil.

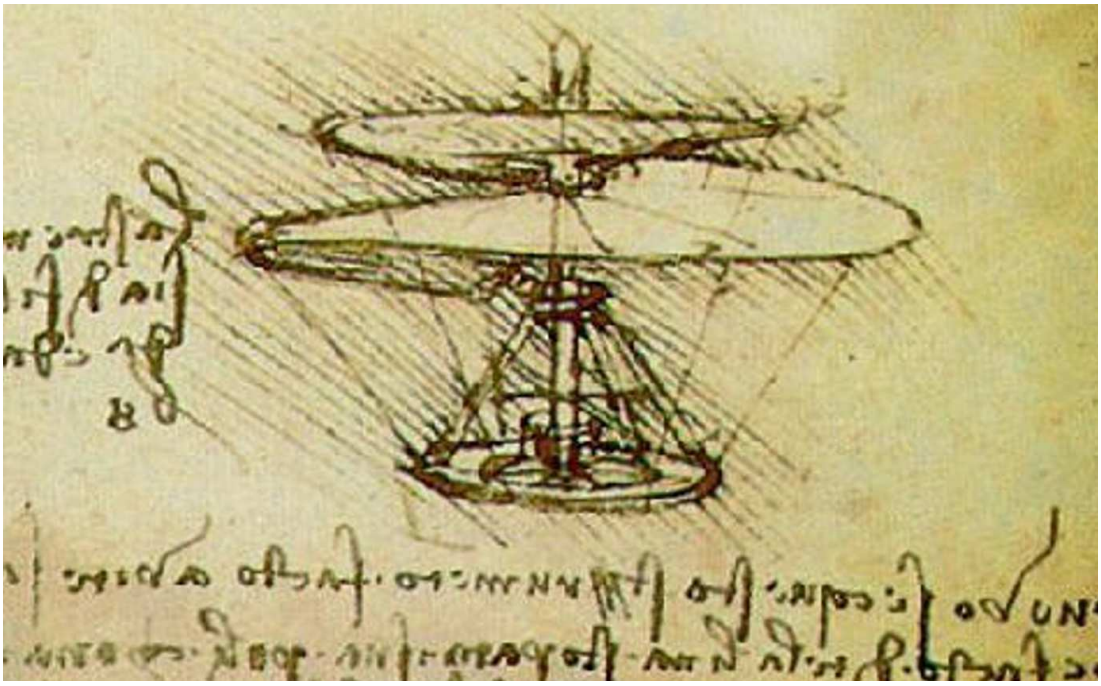

Figure 2.3: 'If this instrument made with a screw be well made - that is to say, made of linen of which the pores are stopped up with starch and be turned swiftly, the said screw will make its spiral in the air and it will rise high.' - Leonardo Da Vinci, 15th century. Credits to [13].

A large number of minor inventions contributed to the advancement of the helicopter between the 15th and 20th centuries. Many extraordinary models were developed by an ever increasing number of great thinkers, but all the pioneers were missing two essentials: a true understanding of the nature of lift and an adequate engine. All models at this time lacked suitable power to achieve flight and were both bulky and heavy. Further successes in the development of modern helicopters had to wait a bit longer.

In the 18th century, some inventions were made based in the rotary-wing ideas for flight machines. In 1754, Russian Mikhail Lomonosov suggested a coaxial rotor machine to elevate meteorological instruments [14]. It was modelled after the Chinese toy but powered by a wound-up spring device. The device flew freely and climbed to a good altitude.

In 1784, French Bienvenu and Launoy developed another version of the Chinese toy, which had at each end of its shaft two propellers driven by a bowdrill system

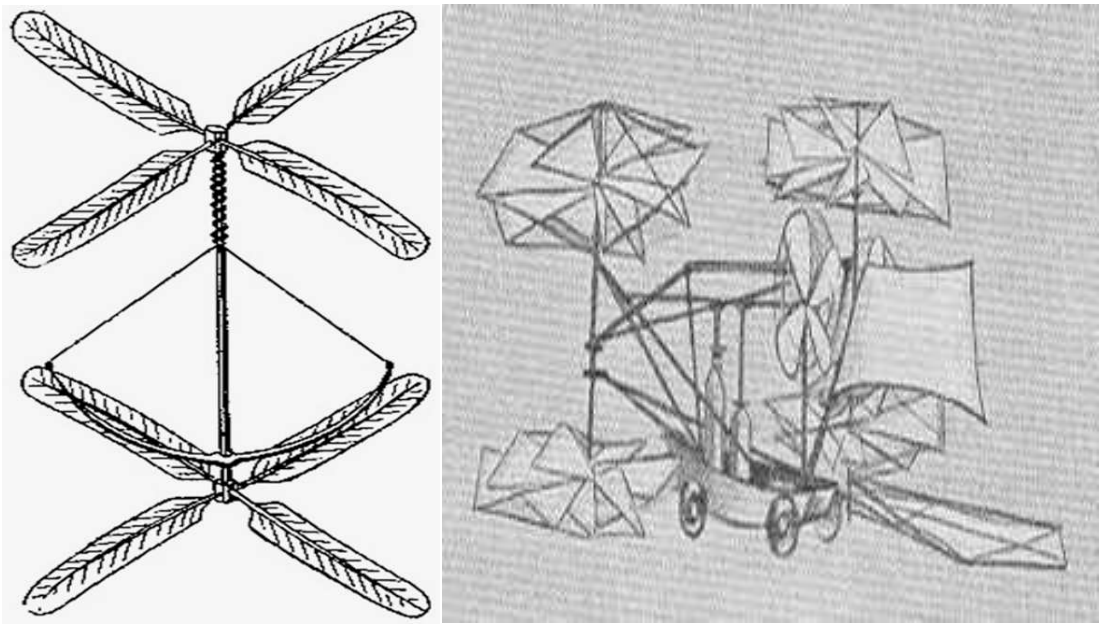

Figure 2.4: Left: Launoy & Bienvenu's invention, 1784 [15]. Right: Sir George Cayley's helicopter, 1796 [13].

[14]. It was a model consisting of a counter rotating set of turkey feathers that could take off and fly using its own power. This proved that an object which is heavier than air could fly.

In England, in 1796, George Cayley, already famous for his work on the basic principles of flight, had constructed several successful vertical-flight models with rotors made of sheets of tin and driven by wound-up clock springs [14]. However, Cayley's device remained only as an idea as the only power plants available at the time were steam engines, and these were too heavy to allow a successful powered flight.

In the 19^{th} century, the invention of the internal combustion engine made it possible for the pioneers to develop full-sized models with an adequate power source.

In 1878, Enrico Forlanini, an Italian civil engineer, constructed a steam driven model helicopter that only weighed 3.5 kg, reached 9 meters and remained in flight for 30 seconds. In 1880, Thomas Edison was the first American to perform any notable research on helicopters. Edison built a test stand and tested several

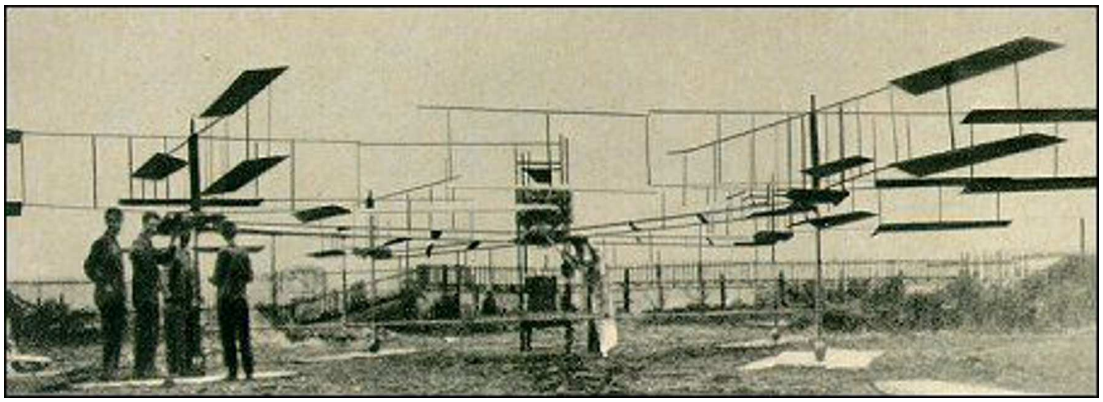

Figure 2.5: Gyroplane No. 1 built by Louis and Jacques Breguet, 1907 [16].

different propellers using an electric motor [14]. He deduced that in order to create a feasible helicopter, he needed a lightweight engine that could produce a large amount of power. In fact, he recognized that the problem was the lack of an adequate engine. He concluded that no helicopter would be able to fly until engines with a weight-to-power ratio below 1 to 2 kg/hp were available.

In addition to the names cited above, special mention is made of Viscomte Gustave de Ponton d'Amecourt (France, 1873) as he built a small steam-driven model; he also invented the word helicopter [14]. It can be summarized that in the last half of the 19^{th} century many inventors were concerned with helicopter design and building, there were some practical advances but no successful vehicle saw the light.

The beginning of the 20^{th} century saw the pioneers experimenting and resolving many of the problems that appeared with each advancement. It was not until the mid-1920's that engines with enough power and with high power to weight ratios suitable for vertical flight became more widely available. The biggest problem with the various early helicopter designs produced during this time was that although they could lift off the ground, they could not be controlled in flight. Inventors did not understand the aerodynamic forces the helicopters were subjected to and did not know how to design mechanical devices to address these forces.

The first vertical take-offs were the work of pioneering French engineers. Paul

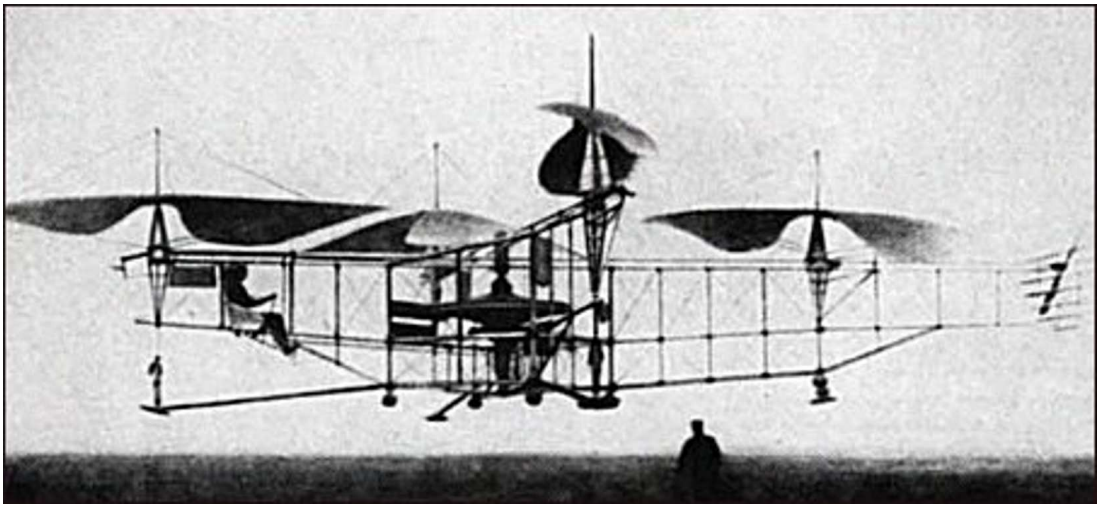

Figure 2.6: Oehmichen No. 2 design picture. On May 4th 1924, it was the first helicopter to fly the distance of one kilometer in a closed-circuit, landing at its starting point [16].

Cornu, who achieved the most successful take-off, near Lisieux on November 13th, 1907, he managed to lift a twin-rotored helicopter into the air entirely without assistance from the ground for a few seconds [17]. This first flight lifted Cornu about 30 cm and lasted 20 seconds. This is sometimes recognized as the first free helicopter flight with a passenger.

Louis Breguet and Maurice L'eger, responsible for previous attempts the same year, were at the heart of these events. They built the first known quadrotor configuration helicopter who achieved to lift itself and pilot into the air, even it did not performed a free flight, as four men were used to steady the structure, the Gyroplane No. 1. Their design was improved and a Gyroplane No. 2 appeared the following year. It was reported to fly successfully more than once in 1908.

In the 1920's, the Marquis Raul Pateras Pescara, an Argentinean working in Europe, achieved one of the first successful applications of cyclic pitch in helicopters [14]. He was also the first to demonstrate that a helicopter with engine failure could still reach the ground safely by means of autorotation, the phenomenon that caused blades to turn even without power being applied to them that resulted from the flow of air as the craft moved through it.

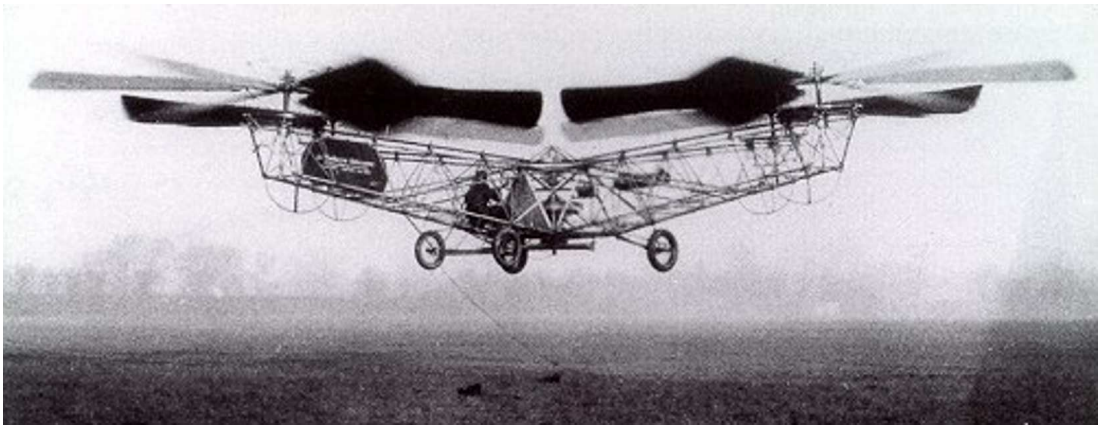

Figure 2.7: The de Bothezat helicopter, known as the "Flying Octopus", undergoes a test flight, 1923 [16].

The French Etienne Oehmichen experimented with rotorcraft designs in the 1920s. Among the different designs he tried, his helicopter No. 2 had four rotors and eight propellers, all driven by a single engine. The Oehmichen No. 2 used a steel-tube frame, with two-bladed rotors at the ends of the four arms. The angle of these blades could be varied by warping. Five of the propellers, spinning in the horizontal plane, stabilized the machine laterally. Another propeller was mounted at the nose for steering. The remaining pair of propellers were for forward propulsion. The aircraft exhibited a considerable degree of stability and controllability for its time, and made more than a thousand test flights during the mid 1920s. By 1923 it was able to remain airborne for several minutes at a time, and on April 14^{th}, 1924 it established the first-ever FAI distance record for helicopters of 360 m. It demonstrated the ability to complete a circular course and later, it completed the first 1 kilometer closed-circuit flight by a rotorcraft. It was a historic flight taking 7 minutes and 40 seconds at an average speed of 7.8 km/hr [14]. The machine, however, was impractical for any realistic use.

In 1922, Dr. George de Bothezat and Ivan Jerome developed the Bothezat quadrotor, with six bladed rotors at the end of an X-shaped structure [14]. Two small propellers with variable pitch were used for thrust and yaw control. The vehicle used collective pitch control. Built by the US Air Service, it made its first flight in October 1922. About 100 flights were made by the end of 1923. The high-

Figure 2.8: Convertawings revived the concept tried in France by Oemichen and by G. de Bothezat in the United States, 1956 [16].

est it ever reached was about 5 m. Although demonstrating feasibility, it was, underpowered, unresponsive, mechanically complex and susceptible to reliability problems. Pilot workload was too high during hover to attempt lateral motion.

The Convertawings Model A Quadrotor, developed in 1956, was intended to be the prototype for a line of much larger civil and military quadrotor helicopters [16]. The design featured two engines driving four rotors with wings added for additional lift in forward flight. No tailrotor was needed and control was obtained by varying the thrust between rotors. Flown successfully many times in the mid-1950s, this helicopter proved the quadrotor design and it was also the first four-rotor helicopter to demonstrate successful forward flight. Due to a low demand for commercial or military versions however, the project was terminated.

The Curtiss-Wright VZ-7 was a VTOL aircraft designed by the Curtiss-Wright company for the US Army [16]. Two prototypes were delivered to the US Army in mid-1958. The VZ-7 had a fuselage with the pilot's seat, fuel tanks and flight

Figure 2.9: Image of the Curtiss-Wright VZ-7, a quadrotor configuration helicopter designed for the US army in the 1950's [16].

controls. On both sides of the fuselage the propellers were attached, unshrouded (the aircraft did originally have shrouds, but these were later removed). There were four propellers in total. The VZ-7 was controlled by changing the thrust of each propeller. The flying platform was maneuvrable and easy to fly. The aircraft performed well during tests, but was not able to meet the Army's standards, therefore it was retired and returned to the manufacturer in 1960.

After all these attempts of manned quadrotor configuration helicopters, and given the lack of orders for civilian or military use, the quadrotor vehicle idea was abandoned until a few decades ago when smaller-size unmanned quadrotor vehicles started to become popular again.

2.2 Quadrotors in the modern era

In the last decades, small scale unmanned aerial vehicles have become commonly used for many applications. This kind of vehicles present numerous advantages

in high risk missions, with high manoeuvrability or reduced dimensions.

The constant evolution of technologies used in UAVs, the sensors and actuators miniaturization and the progress made in communications, point towards an increase on the generalized employment of these platforms [18]. They have demonstrated a good performance in high risk operations as natural disasters and facilities and structures inspection at high altitude or difficult to access locations as well as applications in which the aircraft operation elevated cost does not compensate for the obtained results [19]. Quadrotors also present vertical take-off and landing (VTOL) possibilities and hover manoeuvring, which make of it a suitable vehicle in small spaces manoeuvring cases.

In order to achieve a correct performance in quadrotors actuations in all its applications, it is necessary to have a complete understanding of the vehicle's dynamics and a stable behaviour able to track accurately defined trajectories. It is crucial to avoid control actions which can unstabilize the platform or introduce undesired vibrations. Since quadrotors are semi-autonomous vehicles, increasingly used for reconnaissance missions, a good performance of the telemetry and image capturing systems mounted on the vehicle is crucial. Therefore a free vibrations platform or measuring system is essential for these operations. In this section, the main approaches to quadrotors dynamic and aerodynamic modelling is presented, as well as different sensors and actuators devices usually employed in the quadrotor control and guidance field. Also, the aeroelastic effects studied in quadrotor vehicles are shown here, together with some other works that have considered the vibrations produced in rotary-wing vehicles.

When modelling a quadrotor there are always two different coordinate systems for defining the equations of motion of this kind of vehicles: an inertial earth frame used to locate the vehicle in space; and a second reference system, a body-fixed frame with its origin at the cross section of the two arms of the quadrotor, in which the speeds, forces and moments are expressed. In order to obtain the

equations of motion a series of assumptions are usually made: the vehicle is symmetric, the inertia-matrix is diagonal and invariant and the mass centre of the vehicle coincides with the origin of the body-fixed reference system. There are authors that model the full motion of the vehicle, i.e., with six degrees of freedom, three rotational and three translational, [20–28]. Also a simplified version of this model is quite common; since the lateral and longitudinal motion is determined by the angular position of the vehicle and the total lift forces, only the angular degrees of freedom, [29–35] or the angular motion plus the altitude, [36–38], are considered. Some authors have as well modelled variable configurations, such as a tilt-wing aerial vehicle that is capable of flying in horizontal and vertical modes, [39–41]. Different authors consider more details on the dynamics involved on the quadrotor motion than others; the more simple dynamic model, that can be found in control oriented research, only considers the motion of the vehicle body as a function of the external aerodynamic forces, not considering the gyroscopic or inertial effects, [42–44]. Other authors go one step further by considering the gyroscopic effects acting on the structure [45–47]. However, in order to include all the nonlinearities present in the quadrotors' motion, the gyroscopic [48–52] and inertial effects [53] of the rotors need to be considered.

The most common approach in order to obtain the vehicle's equations of motion is to use the Newton-Euler formalism. It is based on the combination of the two Euler's laws, the linear and angular momentum equations, for obtaining the equations governing the spatial behaviour of a rigid body subjected to external forces and moments [24, 25, 45, 47, 54–60]. Also common is the use of the Euler-Lagrange formalism for obtaining the vehicle's equations of motion. It consists on the application of the Lagrangian differential equation to the Lagrangian of the system, which is obtained from energy considerations [35–37, 61–67]. Even these methodologies part from different principles, the literature shows that the equations of motion obtained with both of them are the same for the quadrotor vehicle.

Even the Euler angles' representation has always been the most widely used to describe the spatial orientation of aircrafts, other authors prefer the quaternion representation for the angular orientation of quadrotors [26, 28–31, 52, 68–73]. This is because there exits a singularity in the Euler angles' spatial representation when the pitch, or rotation around X axis, reaches 90 degrees, [74]. In conventional aircrafts, this singularity does not represent an impediment, however, due to the high manoeuvrability of the quadrotors, this condition may be reached, both during simulation or flight. By using the quaternions spatial representation - which consists on the use of a four dimensional vector for the three dimensional rotation of objects [75] - this singularity, known as gimbal lock in the quadrotor field, can be avoided and it is also numerically more efficient and stable when compared to traditional rotation matrices.

Regarding the control methodologies applied to quadrotors stabilization and tracking, several strategies have been adapted and developed to adjust the high operational demands of these vehicles, and so many research groups still studying the design and implementation of different controllers.

Quadrotors present a very nonlinear behaviour, however there are many linear approaches which are widely used in the stabilization and guidance of quadrotor vehicles. One of the most used is the PID controller that consists on feeding back a control action proportional to the position, integral and derivative error, hence its name [38, 47, 63, 76–81]. Some variations based on this structure are quite common, as the proportional derivative controller PD [27, 28, 43–45, 61, 62, 82] or the proportional double derivative PD^2 [72, 73]. The linear quadratic regulator approach, LQR, is very common for the control of this kind of vehicles as well. This control method uses the space-state linear representation of the vehicle's system and tries to find the feedback control law that minimizes the value of a given cost function by solving the associated constant coefficients Riccati equation [33, 54, 60, 63, 83, 84]. Other authors expand the application of this method to nonlinear systems by solving the state-dependent Riccati equations for each

state [85, 86]. The feedback linearization is also a common approach used in controlling nonlinear systems as the quadrotor vehicles [51, 87, 88]. It consists on the transformation of the nonlinear system into an equivalent linear system through a change of variables and a suitable control input. To ensure that the transformed system is an equivalent representation of the original system, the transformation must be invertible and both, the transformtation and its inverse have to be smooth so that differentiability in the original coordinate system is preserved in the new coordinate system. This technique is also widely employed in combination with other control methodologies, as PID controllers [58], backstepping techniques [89] PD and backstepping PID [55], adaptive control [90] and adaptive sliding modes [91].

Other authors prefer more sophisticated nonlinear control methodologies. Quite common in the control of quadrotors is the use of sliding modes control techniques in which the control inputs typically take values from a discrete set or from a limited collection of prespecified feedback control functions. The switching logic is designed in such a way that the control system leads to the stabilization on the desired trajectories [26, 64, 70, 92–94]. This control technique present the advantage of robustness against perturbations and model uncertainties which makes an ideal candidate for experimental applications, however, it also has an important drawback when studying the vehicle vibrations: the chattering phenomenon, that may excite unmodelled high frequency modes and degrade the performance of the system. The backstepping control approach is also widely used for the control of quadrotors [34, 56, 59, 71, 95–99]. Since the modelling of the complex systems such as quadrotors may be sometimes hazardous, some authors opt for adaptive techniques, which are able to affect the control law depending on the changing conditions of the system or on the unknown values of the system parameters [32, 100–102], many times used for system identification. Less common but also employed in the quadorotors control is the predictive control method which uses the system states, measurements and information from the vehicle model

in order to anticipate the future changes in the dependent variables, enabling the optimization of the current time slot performance while taking the future time slots into account [103–105] and the neural networks based control systems [66, 85, 106].

Obviously, there are multitude of control techniques for the stabilization and guidance of vehicles and different approaches have been used in the control of quadrotors in the last years, each of them presenting different advantages and disadvantages, being chosen for the specific end of the work they were framed in. For the study of vibrations, a relatively straightforward control able to smoothly stabilize the vehicle with small computational load is preferable, so the control system does not introduce any undesired vibration on the vehicle.

To implement the previous mentioned control systems, it is necessary to access the state variables of the vehicle -namely linear and angular positions, speeds and accelerations of the platform and rotors-, which is made through observers, filters and sensors mounted on the quadrotors' structure, in order to affect the actuators adequately. The behaviour of these actuators and sensors has been studied by several authors and included in the theoretical modelling and experimental validation of the quadrotor vehicles.

The quadrotors are usually equipped with accelerometers and gyroscopes. The first ones measure the earth gravity vector and thus can directly observe roll and pitch angles, however, the signals are high sensitive to vibrations induced by the propellers. The gyroscopes measure the angular rates along the rotational axis and the absolute rotation is obtained by integration of the angular rate signals over time. The gyroscopes are less sensitive to the vibrations, however they tend to drift. The use of the Kalman filter is widely used in the quadrotors filed in order to combine the available measurement data coming from the accelerometers and gyroscopes, either in simulations or experimentally, plus prior knowledge about the system and measuring devices, to generate an estimate of

the state variables in such a manner that the error associated to the measure is minimized statistically [33, 68, 77, 96, 97]. It is also common to find authors who use commercial IMUs (inertial measurement units) for the angular estimation of the vehicle, which consist on a series of MEMS (Micro Electrical-Mechanical Systems) sensors, usually combining accelerometers, gyroscopes and magnetometers [53, 78]. There are authors that even consider the data loss from magnetometers and accelerometers, implementing an extended Kalman filter in order to supply an estimation of the angular variables when the interruption in the measurement occurs [29].

In order to tackle the positioning and guidance of the quadrotors, it is also necessary to obtain measurements of the linear variables besides the angular orientation. A popular approach for the obstacles recognition and avoidance in quadrotors is the optical flow based methods, widely used due to the small size and weight of the necessary hardware. Using image feature tracking, the optical flow of two images taken with a short time interval is calculated. Being this optical flow caused by translation and rotation of the vehicle, and having the data provided by IMUs or other angular measurement system, the optical flow effects caused by rotation can be compensated, being possible to obtain a depth estimation of the nearby objects from the optical flow caused by translation [107–110]. Other authors combine the use of optical sensors based on a modified optical mouse sensor, effective for the measurement of the lateral and longitudinal displacements, in conjunction with a commercial IMU and a sonar device for the estimation of the angular and height variables and an extended Kalman filter for the translational speed estimation [50].

An alternative for obtaining the state variables when these can not be directly measured is the use of observers. A state observer is a system that provides an estimate of the internal state of a system from measurements of the inputs and outputs, in which the estimated output - based on the estimated state - is forced to match the actual measured output state. There are authors that use sliding mode

observers in order to estimate the effect of the external disturbances such as wind and noise [57] and also for the observation of the quadrotor speed and estimation of parameter uncertainties [59]. Other authors even achieve disturbance rejection with the use of these observers [36, 44, 61]. Less common is the use of neural network observers for the estimation of the rotational and translational speeds of the vehicle [106].

Because of the nonlinearity and complexity involved in the mechanics of the quadrotor motion and in order to introduce the uncertainty present in the theoretical modelling of complex systems, uncertainty in the modelling parameters is sometimes included. Usually the mass centre is considered to match the geometrical centre of the vehicle, however, due to the location of the telemetry and processing systems this assumption is not always true. Some authors have performed stability analysis of the vehicle depending on the height of the mass centre with respect to the rotor plane for forward flight and subject to wind disturbances [23], others estimate the real in-plane position of the mass centre based on the roll and pitch steady state error that the vehicle experiences [100] and others even present adaptive controllers that compensate the dynamical changes that may be produced in the mass centre of the quadrotor during flight [90].

Also the uncertainties in the modelling parameters have been widely studied in quadrotor vehicles, as variations of the mass, lengths and inertias from their nominal values. These uncertainties, and others as external disturbances, are usually overcome by the robustness of the control method chosen, as is the case of [56, 65, 87, 93–95]. There are different authors that go one step further when modelling uncertainties and include the environmental conditions the vehicle may be subjected to. A common environmental disturbance studied for its effect on the quadrotor's behaviour is the wind gust, modelled in [111] and experimentally verified in [103, 112]. Also external wind disturbances, this time in the form constant wind speeds [50] and the forces and/or moments they usually produce [87,95,100,113] have been considered for different authors. Also the ground effect,

consisting on an increasing of the lift force and a decreasing of the aerodynamic drag of the rotor due to the interruption of the bladetip vortices and flow downwash when the vehicle is flying close to the ground, has been considered in the behaviour of the quadrotors [91, 101].

With the information coming from the sensors and the quadrotor model information, the control system provides the control law for stabilizing and guiding the vehicle, that is then applied by the actuators. The actuators usually used on quadrotors consist on an electric motor with a micro controller that receives a PWM signal from the CPU and transforms this command into rotational speed of the propeller and therefore aerodynamic forces and moments. The dynamic behaviour of the electric motors can be modelled by a system of two differential equations, one for the electrical part and other for the mechanical part. However, due to the very low inductance of the small engines used in quadrotors, the behaviour of the motor can be approximated to a first order differential equation that combines the electrical and mechanical part [34, 35, 49, 55, 56, 63, 89, 94]. Another equivalent method to model the behaviour of the actuator is by means of a first order transfer function [33, 53, 96, 114]. In both cases, the motor parameters on the equation can be obtained from the motor specifications, experimentally or from available literature. Less usual, but also employed is the modelling of the actuator with a linear relation between the control input and the rotational speed, obtained experimentally [115].

There are authors that model and consider the effects of sudden failures on the rotors, usually as a power loss in one of the rotors, and different approaches are used in order to maintain an adequate performance: [102], [58] and [111] use adaptive techniques and control reallocation, which consist on the redistribution of the control signals such the effects of the faulty actuators are cancelled by using the remaining healthy actuators in order to overcome the effect of actuator failures, and [101] and [116] set the gain of their control system to some predefined scheduled gains obtained from the study of fault-free and faulty flight conditions.

Even these research works consider the failure of one of the rotors, modelling it as a sudden power loss, no research group considers the effect of lossing part of a blade, which besides the lift force loss causes an imbalance of forces between the two blades of the same motor, inducing a centrifugal acceleration.

The actuators used for quadrotors control, usually electric motors, have two blades attached to the spinning shaft. The blades moving through the air produce the aerodynamic forces - lift force, drag force and the moments produced by these forces - which are the external forces governing the motion of the quadrotor. These aerodynamic forces are function of the relative lifting surfaces' squared speed with respect to the air, where this relative speed is composed by the rotational speed of the blade, the translational speed of the vehicle and the relative wind speed. Other variables that affect the magnitude of the aerodynamic forces are the blades' dimensions, shape and disposition besides the ambient conditions, as the air density [117]. As for the modelling, different approaches have been used in the last years to simulate these aerodynamic forces and their effects on the vehicle's behaviour. The most common aerodynamic model employed in the quadrotors behaviour modelling considers the lift force produced by the two blades of the rotor as a function of only the rotational speed of the blades and a constant parameter that includes the effect of the blades' dimension, shape and the air density, applied at the centre of the rotor. In this model, the drag forces are considered as a moment acting around the rotor shaft, opposite to the rotating direction, that produces a slowdown of the rotational speed, with its magnitude being proportional again to the rotational speed of the rotor and a constant parameter [71–73, 82, 118]. The constant parameter that is used to determine the aerodynamic forces in this model can be obtained experimentally [31, 85, 115, 119], from the manufacturer specifications [83, 104, 112] or from existing literature [97, 98, 120]. This simplified aerodynamic model, with a linearized dynamic quadrotor model, is usually applied to the design of the control system since it does not take the aerodynamic forces variation with translational speed

into account. Other widely used aerodynamic model is based on the momentum and blade element theories, which consist on the consideration of the blade as a sequence of bidimensional airfoils and calculate the differential aerodynamic forces produced by each section, integrating then the distribution to achieve the total forces acting on the rotor [21, 45, 53, 55, 60, 62, 70, 89, 114]. Even this model considers the configuration of the blades in more detail, the translational speed is usually not taken into account, considering that the effect it may have in the aerodynamic forces is negligible when compared to the rotational speed of the rotors. Besides, both aerodynamic models always consider the aerodynamic forces applied at the centre of the considered rotor, usually not taking into account the effect of the different lift and drag forces produced by each blade individually. It will be shown that when studying the vibrations induced on the vehicle's structure by the aerodynamics and the rotors, these simplifications in the modelling suppress important oscillations.

There are few authors concerned with the aeroelastic coupling effects in translational flight, summarized on the difference of the aerodynamic forces produced in the advancing and retreating blade, which cause a moment at the rotor hub if the rotors are considered rigid [48] or the known as flapping effect [121] that may change the magnitude and direction of the aerodynamic forces. The blade flapping effects on the vehicle performance have been studied before, for both high aggressive manoeuvring [79] and for near hovering conditions [79]. However, in neither case the vibrations introduced in the structure by the flapping effects were considered.

When it comes to the vibrations in quadrotor vehicles, there are not many authors studying the effect of the rotary components on the dynamic behaviour. [122] modelled the vibration of a piston engine in a conventional configuration UAV and studied how these vibrations affect the rest of components in the vehicle, however, the vibrations induced are not in any case similar to those produced by the rotating blades of a quadrotor. There are some authors that propose

the use of foams in order to isolate the measurement equipment from undesired vibrations [123], but no study of how these vibrations are produced or transmitted has been found for quadrotor vehicles. An option proposed for the reduction of vibrations in rotary-wing vehicles is the employment of piezoelectric actuators embedded in the blades in order to decrease the vibrations at the source, which is a solution still under investigation for large scale helicopters and starting to be studied in reduced scale blades [124].

These are some of the most representative examples in quadrotor dynamic and aerodynamic modelling, aeroelastic effects consideration and control. Each approach has its own advantages and disadvantages and all of them are suitable for the specific conditions for which they were applied.

2.3 Contribution to the state of the art

In this work a different approach for the modelling of the dynamics and aerodynamics of the vehicle is used. As it will be seen along this document, a multibody software has been used for the modelling of the quadrotor's dynamics. This software uses the Kane formalism for obtaining the equations of motion, which counts with the advantages of the Newton-Euler and Euler-Lagrange formalisms, but with any of their drawbacks.

The aerodynamic forces will be obtained by means of the momentum and blade element theories, but here they will be calculated for each one of the blades and applied at their pressure centre which, as far as we are aware, no other research has been known for doing so. The consequences of these considerations will be shown in the modelling and vibrational analysis chapters.

Despite the large amount of sophisticated methods already proven for the control of quadrotors, a straightforward control method with small computational load

and good smooth trajectory tracking will be implemented in order to obtain a stable platform for the vibrations study and characterization.

This study will be carried out considering the blades elasticity, since they are expected to be the main source of vibration due to their high rotational speed and also the most sensitive part of the vehicle, since they generate the driving forces.

Chapter 3

Quadrotor modelling

3.1 Quadrotor dynamic and aerodynamic overview

Quadrotors are popular vehicles in the unmanned aviation field due to their reduced dimensions, easy handling and high versatility. Their propulsion and elevation is provided by the action of four equispaced rotors distributed around a central structure. The propulsion is created by the blades' angular rotation around the central hub with an angle of attack. Trajectory tracking is achieved by means of an angular speed change of one or more rotors, leading to a change on the propulsion produced by each of them. The control systems and electronic sensors are usually hosted in the centre of the vehicle structure and are used to stabilize the quadrotor [125, 126].

Since quadrotors do not posses cyclic control, they do not have the mechanisms associated to this degree of freedom simplifying and lightening in this way the vehicle's design. Moreover, the smaller size of the rotors compared to a conventional helicopter's main rotor reduces the kinetic energy during flight. This represents higher security in the case of a rotor collision with obstacles and reduces the hazard for the vehicle and nearby objects [48].

3.1.1 Quadrotor dynamics description

The main forces governing quadrotors behaviour are the weight and the aerodynamic forces acting on the blades and on the structure. These are represented in Figure 3.1.

The resultant forces of the weight, W, act at the mass centre of each element and point downwards towards the ground (blue arrows in Figure 3.1). The Translational Drag is a force opposing the motion of the vehicle, produced by the friction of the airflow around it. Since the vehicle is considered symmetric, the resultant Translational Drag (TD) acts at the centre of the structure and is proportional to its linear speed through a drag coefficient, $K_{TD_{x,y,z}}$ [64, 81]. The aerodynamic forces acting on the blades are provided by the pressure and shear distribution over the object surface, both of them appear due to the relative displacement between the object and the surrounding airflow. The total integration of these distributions along the blade surface is the aerodynamic resultant force (RF) applied at the pressure centre. There are different representations of the resultant aerodynamic force, depending on the reference system used to describe them: Lift (L) and Drag (D) forces or Thrust (T) and Torque/Radius (TQR) forces.

Figure 3.2 shows a representation of the projections used to describe the resultant aerodynamic force. The main difference between these representations is the orientation of the reference systems in which the resultant aerodynamic force is expressed, which is given by the angle between the incoming airflow and the rotor plane, α_{in}.

- Lift force (L): It is the component of the aerodynamic force that is perpendicular to the airflow direction.

- Drag force (D): It is the component of the aerodynamic force that is parallel to the airflow direction.

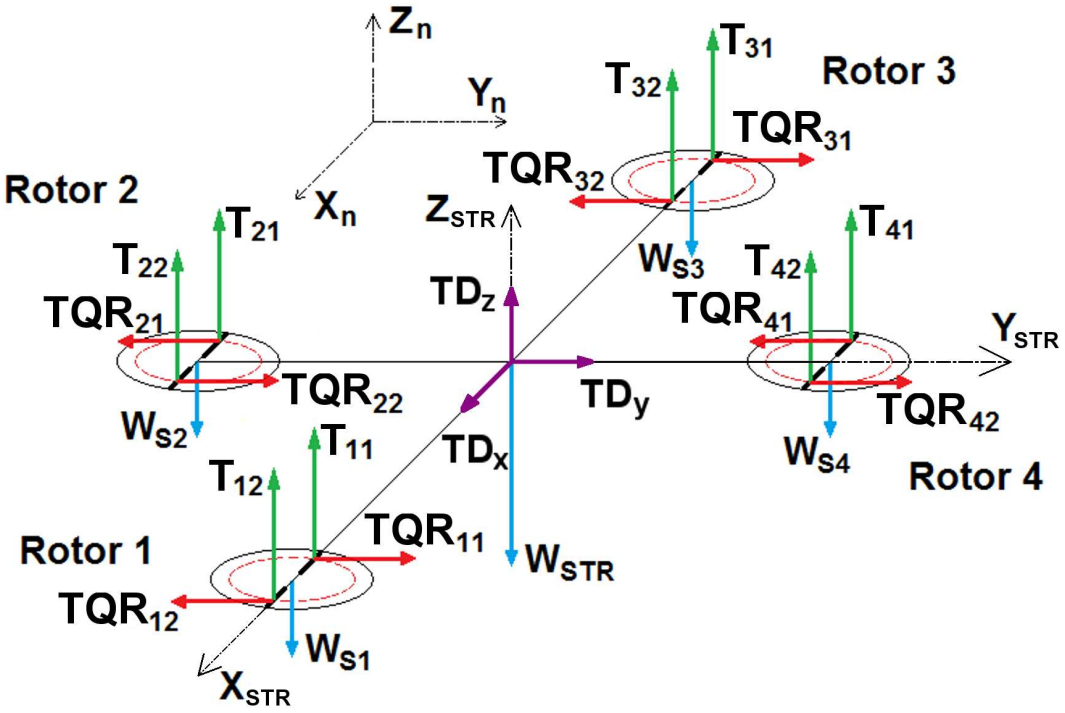

Figure 3.1: Representative diagram of two-bladed rotors' and blades' position around the central body, with the inertial reference system ($[X_n,Y_n,Z_n]$), the body-based reference system ($[X_{STR},Y_{STR},Z_{STR}]$) and the forces involved in the quadrotor dynamics: Thrust (T), Torque/Radius (TQR), Translational Drag (TD) and Weight (W) forces.

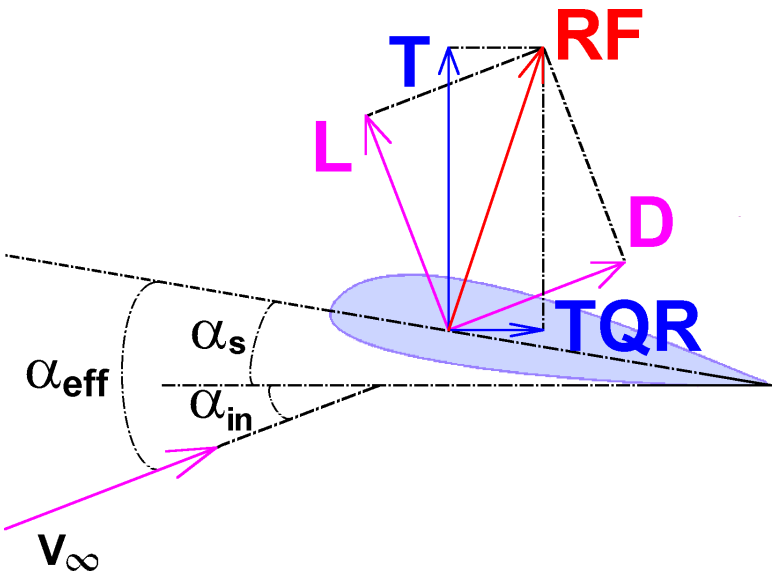

Figure 3.2: Different coordinate system for the definition of the aerodynamic resultant force (RF). Lift (L) and Drag (D) forces are normal and parallel to the incident airflow respectively, Thrust (T) and Torque/Radius (TQR) forces are normal and parallel to the rotor plane respectively.

- Thrust force (T): It is the component of the resultant aerodynamic force normal to the rotor plane.

- Torque/Radius force (TQR): It is the component of the aerodynamic force that acts parallel to the rotor plane.

The relation between the two reference systems is given by the following rotation matrix:

$$\begin{pmatrix} T \\ TQR \end{pmatrix} = \begin{pmatrix} \cos\alpha_{in} & \sin\alpha_{in} \\ -\sin\alpha_{in} & \cos\alpha_{in} \end{pmatrix} \begin{pmatrix} L \\ D \end{pmatrix} \tag{3.1}$$

The subscript i is used along this work to identify the rotor number, the subscript j identifies each corresponding blade in the i$^{\text{th}}$ rotor and the subscript k will be used to identify the blade's segment when elastic blades are considered. In this way, L_{ij} is the Lift generated by the blade j at rotor i and L_i identifies the Lift generated by the rotor i, i.e. by the two blades. Similar notation is used for defining Drag forces, Thrust forces and Torque/Radius forces.

For the type of rotary-wing vehicles consisting of four rotors rotating in opposite directions (rotors 1 and 3 in Figure 3.1 rotate counter-clockwise whilst rotors 2 and 4 rotate clockwise), there will exist four control variables. The control variables considered in this work are the moments applied from the stator to the rotor of the motors. The displacement of the vehicle is achieved by varying the moments applied to each rotor as the rotational speed of the rotors is therefore modified. This way, different aerodynamic forces are obtained and the imbalance of these forces around the different axes associated to the structure induces an acceleration:

- The vertical displacement, $Z(t)$, is given by the total balance of the gravitation force, W, and the total Thrust vertical component, $T = \sum T_{ij}$, $\{\text{i} = 1 \ldots 4, \text{j} = 1, 2\}$. By increasing the rotors angular velocity simultaneously, the total Thrust force increases, and an upward vertical translation appears.

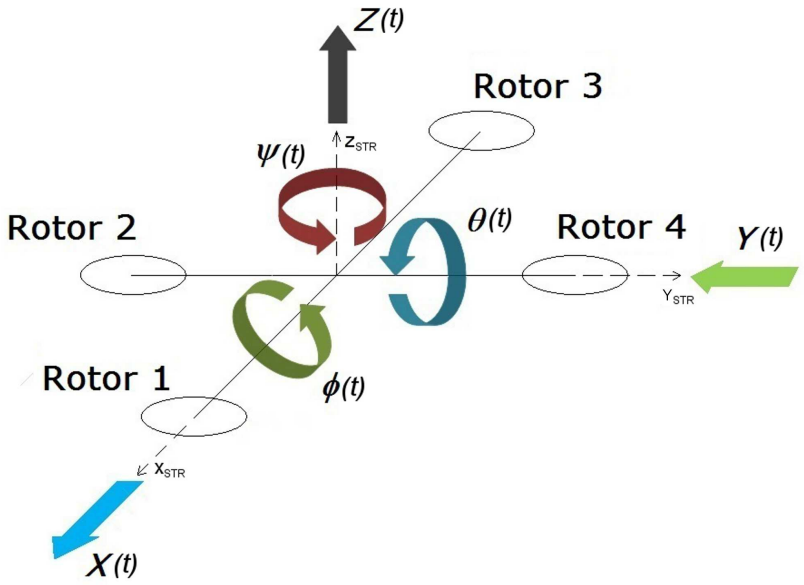

Figure 3.3: Representative diagram of rotors' location around the central body and motions of the quadrotor. The $X(t)$ and $Y(t)$ motions represented correspond to a positive pitch and roll motion, respectively.

On the contrary, by decreasing the angular velocity, the total Thrust force decreases, producing a downwards vertical displacement.

- The roll $\phi(t)$, is the rotation around the structure's longitudinal $\mathtt{X_{STR}}$ axis, it is determined by the moment's imbalance that the Thrust forces generate around this axis, being the main contribution to this moment the forces produced by the rotors aligned along the lateral axis $\mathtt{Y_{STR}}$ (rotors 2 and 4 in Figure 3.3). By increasing the angular velocity of rotor 4 and decreasing the angular velocity of rotor 2 ($T_4 > T_2$), a positive roll turn around $\mathtt{X_{STR}}$ axis is achieved due to the imbalance of Thrust forces T_4 and T_2. By decreasing the angular velocity of rotor 4 and increasing the angular velocity of rotor 2 ($T_2 > T_4$), a negative roll rotation is induced.

- In a similar way, the pitch rotation, $\theta(t)$, around the structure's lateral $\mathtt{Y_{STR}}$ axis is determined by the moment's imbalance that the Thrust forces generate around this axis, being the main contribution to this moment the forces produced by the rotors aligned along the longitudinal axis $\mathtt{X_{STR}}$ (rotors 1 and 3 in Figure 3.3). Similarly to the roll motion case, by increasing the

angular velocity of rotor 3 and decreasing the angular velocity of rotor 1 ($T_3 > T_1$), a positive pitch rotation around $\mathtt{Y}_{\mathtt{STR}}$ axis is produced. On the other hand, by increasing the angular velocity of rotor 1 and decreasing the angular velocity of rotor 3 ($T_1 > T_3$), a negative pitch rotation of the vehicle is achieved.

- The yaw rotation, $\psi(t)$, around the vehicle's vertical axis $\mathtt{Z}_{\mathtt{STR}}$, is determined by the rotors' reaction moments as a response to the control moments applied from the structure. When the control moment is applied to the rotors, it reacts with an opposite moment to the structure. The combination of the moments originated at the four rotors produce a yaw acceleration around the vertical axis associated to the quadrotor. By controlling the moments applied to the rotors, their response into the structure can also be controlled. By applying a larger moment to rotors 2 and 4 than those applied to rotors 1 and 3 ($M_4, M_2 > M_3, M_1$) a positive yaw rotation is obtained, whilst by applying a higher moment to rotors 1 and 3 than those applied to rotors 2 and 4 ($M_3, M_1 > M_4, M_2$) a negative yaw rotation is obtained.

The quadrotor has 6 degrees of freedom; three rotational ($\phi(t)$, $\theta(t)$ and $\psi(t)$) and three translational ($X(t)$, $Y(t)$ and $Z(t)$), and counts with four control inputs; therefore some variables must be related to each other: lateral and longitudinal translations, which are the underactuated variables, are determined by the horizontal component of the Thrust force, which is related to the total Thrust force by means of the quadrotor orientation with respect to the inertial reference system.

- In the particular case of existing only pitch degree of freedom $\theta(t)$, the vehicle's longitudinal translation depends on the horizontal projection of the total Thrust force, $T \sin\theta$. Therefore, by varying the pitch angle adequately, the desired displacement along the longitudinal $\mathtt{X}_{\mathtt{STR}}$ axis can be achieved. By a positive pitch angle increase, a positive displacement along

the longitudinal $\mathtt{X}_{\mathtt{STR}}$ axis is obtained (Figure 3.3), whilst a negative pitch angle change leads to a negative displacement on the longitudinal axis.

- In the case of only roll $\phi(t)$ demands, the lateral translation depends on the horizontal projection of total Thrust force, $T \sin \phi$, thus by varying the roll angle adequately, the desired displacement along the $\mathtt{Y}_{\mathtt{STR}}$ axis is achieved. In contrast to the longitudinal displacement, a positive roll angle produces a negative displacement along the $\mathtt{Y}_{\mathtt{STR}}$ axis, whilst a negative roll angle leads to a positive displacement; this is illustrated in Figure 3.3.

It should be noted that when the quadrotor rotates around any of its axes ($\mathtt{X}_{\mathtt{STR}}$, $\mathtt{Y}_{\mathtt{STR}}$ and $\mathtt{Z}_{\mathtt{STR}}$), the reference system associated to the vehicle is not aligned to the inertial reference system ($\mathtt{X}_{\mathtt{n}}$, $\mathtt{Y}_{\mathtt{n}}$ and $\mathtt{Z}_{\mathtt{n}}$). Therefore, the lateral, longitudinal and vertical displacements would not coincide with the displacements referred to the inertial axes and different reference systems are used in the quadrotors description.

There exists an inertial reference system (IRS) - denoted by the subscript $\mathtt{n}$ in this work - and a body-based reference system (BRS) - denoted by the subscript $\mathtt{STR}$ - that moves with the vehicle. The inertial reference system is commonly used to describe the position of the vehicle with respect to an external reference point, the IRS origin, and the references for guidance are usually given in the IRS. The attitude of the vehicle is given by the relative orientation of the BRS with respect to the IRS, also known as the Euler angles, ϕ, θ and ψ. The external forces acting on the vehicle are usually expressed in the BRS, except for the gravitational force, which is expressed in the IRS.

Since the quadrotor's lateral and longitudinal motions are controlled by the roll and pitch angles, the guidance references need to be expressed in the BRS. Therefore, the references must be transformed from the IRS to the BRS. The relation of the positions expressed in the IRS with respect to those expressed in the BRS

is given by Euler rotation matrix, R:

$$R = \begin{pmatrix} \cos\theta\cos\psi & \cos\theta\sin\psi & -\sin\theta \\ \cos\psi\sin\phi\sin\theta - \cos\phi\sin\psi & \cos\phi\cos\psi + \sin\phi\sin\theta\sin\psi & \sin\phi\cos\theta \\ \sin\phi\sin\psi + \cos\phi\sin\theta\cos\psi & \cos\phi\sin\theta\sin\psi - \cos\psi\sin\phi & \cos\phi\cos\theta \end{pmatrix} \tag{3.2}$$

Therefore, the linear references expressed on the BRS given to the vehicle are:

$$\begin{pmatrix} X_{ref} \\ Y_{ref} \\ Z_{ref} \end{pmatrix}_{BRS} = R \begin{pmatrix} X_{ref} \\ Y_{ref} \\ Z_{ref} \end{pmatrix}_{IRS} \tag{3.3}$$

3.1.2 Aerodynamic forces involved

In this section the basic aerodynamic forces acting on a moving body through the air are revised.

The aerodynamic Lift force and Drag forces appearing in a moving body are:

$$L = C_L q_\infty S \tag{3.4}$$

$$D = C_D q_\infty S \tag{3.5}$$

S represents a reference surface and the dynamic pressure is:

$$q_\infty = \frac{1}{2}\rho_\infty V_\infty^2 \tag{3.6}$$

C_L and C_D are the adimensional Lift Coefficient and Drag Coefficient respectively, which can be obtained experimentally. ρ_∞ is the reference air density and V_∞ is the relative velocity between the airflow and the moving object. It can be seen that the aerodynamic forces depend on the squared velocity between the

airflow and the object and the aerodynamic coefficients C_L and C_D, besides the air density and the representative surface which can be taken as constant. Therefore:

$$L = C_L q_\infty S = C_L \frac{1}{2} \rho_\infty V_\infty^2 S \tag{3.7}$$

$$D = C_D q_\infty S = C_D \frac{1}{2} \rho_\infty V_\infty^2 S \tag{3.8}$$

The aerodynamic coefficients C_L and C_D are functions of several parameters [117]:

$$C_L = C_L(\alpha, Re, M_\infty) \tag{3.9}$$

$$C_D = C_D(\alpha, Re, M_\infty) \tag{3.10}$$

However, for a big range of usual values of Reynolds Number, Re, and Mach Number, M_∞, in quadrotors applications, their influence can be neglected and the aerodynamic coefficients are usually considered only dependent on the blade angle of attack, α [127]:

$$C_L = C_L(\alpha) = C_{L_0} + C_{L_\alpha} \alpha \tag{3.11}$$

$$C_D = C_D(\alpha) = c_d(\alpha) + C_{D_i}(\alpha) \tag{3.12}$$

C_{L_0} is the Lift Coefficient at zero angle of attack, C_{L_α} is the slope of the Lift Coefficient-Angle of attack curve shown in Figure 3.4 and α is the effective angle of attack between the blade's chord and the airflow. Usually the blades in quadrotors do not have feather degree of freedom - rotation around longitudinal axis - therefore the angle of attack is determined by the structural angle of attack, α_s, which is fixed, and the flow incidence angle, α_{in}. c_d represents the profile Drag Coefficient and C_{D_i} represents the induced Drag Coefficient which can be obtained from the Prandtl's Lifting-Line Theory [127]:

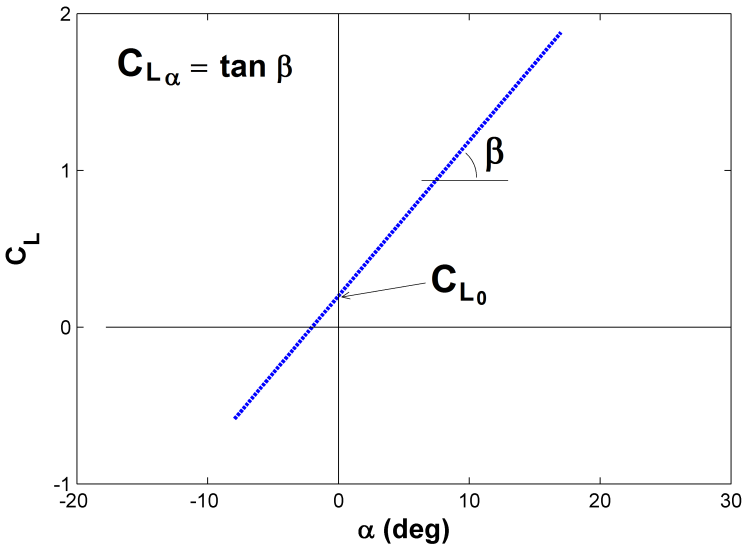

Figure 3.4: A typical curve showing section the Lift coefficient versus angle of attack for a cambered airfoil. It does not include the stall phenomenon since it has not been modelled in this work.

$$C_{D_i} = kC_L^2 \tag{3.13}$$

$$k = \frac{1}{\pi e AR} \tag{3.14}$$

AR is the aspect ratio of the blade and e is the span efficiency factor. These parameters can be obtained from the expressions (3.15) and (3.16).

$$AR = \frac{R^2}{S} \tag{3.15}$$

$$e = \frac{2}{2 - AR + \sqrt{4 + AR^2}} \tag{3.16}$$

By introducing the previous expression in equation (3.12) a expression for C_D dependant on C_L can obtained.

$$C_D = c_d + kC_L^2 \tag{3.17}$$

This relation is known as Drag polar equation and is represented in Figure 3.5. That said, it is concluded that the aerodynamic Lift and Drag forces are only dependent on the blades' speed relative to the air and its incidence angle since

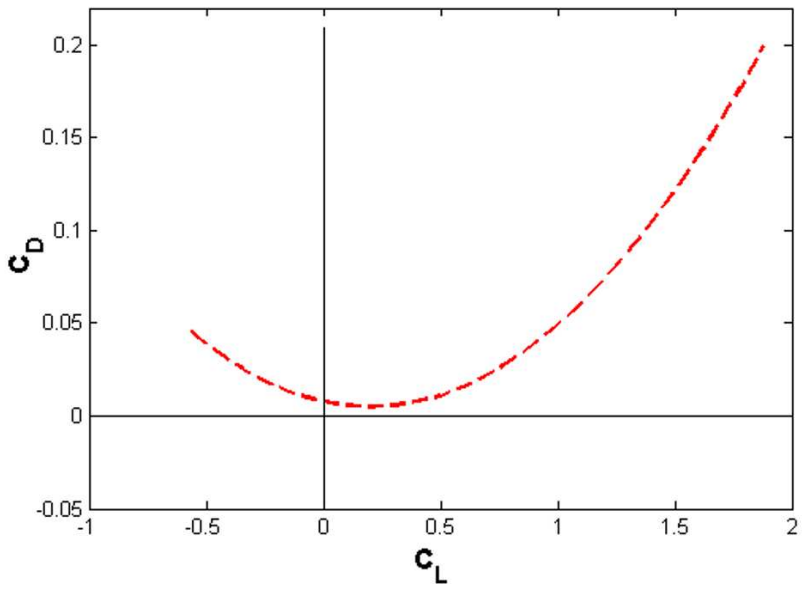

Figure 3.5: A typical drag polar curve for a cambered airfoil.

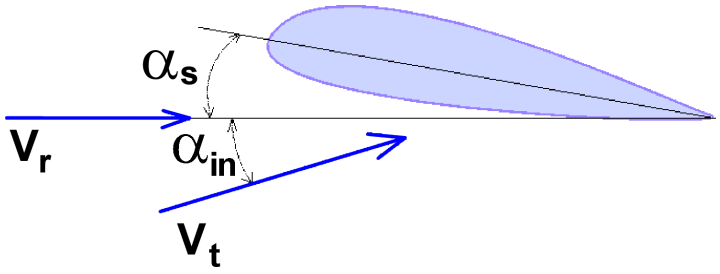

Figure 3.6: Relative velocities and incidence angles of attack in a cambered airfoil considered in the aerodynamic forces modelling.

all the other parameters can be considered constant for a quadrotor.

The relative speed considered in the aerodynamic forces calculus is composed by different contributions: the rotational speed of the blade, V_r, and the translational speed, V_t, as it is shown in Figure 3.6.

3.2 Modelling tool: VehicleSim

The software used for modelling purposes is VehicleSim [128]. It is a modelling and simulation multibody rigid software. The old version of this software, AutoSim, has been used previously by members of this research group in modelling and control of various vehicle systems such as motorcycles [129–133] and heli-

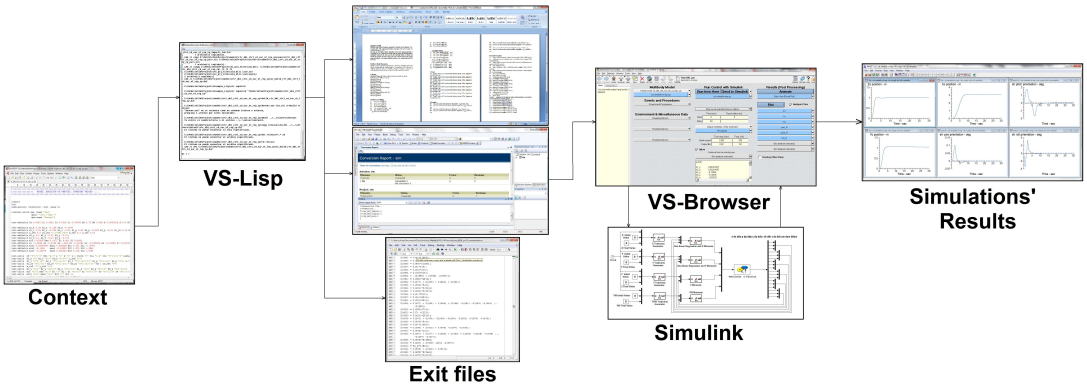

Figure 3.7: Interconnection diagram of VehicleSim components and other softwares employed in the simulations.

copters [134–137]. VehicleSim is the base code of commercial simulators such as TruckSim, CarSim and BikeSim. It consists of a group of LISP macros which allow the description of mechanical systems integrated by several bodies, with the possible addition of non-mechanical systems. It allows the implementation of complex models by a multibody approach; the commands are used to describe the system as a parent-child structure according to the physical constraints between the various bodies conforming the system.

VehicleSim consists of two independent but correlated programs; VS-Lisp and VS-Browser. In VS-Lisp, each body is considered as a rigid body and it is defined by its degrees of freedom (rotation and translation), mass, inertia matrix and by its relation with other bodies. This relation is parental, a reference system is created for each body, which is dependent on the reference system of the ascendant body. It is also necessary to define the forces and moments applied to each body. VS-Lisp extends the performance of Lisp programming language and converts it in a multibody modeling software. Using an advanced formulation of Kane's equations [138] the software obtains the equations of motion from the model's physical description. VS-Lisp solves the differential equations' system, and the output can be in three different formats: (a) .rtf file, which contains the symbolic equations of the described system, (b) a C file containing the model parameters and the simulation control commands or (c) Matlab file containing

the equations of system's motion and the states' matrices A, B, C and D for the linear analysis. Once the model has been generated and compiled, the resultant file is independent from VehicleSim and it can be executed as many times as needed, without modelling or compiling again the system, even in the case the state variables' initial conditions change. The VS-Browser uses the outputs given by VS-Lisp in order to carry out the modelled system's simulations, being possible to carry out the simulation under several different operative conditions. An advantage of this software is the ease of the syntactic rules and its flexibility when describing the bodies and their joints.

Despite the great offer of available programming software, VehicleSim is used due to the advantages it presents: representation of complex systems composed by different bodies and non-mechanical devices, quantification of the interaction between these bodies, lineal and nonlinear equations' derivation, fast numerical solution of these equations and compatibility between this software and other platforms specialized in simulation and control like Simulink, which has been used to implement the control system in this work.

3.2.1 VehicleSim modelling software, VS-Lisp

The beginning of the modelling process consists on the environment definition: units system, linear or nonlinear simulation mode and force fields. VS-Lisp provides different predefined units system (`si`, `mks`) and also allows to define or change the units in a specific units system. In this work the International System of units (SI) is adopted, including also the 'degree' units for angular position. The gravitational field has been included, considered constant, with gravity g=9.80665 m/s^2, and the nonlinear simulation mode has been selected.

An inertial reference system is added automatically to all models, `n`, which has a fixed origin point $\mathtt{n}_0$, and three associated perpendicular directions [$\mathtt{X}_\mathtt{n}$, $\mathtt{Y}_\mathtt{n}$, $\mathtt{Z}_\mathtt{n}$]. Based on this inertial reference frame, the bodies that conform the model

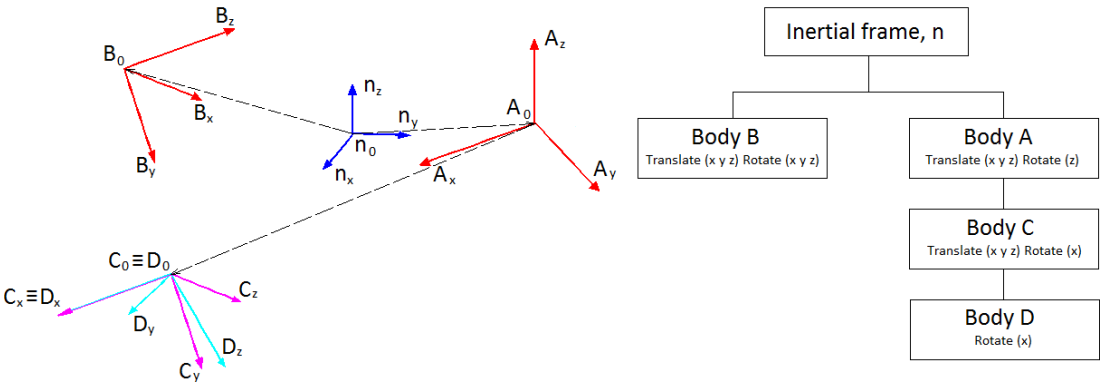

Figure 3.8: Example of Cartesian coordinate systems associated to different bodies in VS-Lisp and their parent-child structure.

are added sequentially, indicating their physical properties (mass, inertia, mass centre, etc.) and their degrees of freedom with respect to the parent (translations and rotations). Each body has an associated local Cartesian coordinate system, which their "child's" coordinates are expressed in. This coordinate system is defined by (i) a reference system which the coordinate system is associated to, (ii) an origin point, and (iii) three mutually orthogonal directions that define the local axes. An example of the coordinate systems associated to each body in a multibody system developed in VS-Lisp is given in Figure 3.8.

Besides their degrees of freedom and restrictions, each body has its own parameters. These parameters are identified with the symbol of the parameter with a subscript indicating the body it is referred to, so the mass of a body named E is $\texttt{M}_\texttt{E}$, the position of its mass centre is $\texttt{MC}_\texttt{E}$ and so on. All the available options for defining a body are listed on Table 3.1 for a body named E with a parent named G.

Once the structural layout is fully defined and the restrictions between bodies are established, the external forces and moments acting on the system are included in the model. As in the bodies description, the forces and moments have some parameters to be fully described. The options and parameters for describing forces and moments are listed in Table 3.2.

Table 3.1: Degrees of freedom and parameters for defining a body in VS-Lisp

Keyword	Symbol	Definition	Default
Body	E	Symbol used to identify the body later.	-
Name	E	String of text used in documentation.	String version of Body.
Parent	G	Body used to locate E and define its movements.	n
Joint Coordinates	JC_E	Point's coordinates where the body is attached to its parent.	Origin of Parent.
CM coordinates	MC_E	Coordinates of mass centre of E.	(0 0 0)
Coordinate system	-	Symbol of body whose coordinate system is used for coordinates specified forJC_E and MC_E.	For JC_E is Parent and for MC_E is Body.
Mass	M_E	Scalar expression for mass of E.	The default is a symbol made by adding M as a prefix to the symbol Body.
Inertia Matrix	I_E	Moments and products of inertia for E about its mass centre.	3x3 matrix with symbols based on Body.
Inertia Matrix Coordinate System	-	Coordinate system in which the inertia matrix is defined.	Body.
Parent Rotation axis	-	Vector expression for the direction, fixed in Parent, of the first rotation Body can make relative to Parent.	If Body Rotation axes is given, default is set to the axis in Parent that coincides with the first element of Body Rotation Axes.
Body Rotation Axes	G_x, G_y, G_z	List of 0 to 3 axis indices indicating sequence of rotations of E relative to parent. If this argument and Parent Rotation Axes are omitted, then Body cannot rotate relative to Parent.	If Parent Rotation Axis is specified, the default is a list of length 1, containing the first axis contributing to the vector direction in Parent Rotation Axis.
Reference axis	-	Vector expression for a direction, fixed in Parent, that defines the orientation of Body when all generalized coordinates are zero. If the first element of Body Rotation Axes is X, Y or Z, then Reference Axis defines the orientation of the Y, Z or X respectively.	-
Translate	G_x, G_y, G_z	List of 0 to 3 vector expressions defining directions of translational movements of E_0 relative to JC_E.	If this argument is omitted, then Body cannot translate relative to Parent.

Table 3.2: Parameters defining forces and moments in VS-Lisp

Keyword	Symbol	Definition
Symbol	F, M	Symbol used later to identify the force or moment.
Name	Force, Moment	String used for comments and generating output variables.
Direction	-	A vector expression for the direction of the force/moment vector. It must be a unit vector, or else the equations of motion will be in error.
Magnitude	-	A scalar expression for the magnitude of the force/moment vector. The default is a constant parameter with the label Symbol.
Point 1 (Forces)	P_1	A point on the line of action of the force. This argument must be provided or an error will be signalled.
Point 2 (Forces)	P_2	A point that may be used to (1) define the body which reacts the force and/or (2) help determine the magnitude of the force. The default is the origin of the inertial reference.
Body 1 (Forces)	B_1	The body upon which the moment acts. The default is the body containing P_1.
Body 2 (Forces)	B_2	The body upon which the moment reacts. The default is the body containing P_2.
Body 1 (Moments)	B_1	The body upon which the moment acts.This argument must be provided or an error will be signalled.
Body 2 (Moments)	B_2	The body upon which the moment reacts. The default is n, the inertial reference.

At this point of the modelling process, with the structure fully defined and the external forces applied, the system would be fully modelled and the system's dynamic equations could be obtained by compiling the file with VS-Lisp.

3.2.2 Equations of motion

Essentially all methods for obtaining equations of motion are equivalent. However, the ease of use of the various methods differs; some are more suited for multibody dynamics than others. Quadrotors are usually modelled as single rigid bodies, and so the Newton-Euler and Lagrange methods are commonly used for obtaining the motion equations. However, in this work a multibody approach is used to model the quadrotor vehicle as these methods are not so efficient when dealing with multibody systems.

The Newton-Euler method is comprehensive in that a complete solution for all the forces and kinematic variables are obtained, but it is inefficient. Applying the Newton-Euler method requires force and moment balances to be applied to each body taking in consideration every interactive and constraint force. Therefore, the method is inefficient when only a few of the system's forces need to be solved for.

Lagrange's equations provide a method for disregarding all interactive and constraint forces that do not perform work. The major disadvantage of this method is the need to differentiate scalar energy functions (kinetic and potential energy). This is not much of a problem for small multibody systems, but becomes an efficiency problem for large multibody systems.

Kane's method offers the advantages of both the Newton-Euler and Lagrange methods without the disadvantages. With the use of generalized forces the need for examining interactive and constraint forces between bodies is removed. Since Kane's method does not use energy functions, differentiating is not a problem.

The differentiating required to compute velocities and accelerations can be obtained through the use of algorithms based on vector products.

A brief introduction of the Kane's equations is given below, and more information about this topic with applications can be found at [138–141].

Consider a multibody system of N interconnected rigid bodies, each subject to external and constraint forces. The external forces can be transformed into an equivalent force and torque ($\vec{F}_\kappa$ and $\vec{M}_\kappa$) passing through MC_κ, the mass centre of the body κ (κ = 1,2...N). Similar to the external forces, the constraint forces may be written as $\vec{F}^c_\kappa$ and $\vec{M}^c_\kappa$.

Using d'Alembert's principle for the equilibrium of body κ, the next expression is obtained:

$$\vec{F}_\kappa + \vec{F}^*_\kappa + \vec{F}^c_\kappa = 0 \tag{3.18}$$

where $\vec{F}^*_\kappa = -m_\kappa a_\kappa$ is the inertia force of body κ.

In a system formed by N bodies with 3N degrees of freedom - which can be described using q_r (r = 1,2...3N) generalized coordinates with force components F_1, F_2,...F_{3N} applied to the mass centre of the bodies along the corresponding generalized coordinates -, the virtual work can be defined as follows:

$$\delta W = \sum_{m=1}^{N} \vec{F}_m \cdot \delta r_m \tag{3.19}$$

where $\vec{F}_m$ is the resultant force acting on the m^{th} body and r_m is the position vector of the m^{th} mass centre in the inertial reference frame. δr_m is the virtual displacement of the m^{th} body, which is imaginary in the sense that is assumed to occur without the passage of time.

Applying the concept of virtual work to the multibody system, considering only

the work due to the forces on the system, the next expression can be obtained:

$$\delta W = \left(\vec{F}_\kappa + \vec{F}^*_\kappa + \vec{F}^c_\kappa\right) \delta r_\kappa \qquad (\kappa = 1, 2...N) \tag{3.20}$$

Since the common constraints usually do not allow any work to be produced, the previous expression can be simplified to:

$$\delta W = \left(\vec{F}_\kappa + \vec{F}^*_\kappa\right) \delta r_\kappa \qquad (\kappa = 1, 2...N) \tag{3.21}$$

or

$$\delta W = \left(\vec{F}_\kappa + \vec{F}^*_\kappa\right) \frac{\partial \vec{r}_\kappa}{\partial q_r} \delta q_r \qquad (\kappa = 1, 2...3N) \tag{3.22}$$

The position vector may also be written as:

$$\vec{r}_\kappa = \vec{r}_\kappa(q_r, t) \tag{3.23}$$

and its derivative with respect to time as:

$$\dot{\vec{r}}_\kappa = \frac{\partial \vec{r}_\kappa}{\partial q_r} \frac{\mathrm{d}q_r}{\mathrm{d}t} + \frac{\partial \vec{r}_\kappa}{\partial t} = \frac{\partial \vec{r}_\kappa}{\partial q_r} \dot{q}_r + \frac{\partial \vec{r}_\kappa}{\partial t} \tag{3.24}$$

Taking the partial derivative of $\dot{\vec{r}}_\kappa$ with respect to $\dot{q}_r$, it yields to:

$$\frac{\partial \dot{\vec{r}}_\kappa}{\partial \dot{q}_r} = \frac{\partial \vec{r}_\kappa}{\partial q_r} \tag{3.25}$$

which can be rewritten as:

$$\frac{\partial \vec{v}_\kappa}{\partial \dot{q}_r} = \frac{\partial \vec{r}_\kappa}{\partial q_r} \tag{3.26}$$

Substituting (3.26) into (3.22), it yields to a new expression of the virtual work:

$$\delta W = \left(\vec{F}_\kappa + \vec{F}^*_\kappa\right) \frac{\partial \vec{v}_r}{\partial \dot{q}_r} \delta q_r \tag{3.27}$$

Since the virtual displacement δq_r is arbitrary without violating the constraints,

the following equality must be satisfied:

$$f_r + f_r^* = 0 \tag{3.28}$$

where f_r and f_r^* are the generalized active and inertia forces respectively, defined as follows:

$$f_r = \vec{F}_\kappa \cdot \frac{\partial \vec{v}_\kappa}{\partial \dot{q}_r} \tag{3.29}$$

$$f_r^* = \vec{F}_\kappa^* \cdot \frac{\partial \vec{v}_\kappa}{\partial \dot{q}_r} \tag{3.30}$$

In a similar fashion, it can be shown using the virtual work principle that the moments can be written as:

$$M_r + M_r^* = 0 \tag{3.31}$$

where M_r and M_r^* are the generalized active and inertia moments respectively and are defined as follows:

$$M_r = \vec{T}_\kappa \cdot \frac{\partial \vec{\omega}_\kappa}{\partial \dot{q}_r} \tag{3.32}$$

$$M_r^* = \vec{T}_\kappa^* \cdot \frac{\partial \vec{\omega}_\kappa}{\partial \dot{q}_r} = -\left(\vec{\alpha}_\kappa \cdot \vec{\vec{I}} + \vec{\omega}_\kappa \times \vec{\vec{I}} \cdot \vec{\omega}_\kappa\right) \cdot \frac{\partial \vec{\omega}_\kappa}{\partial \dot{q}_r} \tag{3.33}$$

By superposition of the force and moment equations (3.28, 3.31), the Kane's equations are obtained:

$$F_r + F_r^* = 0 \tag{3.34}$$

where $F_r = f_r + M_r$ and $F_r^* = f_r^* + M_r^*$.

3.2.3 VehicleSim solvers

Once the bodies that conform the vehicle have been fully defined and the external forces and moments have been applied, the motion equations of the complete vehicle are obtained. The VehicleSim solver performs a run by executing calculations at closely spaced intervals of time, using the motion equations that define the math model. The current state of the vehicle's model is defined by a set of

independent variables, state variables, x. Traditionally, the state variables for a multibody vehicle model are defined exclusively with differential equations. Indeed, most of the state variables in a VehicleSim model are defined by a set of ordinary differential equations (ODE's).

This section describes the numerical methods used to solve the differential equations in the vehicle math models.

3.2.3.1 Overview of numerical integration methods

VehicleSim math models have been set up to work with one of five numerical explicit fixed-step integration algorithms. In theory, each state variable is a continuous function of time $x(t)$. However, in a simulation run, calculations are made at discrete intervals of time. Figure 3.9 shows the history for a state variable x at discrete values of time separated by a constant step ΔT. At each step, identified with a count s, there is a corresponding value of x_s and its derivative, indicated as $\dot{x}_s$.

The solver program computes the values of each output variable in the math model at each time interval, using current values of the state variables (x) and possibly their derivatives. The state variables are in turn calculated using numerical integration. If the time t and value of x are known at interval s (time = T_s, x = x_s), then ODEs in the math model can be used to calculate the corresponding value of the derivative $\dot{x}(t)$. The correct value of the state variable at the next interval (s+1) is:

$$x_{s+1} = x(T_s + \Delta T) = x_s + \int_{T_s}^{T_s+\Delta T} \dot{x}(t)\mathrm{d}t \tag{3.35}$$

where $\dot{x}(t)$ is a continuous function of x and possibly other variables that might be imported into the math model from other software or measurements from

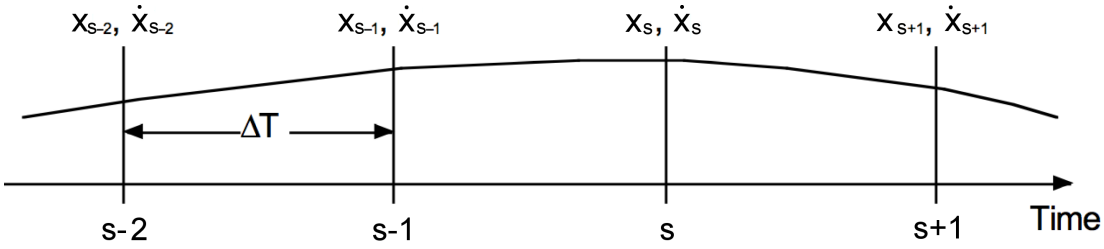

Figure 3.9: Sketch of the time discretization of a state variable x and its time derivative $\dot{x}$.

hardware in the loop. In reality, the behavior of the many variables that influence $\dot{x}(t)$ are not known over the interval. Therefore, approximations are used to calculate the new value of x_{s+1} via numerical integration. The simplest method of numerical integration, called Euler integration, is to project the last known derivative forward to estimate the new value of x:

$$x_{s+1} = x_s + \Delta T \dot{x}_s \tag{3.36}$$

Euler integration does not account for any change in the derivative over the time interval and is not accurate unless ΔT is so small that changes in the derivative are negligible over the step. It is shown here to introduce the concept of numerical integration, but is not used in VehicleSim solver programs. Many numerical integration methods are available for solving equations of motion for multibody systems. Overall, the best method is the one that can calculate all of the state variables with acceptable accuracy over the range of time needed by the user, with the fastest computation time.

VehicleSim solver programs support five methods for numerical integration. Four of these methods involve calculations at a half step, at interval $s + 1/2$, as shown in Figure 3.10. With these methods, an estimation of the state variables at half-step is calculated $x_{s+1/2}$, which is used to calculate the derivative at half-step $\dot{x}_{s+1/2}$, which is then used to calculate a corrected and more accurate value of the full-step state variable x_{s+1}.

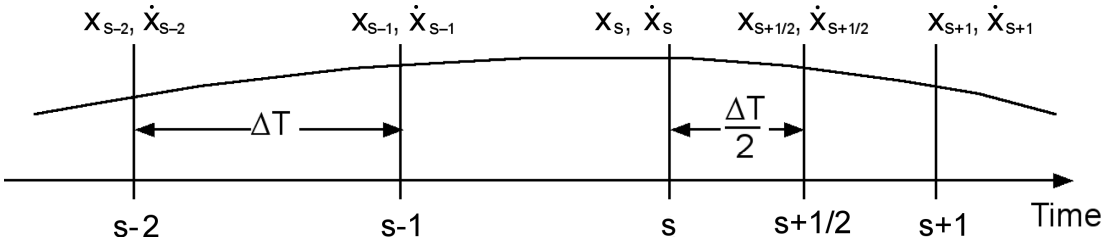

Figure 3.10: Sketch of the time discretization for the half-step numerical integration.

3.2.3.1.1 Adams-Moulton 2nd Order Method

VehicleSim solvers support three Adams-Moulton methods. Each calculates the state variables at the half step to obtain derivatives that are then used to calculate the state variables at full-step time. In the second-order method, the derivatives from the previous step are used to account for some curvature in predicting the state variables at the half step. The two equations are:

$$x_{s+1/2} = x_s + \frac{\Delta T}{8}(5\dot{x}_s - \dot{x}_{s-1}) \tag{3.37}$$

$$x_{s+1} = x_s + \Delta T \dot{x}_{s+1/2} \tag{3.38}$$

This method is the default in all VehicleSim solver programs.

3.2.3.1.2 Adams-Moulton 3rd Order Method

The third-order version accounts for more curvature by going back an additional step. The equations are:

$$x_{s+1/2} = x_s + \frac{\Delta T}{24}(17\dot{x}_s - 7\dot{x}_{s-1} + 2\dot{x}_{s-2}) \tag{3.39}$$

$$x_{s+1} = x_s + \frac{\Delta T}{18}(20\dot{x}_{s+1/2} - 3\dot{x}_s + \dot{x}_{s-1}) \tag{3.40}$$

This method gives performance similar to the AM-2 method. It is better for conditions that have high-frequency vibrations that involve simple springs and

dampers. For example, oscillations of tires when braking to a stop can sometimes be predicted better with AM-3 than with AM-2. On the other hand, simulation of manoeuvres that involve controls or road geometries with abrupt changes in slope can run more efficiently with AM-2.

3.2.3.1.3 Adams-Moulton 4th Order Method

The fourth-order version goes back one more step to provide more accuracy if the variables change smoothly over several steps. The equations are:

$$x_{s+1/2} = x_s + \frac{\Delta T}{384}(297\dot{x}_s - 187\dot{x}_{s-1} + 107\dot{x}_{s-2} - 25\dot{x}_{s-3}) \tag{3.41}$$

$$x_{s+1} = x_s + \frac{\Delta T}{30}(36\dot{x}_{s+1/2} - 10\dot{x}_s + 5\dot{x}_{s-1} - \dot{x}_{s-2}) \tag{3.42}$$

3.2.3.1.4 Runge-Kutta 2nd Order Method

This real-time Runge-Kutta method is similar to the AM-2 method. It differs by using Euler integration to obtain the state variables at the half-step.

$$x_{s+1/2} = x_s + \frac{\Delta T}{2}\dot{x}_s \tag{3.43}$$

$$x_{s+1} = x_s + \Delta T\dot{x}_{s+1/2} \tag{3.44}$$

For many conditions, results from RK-2 are nearly identical to AM-2. However, the AM-2 works a little better at handling high-frequency vibrations (such as tire spin when braking to a stop), so the AM-2 is usually preferred. Because it does not use old calculated derivatives, RK-2 is less affected by discontinuous inputs, and might be preferable when dealing with sampled data in hardware in the loop systems or slope discontinuities in tables.

3.2.3.1.5 Adams-Bashforth 2nd Order Method

The Adams-Bashforth second-order method performs all calculations at the main time step ΔT, with no additional calculations.

$$x_{s+1} = x_s + \frac{\Delta T}{2}(3\dot{x}_s - \dot{x}_{s-1}) \tag{3.45}$$

This uses one old derivative to predict some curvature and provide better accuracy than Euler integration nearly all of the time. It provides the most consistent communication with other software (e.g., Simulink), with all variables always having the same accuracy. In contrast, the other methods are more accurate at the full step values than at the mid-step. When AB-2 is used, the time step ΔT should be cut roughly in half to obtain comparable accuracy relative to the other methods. This also results in comparable computational efficiency.

3.3 Structural modelling

In this section a detailed description of the system modelled is given, pointing the different bodies composing the vehicle, their respective degrees of freedom and their properties.

Along this work, two main different structural models have been designed: one considering rigid blades and other one considering elastic blades. Figure 3.11 is a representative image of the quadrotor's bodies spatial distribution and shows the parental structure used in the multibody system's definition explained in this section, considering blade i1 rigid and blade i2 elastic.

A quadrotor is usually composed by two equal arms in a cross, whose intersection hosts the batteries, the electronic control circuit, the IMU sensor and the devices needed for the adequate performance of the quadrotor. All these elements, the

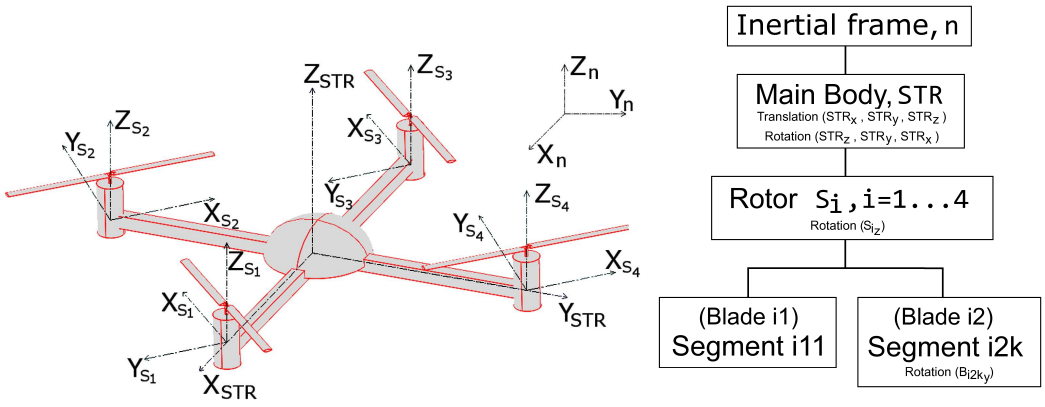

Figure 3.11: Left: Schematic sketch of quadrotor's bodies distribution and the structure's and rotors' associated axes for rigid blades. Right: Parent-child structure employed in the definition of the quadrotor as a multibody system, with blade i1 considered rigid and blade i2 considered elastic.

arms and the electronic devices, have been modelled in this work as a lumped rigid body, STR. The main body is defined at the inertial reference system, `n`, with six degrees of freedom with respect to it, with no restrictions, so STR's motion is only governed by the forces and moments' imbalance around the [X_{STR}, Y_{STR}, Z_{STR}] axes.

The code employed to generate the structure is included below:

```
(add-body str:name "structure"
              :parent n
              :joint-coordinates n0
              :cm-coordinates str0
              :mass Mstr
              :inertia-matrix (Ixstr Iystr Izstr)
              :inertia-matrix-coordinate-system str
              :body-rotation-axes (z y x)
              :reference-axis [nx]
              :translate (x y z))
```

One rotor is placed at the end of each arm, the model has a total of four rotors. Each rotor is identified by its name, S_i, and they are allowed one degree of freedom: rotation around their corresponding local Z axis, Z_{S_i}, i=1,...,4 .

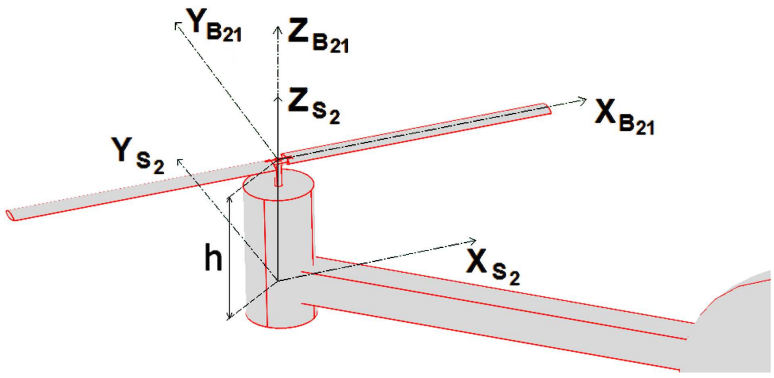

Figure 3.12: Sketch of rotor number 2, S_2, including rigid blades' distribution and associated axes.

```
(add-body Si:name "shafti"
            :parent str
            :joint-coordinates jcSi
            :cm-coordinates Si0
            :mass Ms
            :inertia-matrix (0 0 Jr)
            :inertia-matrix-coordinate-system Si
            :body-rotation-axes z
            :reference-axis [strx])
```

There are two opposite blades attached to each rotor i, B_{ij} j=1,2. For simplicity, untwisted blades are considered with a constant symmetric airfoil along the span. It leads to a constant structural angle of attack, α_s.

3.3.1 Rigid blades' model.

The different structural models developed start differing at this point. In the rigid structural model, the blades have been modelled as rigid single elements attached to the rotor. They have not been allowed any degree of freedom, so they spin with the rotor. The blades' layout and their associated axes are shown in Figure 3.12, and the describing code is as follows:

```
(add-body Bij:name "Bij"
              :parent Si
              :joint-coordinates (0 0 0)
              :cm-coordinates (cmb 0 0)
              :mass Mb
              :inertia-matrix (Ixb Iyb Izb)
              :inertia-matrix-coordinate-system Bij
              :no-rotation true)
```

3.3.2 Elastic blades' model.

Since the main purpose of this research is the vibrational study of the vehicle, elastic blades need to be considered as rotating elastic members are one of the main sources of vibrations in full scale rotorcrafts.

VehicleSim is a multibody rigid software and does not allow the modelling of elastic components in a straight forward manner. Therefore the blades have been discretized and given the flap degree of freedom only, since due to the short length of the blades, torsion and lag is less likely to occur. In order to assimilate the continuous body of the blade to the discretized model, a restoring moment will be applied to represent the material elastic and structural properties.

In order to obtain a behaviour of the discretized system similar to the continuous blade's case, first the continuous system needs to be fully described. To all effects, the blade will be represented by a pinned-free constant mass distribution and constant cross section area beam. Therefore, from classic beam theory [142], the static deflection of the beam subjected to a punctual force applied at the free tip will respond to expression (3.46), where P represents the load, R the length of the beam, E is the elastic modulus of the material, I is the second moment of inertia of the beam cross section, m is the mass of the blade, and the beam

natural frequencies of vibration will respond to the expression (3.47).

$$w_{tip} = \frac{PR^3}{3EI} \tag{3.46}$$

$$\omega_n = \alpha_n^2 \sqrt{\frac{EI}{mR^3}}, \quad \alpha_n = 1.875, 4.694, 7.885 \tag{3.47}$$

The previous equations describe the static behaviour of the beam; as for the dynamics, the beam will also present structural or hysteretic damping [143]. This damping is proportional to the square of the deflection amplitude and is generated by internal friction, local plastic deformation and plastic yielding. The energy dissipated by hysteretic damping can be equated to the energy dissipated by a viscous damping, obtaining a viscous damping equivalent to the hysteretic damping. This approximation is commonly used since viscous damping leads to a simple formulation of the equation of motion. The free beam's tip deflection when the equivalent viscous damping is considered responds to the expression (3.48), where λ can be found to be $2\pi\xi\omega_n$ [144].

$$w(t) = w_o \cos(\omega_n t) e^{-\lambda t} \tag{3.48}$$

w_o is the initial perturbation, ξ is the damping ratio, characteristic of the material, and ω_n is the beam's first natural frequency.

Now that the static and dynamic properties of an elastic beam have been introduced, the equivalent rigid discretized system and the derivation process of the modelling parameters to reproduce the behaviour of a continuous elastic blade will be explained.

The discretized blade model will consider rotational springs to reproduce the material elastic and vibrational behaviour and dampers to reproduce structural dissipation.

Starting with a single element discretization, as seen in Figure 3.13, the equilib-

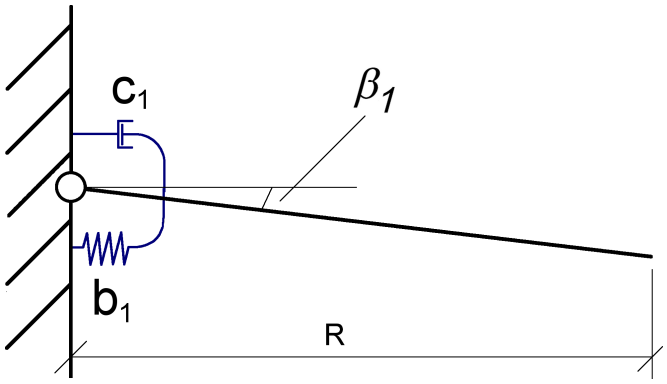

Figure 3.13: Representation of a blade discretization in a single element, with rotational spring for the elastic and vibrational characterization and damper for the dynamic characterization.

rium point when a force is applied to the tip responds to expression (3.49), so by equating the continuous system maximum deflection (3.46) and the discretized system (3.49), an equivalence between the elastic modulus and the rotational spring constant can be found (3.50).

$$w_{tip} = \frac{PR^2}{b} \tag{3.49}$$

$$b = \frac{3EI}{R} \tag{3.50}$$

This equivalent rotational spring constant, b, provides the same maximum deflection as a continuous beam subjected to the same load, and the same vibrational frequency. When considering the blade discretized in n segments - as shown in Figure 3.14 -, the relation between the torsional spring constants - assuming all have the same value - and the elasticity modulus of the material is as follows:

$$b(n) = \frac{3EI}{R}\left(\frac{1}{2} + \frac{1/2}{n}\right) \tag{3.51}$$

The previous expression allows to find the value of the torsional spring parameters for a blade discretized in n elements that reproduces the maximum deflection of a continuous elastic beam.

When the blade is discretized in more than one element, the relation between

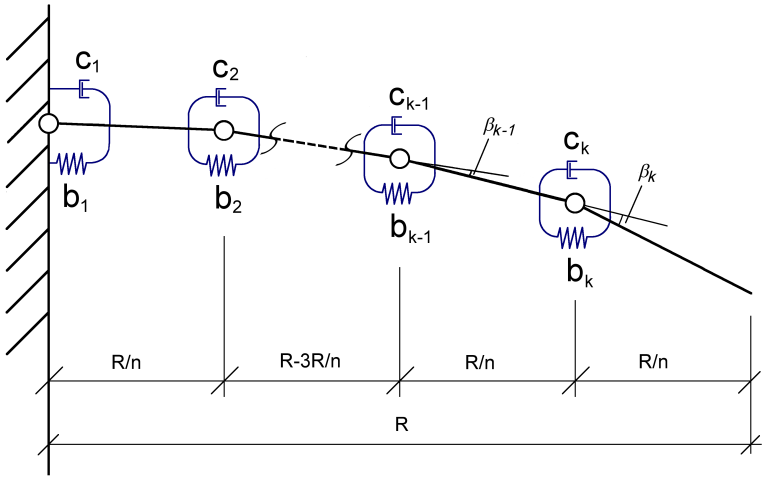

Figure 3.14: Blade discretization in n elements, with rotational spring as equivalent of the elastic properties and damper as equivalent of structural damping.

the damper parameters $c(n)$ and the hysteretic damping of the material, ξ, is not clear. Therefore, in order to obtain the equivalence between the constant damping parameters $c(n)$ and the structural damping of an specific material, the responses of the continuous system and the discretized system have been compared: the response of the discretized model is plotted together with the exponential component of the continuous system (3.48) varying the parameter $c(n)$ until the maximum displacements of the discretized system match the exponential curve of the continuous system. An example of the $c(n)$ damper parameter adjustment for the discretized blade can be found in Figure 3.15 for the case of a balsa wood blade, with elastic modulus $E = 4$ GPa and damping ratio $\xi = 0.03$.

This way, obtaining the spring constant $b(n)$ from (3.51) and the damper parameter $c(n)$ by adjusting the behaviour of the discretized beam, both the static and the dynamic behaviour of the elastic blade can be reproduced by the rigid discretized system.

For the modelling process in VehicleSim, the blade has been discretized in several segments and each segment has been given one rotational degree of freedom

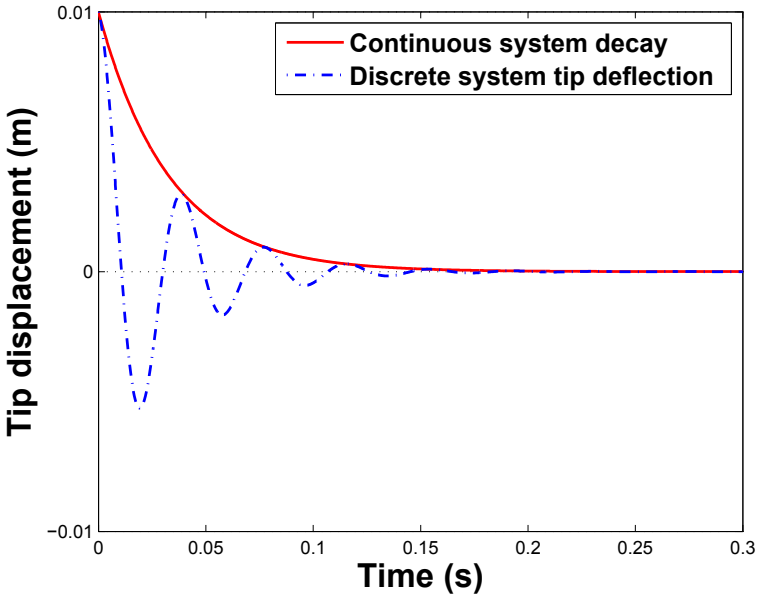

Figure 3.15: Adjusted dynamic displacement of the balsa wood discretized beam tip when initially disturbed (-·-) and expected decay of the continuous beam oscillations amplitude (—): $A_o e^{-2\pi\xi\omega_n t}$

around its Y axis, corresponding to their respective flap motion. Also, a restoring moment has been applied to each segment in order to represent the elasticity and the internal damping, which responds to expression (3.52), where β_{ijk} is the flap angle of the k$^{\text{th}}$ segment, k = 1...n, in blade j, rotor i.

$$M_{r_{ijk}} = b(n)\beta_{ijk} + c(n)\dot{\beta}_{ijk} \tag{3.52}$$

An example of the code implemented to describe the segments of the elastic blades and their respective restoring moments is shown below:

```
(add-body Bijk:name "Bijk"
              :parent Bij(k-1)
              :joint-coordinates ("R/n" 0 0)
              :cm-coordinates (cmbn 0 0)
              :mass Mbn
              :inertia-matrix (0 Iybn 0)
              :inertia-matrix-coordinate-system Bijk
              :body-rotation-axes y
              :reference-axis [Bij(k-1)z])
```

```
(add-moment Mrijk:name "Mijk"
                  :direction Bijky
                  :magnitude "@Mrijk"
                  :body1 Bijk
                  :body2 n)
```

3.4 Aerodynamic modelling

As it was explained in Section 3.1.1, the total aerodynamic load acting on a blade can be divided in two components: Lift force (L) and Drag force (D) or Thrust force (T) and Torque/Radius force (TQR). Different authors have modelled these forces in various ways: neglecting the translational velocity when compared to the rotational velocity [103], considering the Lift force of the blades to be applied at the shaft centre [82], modelling the Drag forces as a moment around the shaft axis [118], considering the variation of total Thrust in translational flight [48], considering blade flapping effects on Lift force and Drag forces [23], etc.

In this work, two aerodynamic models have been implemented in VS-Lisp. In this section both of them are described and the simulations' results carried out with these models will be presented in next chapters.

The first model consists on a simplified aerodynamic model which neglects the effect of the translational speed on the aerodynamic forces calculus. This model has been used for designing and testing the control system.

The second model is a more advanced one and considers the contribution of the quadrotor's translational speed to the aerodynamic forces' calculus. In the implementation of this complete model two submodels have been derived; the first one considers the aerodynamic forces calculated with the stationary representative point and applied at the stationary pressure centre and the second one calculates

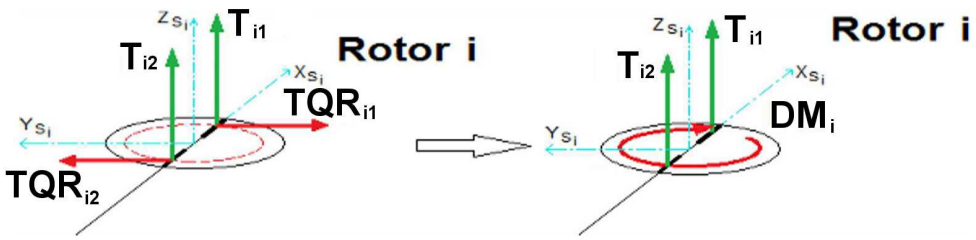

Figure 3.16: Equivalence between Torque/Radius forces, TQR_i, and Drag Moment, DM_i, acting on the rotor i.

the aerodynamic forces with the real representative point instead and applies them at the real pressure centre. The consequences of these considerations will be shown when the models are introduced.

It has been shown that there are different forms to express the aerodynamic forces. In this work both forms are used: the Lift and Drag forces form is calculated from the data provided by the *ai2*[1] and then, for computational convenience, these aerodynamic forces are transformed to the Thrust and Torque/Radius representation (3.53-3.54) and then applied to the vehicle's model.

$$T_{ij} = L_{ij} \cos \alpha_{in_{ij}} + D_{ij} \sin \alpha_{in_{ij}} \tag{3.53}$$

$$TQR_{ij} = D_{ij} \cos \alpha_{in_{ij}} - L_{ij} \sin \alpha_{in_{ij}} \tag{3.54}$$

For all the models here considered, the aerodynamic Torque/Radius forces have been modelled as their equivalent moment around the vertical axis of each of the rotors, as shown in Figure 3.16.

$$DM_i = \sum_{j=1}^{2} r_{cp_{ij}} TQR_{ij} \tag{3.55}$$

The Drag Moment reduces the rotational speed of the rotor and needs to be compensated in order to keep an adequate rotational velocity. This will be considered

[1]Instituto de Auntomática e Informática Industrial, Universidad Politécnica de Valencia, Spain.

in the control design process in Chapter 4.

The aerodynamic models developed are here explained for rigid blades case, and they will be further extended for the elastic blades case.

3.4.1 Aerodynamic forces as a function of the rotational speed.

The most common aerodynamic model for control purposes in quadrotors considers the aerodynamic forces as a function of the rotational speed and some fixed parameters, being the aerodynamic forces applied at the rotor centre. The simplest aerodynamic model developed here is similar to these models, used in this work in order to design the initial control system.

As seen in Section 3.1.2, Lift and Drag forces mainly depend on the Lift and Drag coefficients, C_L and C_D, the angle of attack, α, and the relative speed between the blade and the surrounding flow. Lift and Drag forces generated by the rotors have been modelled for non translational speed as follows:

$$L_{ij}(\alpha_{ij}) = \frac{1}{2}\rho_\infty S C_L(\alpha_{ij}) \left[r_{rep_0}\Omega_i\right]^2 \tag{3.56}$$

$$D_{ij}(\alpha_{ij}) = \frac{1}{2}\rho_\infty S C_D(\alpha_{ij}) \left[r_{rep_0}\Omega_i\right]^2 \tag{3.57}$$

Since this simple real model does not consider the translational speed in the aerodynamic forces calculus, the incident angle on attack, α_{in}, is zero. Therefore, in this case, Thrust matches the Lift force and Torque/Radius matches Drag force.

The Drag Moment in this model is given by:

$$DM_i(\alpha_{ij}) = \sum_{j=1}^{2} r_{cp_0} TQR_{ij}(\alpha_{ij}) \tag{3.58}$$

In the previous equations, r_{rep_0} is the position of the representative point of the blade j in stationary conditions and r_{cp_0} is the pressure centre of the blade j calculated in stationary conditions, their positions are calculated in Appendices A and C respectively.

The representative point is such a point that assuming its speed constant along the blade, a Lift force equal to a Lift force distribution is obtained and the pressure centre is the point in which the aerodynamic forces act.

The VS-Lisp code implemented to apply the aerodynamic forces in this model is presented below:

```
(add-line-force Tij:name "thrustij"
                    :direction [Siz]
                    :magnitude @Tij
                    :point1 cp0
                    :body1 Bij
                    :body2 n)


(add-moment DMi:name "DMi"
                :direction [Siz]
                :magnitude @DMi
                :body1 Si
                :body2 n)
```

The transformation between the different representations of the aerodynamic resultant force is the same for all the aerodynamic models:

```
(setsym   @Tij     "@Lij*cos(@alpha_ij) + @Dij*sin(@alpha_ij)")
          @TQRij   "@Dij*cos(@alpha_ij) - @Lij*sin(@alpha_ij)")
```

The aerodynamic forces and moments variables `@Lij`, `@Dij` and `@DMi` vary from

model to model, and for the simple aerodynamic model have been defined as:

```
(setsym   @Lij   "0.5*rho*(1-e)*R*chord*Cla*(alphas +
                 @alphai_ij))*(prep0*(ru(str,1) + ru(Si,1))^2))"
          @Dij   "0.5*rho*(1-e)*R*chord*@CDaij*(prep0*(ru(Si,1) +
                 ru(Si,1))^2)"
          @DMi   "cp0*@TQRi1 + cp0*@TQRi2")
```

Both the Lift and Drag forces are calculated considering the stationary values of the representative point, r_{rep_0}, and the pressure centre, r_{cp_0}. This provides a simpler model which has been used to implement the initial control system design.

3.4.2 Aerodynamic forces as a function of the rotational and translational speed.

Once the control system has been designed for the simple quadrotor's aerodynamic model and it has been validated, the aerodynamic model can be improved further and its complexity increases. In this section, the translational speed is also considered on the aerodynamic forces calculations.

Lift and Drag forces are now dependent on the translational speed as well:

$$L_{ij}(\alpha_{ij}) = \frac{1}{2}\rho_\infty S C_L(\alpha_{ij}) \left[V_{t_{ij}} + r_{rep_{ij}}\Omega_i\right]^2 \tag{3.59}$$

$$D_i(\alpha_{ij}) = \frac{1}{2}\rho_\infty S C_D(\alpha_{ij}) \left[V_{t_{ij}} + r_{rep_{ij}}\Omega_i\right]^2 \tag{3.60}$$

$V_{t_{ij}}$ is the relative speed between the airflow and the blade j caused by the translational displacement.

Two submodels based in this aerodynamic model have been derived, they differ on the choice of the representative point and the forces' application point:

3.4.2.1 Aerodynamic forces as a function of the rotational and translational speed applied at the blade's stationary pressure centre.

As mentioned in the theoretical introduction of the aerodynamic forces, the resultant aerodynamic force acts on the pressure centre of the blade, which is not a fixed point, it varies with the flight conditions. However, as a first approach, the aerodynamic forces are applied at the stationary pressure centre, r_{cp_0}, which actually is a fixed point.

This simplification is also applied to the calculus of these aerodynamic forces with the stationary representative point, r_{rep_0}, so the equations that represent the aerodynamic forces in this model, both of them applied at r_{cp_0} are as follows:

$$L_{ij}(\alpha_{ij}) = \frac{1}{2}\rho_\infty S C_L(\alpha_{ij}) \left[V_{t_{ij}} + r_{rep_0}\Omega_i\right]^2 \tag{3.61}$$

$$D_{ij}(\alpha_{ij}) = \frac{1}{2}\rho_\infty S C_D(\alpha_{ij}) \left[V_{t_{ij}} + r_{rep_0}\Omega_i\right]^2 \tag{3.62}$$

$$DM_i(\alpha_{ij}) = \sum_{j=1}^{2} r_{cp_0} TQR_{ij} \tag{3.63}$$

This increases the complexity of the modelling process, there are two main reasons for it:

i) For control systems validation purposes, the simple aerodynamic model is used: The individual effects of the variations from model to model can be characterized separately and the appropriate adjustments to the control system can be included if necessary.

ii) In order to obtain a model that considers the translational speed and also has a small computational load. Since the representative point and the pressure centre are not calculated at each simulation step (they have a constant value), the computational time of simulation is significantly reduced.

The code used to define the aerodynamic forces for this model can be found below.

```
(add-line-force Tij:name "thrustij"
                    :direction [Siz]
                    :magnitude @Tij
                    :point1 cp0
                    :body1 Bij
                    :body2 n)



(add-moment DMi:name "DMi"
                :direction [Siz]
                :magnitude @DMi
                :body1 Si
                :body2 n)



(setsym  @Lij   "0.5*rho*(1-e)*R*chord*Cla*(alphas +
                + @alphai_ij)*(@VBt_ij + prep0*(ru(str,1) +
                + ru(S1,1)))^2"
         @Dij   "0.5*rho*(1-e)*R*chord*@CDa_i1*(@VBt_ij +
                + prep0*ru(Si,1))^2"
         @DMi   "cp0*@TQRi1 + cp0*@TQRi2")
```

Since the application point of the aerodynamic forces in this model is the stationary pressure centre, the code for the application of the forces is the same as in the aerodynamic simple mode, which also considered the stationary pressure centre. However, the expressions of the Lift and Drag forces include more terms due to the consideration of the translational speed into the aerodynamic forces.

3.4.2.2 Aerodynamic forces as a function of the rotational and translational speed applied at the blade's pressure centre.

A further level of complexity can be added to the aerodynamic model, achieving in this way a more realistic model. It consists on the calculation of the Lift and Drag forces using the real representative point, $r_{rep_{ij}}$, applied at the dynamic pressure centres, $r_{cp_{ij}}$, which are no longer constant.

The equations that represent the Lift and Drag forces and moments for the complete aerodynamic model are:

$$L_{ij}(\alpha_{ij}) = \frac{1}{2}\rho_{\infty} S C_L(\alpha_{ij}) \left[V_{t_{ij}} + r_{rep_{ij}}\Omega_i\right]^2 \tag{3.64}$$

$$D_{ij}(\alpha_{ij}) = \frac{1}{2}\rho_{\infty} S C_D(\alpha_{ij}) \left[V_{t_{ij}} + r_{rep_{ij}}\Omega_i\right]^2 \tag{3.65}$$

$$DM_i(\alpha_{ij}) = \sum_{j=1}^{2} r_{cp_{ij}} TQR_{ij} \tag{3.66}$$

In this case, both Lift and Drag forces are applied at the aerodynamic pressure centre of each blade j, $r_{cp_{ij}}$, which varies at each simulation step, depending on the flying conditions.

The code used to define the aerodynamic forces for this model differs from the previous ones in the choice of the representative point, which in this case is `@prep_ij` instead of `prep0` and the application point of the aerodynamic forces, `@cp_ij` instead of `cp0`.:

```
(add-line-force Tij:name "thrustij"
                    :direction [Siz]
                    :magnitude @Tij
                    :point1 @cp_ij
                    :body1 Bij
                    :body2 n)
```

```
(add-moment DMi:name "DMi"
                :direction [Siz]
                :magnitude @DMi
                :body1 Si
                :body2 n)


(setsym  @Lij   "0.5*rho*(1-e)*R*chord*Cla*(alphas +
                + @alphai_ij)*(@VBt_ij + @prep_ij*(ru(str,1) +
                + ru(Si,1)))^2"
         @Dij   "0.5*rho*(1-e)*R*chord*@CDa_ij*(@VBt_ij +
                + @prep_ij* ru(Si,1))^2"
         @DMi   "@cp_i1*@TQRi1 + @cp_i2*@TQRi2")
```

3.4.3 Aerodynamic forces for elastic blades.

In the previous sections the different aerodynamic models developed during this research have been considered to be applied to rigid blades. In order to simulate a flexible blade, which is a more realistic case, the blade is discretized in more than one segment, the aerodynamic forces now need to be calculated for each of these segments and applied at their respective pressure centres.

The Thrust forces for the elastic discretized case are applied at the pressure centre of each segment and perpendicular to each of the discrete surfaces, as shown in Figure 3.17. Clearly now not only the magnitude of the force is variable, but also its direction.

For the sake of clarity, only the equations for the complete aerodynamic model have been included in here, being possible to obtain the equations for the other models by applying the pertinent simplifications. Assuming constant lift and drag coefficients along the span, the Lift and Drag forces for each segment have the expressions:

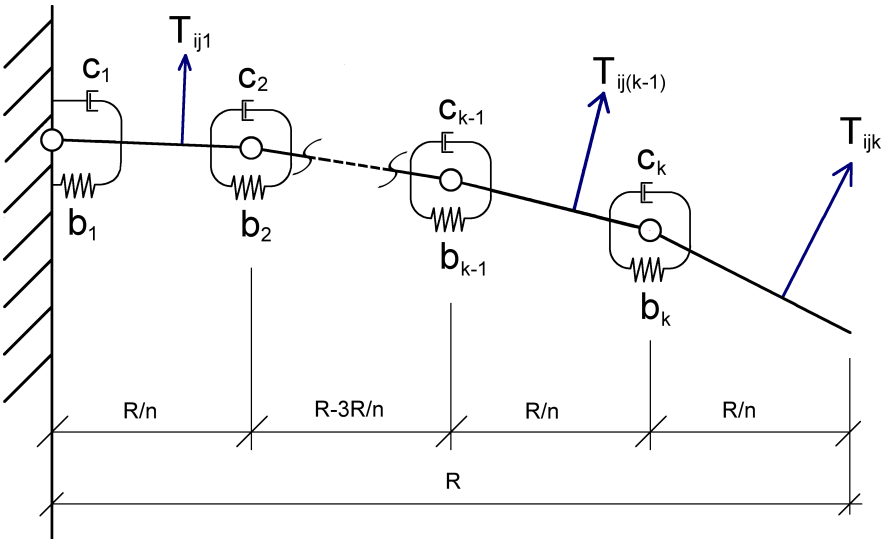

Figure 3.17: Thrust forces are applied perpendicular to each segment surface for elastic blades modelling.

$$L_{ijk}(\alpha_{ij}) = \frac{1}{2}\rho_{\infty} S_k C_L(\alpha_{ij}) \left[V_{t_{ij}} + r_{rep_{ijk}}\Omega_i\right]^2 \tag{3.67}$$

$$D_{ijk}(\alpha_{ij}) = \frac{1}{2}\rho_{\infty} S_k C_D(\alpha_{ij}) \left[V_{t_{ij}} + r_{rep_{ijk}}\Omega_i\right]^2 \tag{3.68}$$

For this structural model, the Drag Moment acting on each rotor is composed by $2n$ elements, one corresponding to each blade's segment:

$$DM_i(\alpha_{ij}) = \sum_{j=1}^{2}\left(\sum_{k=1}^{n} r_{cp_{ijk}} TQR_{ijk}\right) \tag{3.69}$$

S_k is the representative surface of segment k, $r_{rep_{ijk}}$ is the representative point of segment k in blade j, and the forces are applied at the pressure centre of the each segment, $r_{cp_{ijk}}$.

The calculus of the representative point and pressure centre positions of each segment can be found in Appendices B and D respectively.

The code used to define and apply the aerodynamics forces and moments is more

complicated in this case:

```
(add-line-force Tijk   :name "thrustijk"
                       :direction [Bijkz]
                       :magnitude @Tijk
                       :point1 @cp_ijk
                       :body1 Bijk
                       :body2 n)


(add-moment DMi   :name "DMi"
                  :direction [Siz]
                  :magnitude @DMi
                  :body1 Si
                  :body2 n)


(setsym  @Lijk   "0.5*rho*chord*(x_k-x_k-1)*R*Cla*(alphas +
                 + @alphai_ij)*(@VBt_ij + @prep_ijk*(ru(str,1) +
                 + ru(Si,1)))^2"
         @Dijk   "0.5*rho*chord*(x_k-x_k-1)*R*@CDa_ij*(@VBt_ij +
                 + @prep_ijk*(ru(str,1) +ru(Si,1)))^2"
         @DMi   "@cp_i11*@Di11 + @cp_i21*@Di21 +
                 ...
                 + @cp_i1(k-1)*@Di1(k-1) + @cp_i2(k-1)*@Di2(k-1) +
                 + @cp_i1k*@Di1k + @cp_i2k*@Di2k")
```

The code is similar to the most complete aerodynamic rigid case, but now there are n Lift and Drag forces to apply instead of one for each blade and the Drag moments have $2n$ components.

3.4.4 Obtaining the aerodynamic parameters

Regarding the equations given previously (3.56)-(3.69), which describe the aerodynamic forces modelled, there are two parameters whose values have not been determined yet. These parameters are the profile Drag Coefficient, c_d, and the slope of the Lift Coefficient-Angle of Attack curve, C_{L_α}. For this work purposes, these parameters have been deduced from available quadrotor data property of *ai2*.

According to the data provided by *ai2*, the Lift force and Drag moment have been obtained experimentally for non translational speed, which implies a fixed angle of attack ($\alpha = \alpha_s$), and have been modelled by

$$L = a_1 \Omega^2 \tag{3.70}$$

$$DM = a_2 \Omega^2 \tag{3.71}$$

The value of the parameters a_1 and a_2 from equations (3.70) and (3.71) is registered on Table 3.3. Remembering the expressions of the Lift force and Drag

Table 3.3: Aerodynamic parameters of quadrotor courtesy of *ai2*

Parameter	Value	Units
a_1	$3,13 \cdot 10^{-5}$	Ns^2
a_2	$7,5 \cdot 10^{-7}$	Nms^2

Moment for hover conditions, when the Thrust matches the Lift force and the Torque/Radius matches the Drag force:

$$L = \frac{1}{2} \rho_\infty S C_L V_\infty^2$$

$$DM = \sum_{j=1}^{2} r_{cp_j} D_j$$

These equations can be particularized for the non translational speed case as:

$$L = \frac{1}{2}\rho_\infty S C_L (r_{rep_0}\Omega)^2 \tag{3.72}$$

$$DM = \frac{1}{2}\rho_\infty S C_D 2 r_{cp_0} (r_{rep_0}\Omega)^2 \tag{3.73}$$

Taking into account the non translational speed condition and the symmetrical airfoil assumption, the expressions for C_L and C_D become:

$$C_L = \cancelto{0}{C_{L_0}} + C_{L_\alpha}(\alpha_s + \cancelto{0}{\alpha_{in}}) \tag{3.74}$$

$$C_D = c_d + kC_L^2 = c_d + k\left(\cancelto{0}{C_{L_0}} + C_{L_\alpha}\left(\alpha_s + \cancelto{0}{\alpha_{in}}\right)\right)^2 \tag{3.75}$$

Substituting these expressions of C_L and C_D in equations (3.72) and (3.73) respectively yields:

$$L = \frac{1}{2}\rho_\infty S r_{rep_0}^2 (C_{L_\alpha}\alpha_s)\Omega^2 \tag{3.76}$$

$$DM = \frac{1}{2}\rho_\infty S 2 r_{cp_0} r_{rep_0}^2 \left[c_d + k\left(C_{L_\alpha}\alpha_s\right)^2\right]\Omega^2 \tag{3.77}$$

By equating previous expressions, (3.76) and (3.77), with equations (3.70) and (3.71) respectively, the values of the parameters C_{L_α} and c_d can be obtained.

$$C_{L_\alpha} = \frac{a_1}{\frac{1}{2}\rho_\infty S r_{rep_0}^2 \alpha_s} \tag{3.78}$$

$$c_d = \frac{a_2}{\frac{1}{2}\rho_\infty S r_{rep_0}^2 r_{cp_0}} - k\left(C_{L_\alpha}\alpha_s\right)^2 \tag{3.79}$$

Is with these values of the aerodynamic parameters C_{L_α} and c_d that the rest of the study has been carried out.

3.5 Summary of the chapter

In this chapter a general description of the quadrotor layout and operation is given, pointing out and describing the motions allowed and the different reference systems used in the quadrotors guidance. A basic but clear description on quadrotor behaviour and functioning has been presented with the objective of clarifying the main controls involved in the vehicle's guidance. Also an overview of the basic expressions for the aerodynamic forces has been given.

The dynamic modelling software has been presented, showing its interaction with other softwares also used in this work, as Simulink. Its principal features are listed: representation of complex systems through the multibody methodology; the possibility of interaction with other softwares when simulating; obtaining the space-state representation of the model and derivation of lineal and nonlinear equations motion, as desired, which is needed for the robust control design process. The methodology used for obtaining the motion equations has been outlined and a review of the integration methods included in the software has been given.

The structural layout and properties of the bodies comprising the quadrotor have been given, both for rigid blades and elastic blades models, as well as the VS-Lisp code used to model these bodies. The equivalence between the discretized elastic blade and the continuous elastic blade model has been found, making possible the reproduction of the continuous blade static and dynamic characterization.

The different aerodynamic models developed have been presented: the first one, a simplified model, neglects the effect of the translational speed in the aerodynamic forces; the second model takes into account the translational speed in the calculus of the aerodynamic forces, but not in the calculus of the representative point and pressure centre; and the complete model that considers the effect of the translational speed in both, the aerodynamic forces and the position of the points considered.

Also, the VS-Lisp code for the definition and application of the aerodynamic forces and moments is shown for the different structural and aerodynamic models, and the derivation of the aerodynamic coefficients necessary to define the rotors' aerodynamic behaviour has been obtained from experimental data of the same quadrotor described earlier in the chapter, courtesy of *ai2*.

Chapter 4

Control system

This chapter presents the control system used to stabilize and guide the vehicle through predefined trajectories. The vehicle's nonlinear equations of motion are presented, and their controllability analysed. Also the Counter Drag Moment is introduced, as well as the maximum torque and total control actions needed for the quadrotor to follow different trajectories.

The control system design and implementation has been carried out with the Simulink platform [145]. This software is widely used both in modelling (electrical devices [146], electronic devices [147, 148], and mechanical devices [149]) and in control (design and simulation [150] and in real-time control [151]). It is also used in sensors and predictors implementation [152]. Besides, the interaction between the control system implemented in Simulink and the VehicleSim's dynamic model is available in real-time, being this a very good advantage for the simulations.

4.1 Analysis of the nonlinear mathematical model

The software VS-Lisp generates three different output files, one of them is a text file containing the symbolic nonlinear equations that describe the motion

of the multibody system described. From this file, the motion equations have been obtained and written according to the terminology used in this work. These equations represent the rigid blades and aerodynamic complete model, and could be simplified to match the simplifications considered in the other aerodynamic models.

$$\begin{aligned}\ddot{X} = {} & g\sin\phi + \dot{\psi}\dot{Y} - \dot{\theta}\dot{Z} \\ & + \frac{8hM_b\left[I_{x_{STR}} - I_{y_{STR}} - I_{z_{STR}} - J_r - 4d^2\left(M_s + 2M_b\right)\right]\dot{\phi}\dot{\psi}}{I'_y} \\ & + \frac{8hM_b\left[d\left(T_{11} + T_{12} - T_{31} - T_{32}\right) + \sum_{i=1}^{4}\left(cp_{i1}T_{i1} - cp_{i2}T_{i2}\right)\cos\gamma_i\right]\dot{\phi}\dot{\psi}}{I'_y} \\ & - \frac{TD_x\left(I_{y_{STR}} + 4d^2M_b + 2d^2M_s + 8h^2M_b\right)}{I'_y}\end{aligned} \tag{4.1}$$

$$\begin{aligned}\ddot{Y} = {} & -g\sin\theta\cos\phi - \dot{\psi}\dot{X} + \dot{\phi}\dot{Z} \\ & - \frac{8hM_b\left[I_{x_{STR}} - I_{y_{STR}} + I_{z_{STR}} + J_r - 4d^2\left(M_s + 2M_b\right)\right]\dot{\theta}\dot{\psi}}{I'_x} \\ & + \frac{8hM_b\left[d\left(T_{21} + T_{22} - T_{41} - T_{42}\right) - \sum_{i=1}^{4}\left(cp_{i1}T_{i1} - cp_{i2}T_{i2}\right)\sin\gamma_i\right]\dot{\theta}\dot{\psi}}{I'_x} \\ & - \frac{TD_y\left(I_{x_{STR}} + 4d^2M_b + 2d^2M_s + 8h^2M_b\right)}{I'_x}\end{aligned} \tag{4.2}$$

$$\ddot{Z} = -g\cos\theta\cos\phi - \dot{\phi}\dot{Y} + \dot{\theta}\dot{X} + \frac{\mathbf{T} + 8hM_b\left(\dot{\theta}^2 + \dot{\phi}^2\right) - TD_z}{M_t} \tag{4.3}$$

$$\begin{aligned}\ddot{\phi} = {} & \frac{d\left(T_{41} + T_{42} - T_{21} - T_{22}\right) + \sum_{i=1}^{4}\left(cp_{i1}T_{i1} - cp_{i2}T_{i2}\right)\sin\gamma_i}{I''_x} \\ & - \frac{\left(I_{z_{STR}} - I_{y_{STR}}\right)\dot{\theta}\dot{\psi} + J_r\mathbf{\Omega}\dot{\theta}}{I''_x} - \frac{2d^2M_s\left(M_{STR} + M_s\right)}{I''_xM_t} \\ & - \frac{\left[4M_b\left(8d^2\left(M_b + M_s\right) - 2h^2\left(M_{STR} + 4M_s\right) + d^2M_{STR}\right)\right]\dot{\theta}\dot{\psi}}{I''_xM_t} \\ & + \frac{8hM_bTD_y}{I''_xM_t}\end{aligned} \tag{4.4}$$

$$\ddot{\theta} = \frac{d\left(T_{31} + T_{32} - T_{11} - T_{12}\right) - \sum_{i=1}^{4}\left(cp_{i1}T_{i1} - cp_{i2}T_{i2}\right)\cos\gamma_i}{I''_y} + \frac{\left(I_{z_{STR}} - I_{x_{STR}}\right)\dot{\phi}\dot{\psi} + J_r\mathbf{\Omega}\dot{\phi}}{I''_y} + \frac{\left[2d^2M_s\left(M_{STR} + 4M_s\right)\right]\dot{\phi}\dot{\psi}}{I''_yM_t} + \frac{\left[4M_b\left(8d^2\left(M_b + M_s\right) - 2h^2\left(M_{STR} + 4M_s\right) + d^2M_{STR}\right)\right]\dot{\phi}\dot{\psi}}{I''_yM_t} - \frac{8hM_bTD_x}{I''_yM_t} \tag{4.5}$$

$$\ddot{\psi} = \frac{\left[\left(I_{x_{STR}} - I_{y_{STR}}\right)\dot{\theta}\dot{\phi} - \sum_{i=1}^{4} CM_i\right]}{I''_z} \tag{4.6}$$

$$\ddot{\Omega}_1 = \frac{-CM_1 + DM_1}{J_r} \tag{4.7}$$

$$\ddot{\Omega}_2 = \frac{-CM_2 - DM_2}{J_r} \tag{4.8}$$

$$\ddot{\Omega}_3 = \frac{-CM_3 + DM_3}{J_r} \tag{4.9}$$

$$\ddot{\Omega}_4 = \frac{-CM_4 - DM_4}{J_r} \tag{4.10}$$

The parameter g represents the value of the gravity, the parameter γ_i represents the angular position of the first blade in the rotor plane and the parameters M_{STR}, M_s, M_b, M_t, $I_{x_{STR}}$, $I_{y_{STR}}$, $I_{z_{STR}}$, J_r, d and h correspond to the quadrotor property of *ai2* and have been defined in Table 4.1, which includes the rigid modelling parameters employed along this work. $\mathbf{T}$ and $\mathbf{\Omega}$ represent the sum of the Thrust forces and rotational speeds respectively, $\sum_{i=1}^{4}\sum_{j=1}^{2} T_{ij}$ and $\sum_{i=1}^{4}|\Omega_i|$, CM_i and DM_i represent the Control Moment and Drag Moment of the i$^{\text{th}}$ rotor respectively, and $TD_{x,y,z}$ represents the vehicle's translational drag in the $\mathtt{X_{STR}}$, $\mathtt{Y_{STR}}$ and $\mathtt{Z_{STR}}$ directions respectively. The terms I'_x, I'_y, I''_x, I''_y and I''_z respond to expressions (4.11-4.15).

$$I'_x = I_{x_{STR}} M_t + 2d^2 M_r \left(M_{STR} + 4M_s\right)$$
$$4M_b \left[8d^2 \left(M_b + M_s\right) + 2h^2 \left(M_{STR} + 4M_s\right) + d^2 M_{STR}\right] \tag{4.11}$$

$$I'_y = I_{y_{STR}} M_t + 2d^2 M_s \left(M_{STR} + 4M_s\right)$$
$$4M_b \left[8d^2 \left(M_b + M_s\right) + 2h^2 \left(M_{STR} + 4M_s\right) + d^2 M_{STR}\right] \tag{4.12}$$

$$I''_x = I_{x_{STR}} + 8h^2 M_b + d^2(2M_s + 4M_b) - \frac{64h^2 M_b^2}{M_t} \tag{4.13}$$

$$I''_y = I_{y_{STR}} + 8h^2 M_b + d^2(2M_s + 4M_b) - \frac{64h^2 M_b^2}{M_t} \tag{4.14}$$

$$I''_z = I_{z_{STR}} + d^2(4M_s + 8M_b) \tag{4.15}$$

cp_{ij} represents the application point of the Thrust force T_{ij} on the blade ij, which varies with the aerodynamic model considered.

- On the simple aerodynamic model, which considers the forces only as a function of the rotational speed, the application points for all the blades are their stationary pressure centre r_{cp_0}. Since the Thrust force produced by the two blades of each rotor have the same magnitude, the terms considering the pressure centre and the Thrust forces are cancelled.
- For the second aerodynamic model, that considers the translational speed in the calculus of the aerodynamic forces, the application point is also the stationary pressure centre which has a fixed value, r_{cp_0}. However, the Thrust force produced by the blades on each rotor do not have the same magnitude, therefore, the previous term is not cancelled in this model.
- Finally, the more complete aerodynamic model considers the real pressure centre, calculated considering the flight conditions at every simulation step, so every cp_{ij} have a different numeric value.

Table 4.1: Parameters values for the system's bodies in VS-Lisp.

Parameter	Symbol	Value	Units
Structure Mass	$\mathtt{M_{STR}}$	0.750	Kg
STR inertia around $\mathtt{X_{STR}}$ axe	$\mathtt{I_{x_{STR}}}$	0.0081	Nms^2
STR inertia around $\mathtt{Y_{STR}}$ axe	$\mathtt{I_{y_{STR}}}$	0.0081	Nms^2
STR inertia around $\mathtt{Z_{STR}}$ axe	$\mathtt{I_{z_{STR}}}$	0.0016	Nms^2
Rotor Mass	$\mathtt{M_s}$	0.035	Kg
$\mathtt{S}_i$ rotational inertia around $\mathtt{Z_{S_i}}$ axe	$\mathtt{J_r}$	0.00006	Nms^2
Blade Mass	$\mathtt{M_b}$	0.006	Kg
Total Mass	$\mathtt{M_t}$	0.906	Kg
Blade Lenght	R	0.105	m
Blade Offset	e	0.05	-
Distance between $\mathtt{STR}_0$ and $\mathtt{S}_{i_0}$	d	0.3	m
Distance between $\mathtt{B}_{ij_0}$ and $\mathtt{S}_{i_0}$	h	0.0	m

Equations (4.1-4.3) correspond to the linear acceleration of the structure's centre along $\mathtt{X_n}$, $\mathtt{Y_n}$ and $\mathtt{Z_n}$ expressed in the body-based reference system. Equations (4.4-4.6) are the angular accelerations around $\mathtt{X_{STR}}$, $\mathtt{Y_{STR}}$ and $\mathtt{Z_{STR}}$ respectively and (4.7-4.10) are the angular accelerations of the rotor shafts.

This nonlinear model, obtained using VehicleSim modelling, is similar to the one obtained by [90] when the position of the vehicle's centre of gravity matches the centre of the structure and the rotors gyroscopic effect is not considered. Also [119] obtained a model quite similar to the one obtained here that includes the rotor gyroscopic effect and the drag due to the vehicle's motion. However, none of these models consider the effect of having the aerodynamic forces applied at the blade's pressure centre, represented by the terms $cp_{ij}T_{ij}$ in equations (4.1-4.10).

4.2 Controllability of the platform

Before attempting the control system design, a controllability test has been carried out on the nonlinear equations of motion. In this section, the basics of

nonlinear systems controllability will be introduced and the results of the test will be discussed. Let's first introduce some needed concepts:

Let $X \subset \mathbb{R}^n$, and let f and g be vector fields on X. The *Lie bracket* of f and g is another vector field on X defined as follows:

$$[f,g](x) = \frac{\partial g}{\partial x}(x)f(x) - \frac{\partial f}{\partial x}(x)g(x), \tag{4.16}$$

where $\partial f/\partial x$ and $\partial g/\partial x$ denote the Jacobi matrices of f and g [153]. Also, higher order *Lie brackets* can be defined:

$$\begin{gathered}
\left(ad_f^1, g\right)(x) \equiv [f,g](x) \\
\left(ad_f^2, g\right)(x) \equiv [f,[f,g]](x) \\
\cdots \\
\left(ad_f^k, g\right)(x) \equiv \left[f, \left(ad_f^{k-1}, g\right)\right](x)
\end{gathered}$$

Now that the *Lie bracket* has been introduced, the controllability condition of a nonlinear system can be determined.

Take the nonlinear equations of a system where x is a vector of n states and u is a m-dimensional input vector.

$$\dot{x} = f(x,u) \tag{4.17}$$

Assuming that the vector field, f, is affine in the control, the nonlinear system can be rewritten as:

$$\dot{x} = f_0(x) + \sum_{i=1}^{m} u_i f_i(x) \tag{4.18}$$

with $f_0(0) = 0$, such that $(\hat{x}, \hat{u}) = (0,0)$ is an equilibrium point.

If the nonlinear equations of the system can be written as in 4.18, it is possible to say that the system is locally controllable if it satisfies the rank condition established in the following theorem [154].

Theorem 4.2.1 *A necessary condition for the system*

$$\dot{x} = f_0(x) + \sum_{i=1}^{m} u_i f_i(x)$$

with $f_0(0) = 0$*, to be locally controllable around the origin is that the Lie algebra* $Lie\{f_0, ..., f_m\}$ *satisfies the condition*

$$rank\left(Lie\{f_0, ...f_m\}(x)\right) = n, \forall x \in U \tag{4.19}$$

where U *is a neighborhood of the origin and* $Lie\{f_0, ..., f_m\}$ *is the Lie algebra generated by the linear combinations of* $f_0, ..., f_m$ *and all their Lie brackets.*

In order to express the equations of the quadrotor motion as in 4.18, a change of variable is necessary; the state variable Ω_i, rotational speed of the i$^{\text{th}}$ rotor shaft, will now be $\overline{\Omega}_i$ and $\ddot{Z}$ will be $\overline{\ddot{Z}}$, as in (4.20) and (4.21) respectively.

$$\overline{\Omega}_i = \Omega_i - \Omega_0 \tag{4.20}$$

$$\overline{\ddot{Z}} = \ddot{Z} + g = g - g\cos\theta\cos\phi - \dot{\phi}\dot{Y} + \dot{\theta}\dot{X} + \frac{\mathbf{T} + 8hM_b\left(\dot{\theta}^2 + \dot{\phi}^2\right) - TD_z}{M_t} \tag{4.21}$$

This way, equations (4.1-4.10) can be expressed as (4.18) and $f_0(0) = 0$, being this an equilibrium point, known as hover.

Assuming the simple model for the aerodynamic forces (3.4.1) and transforming the second order differential equations to first order differential equations, the equations of the quadrotor system can be expressed as :

$$\dot{\overline{x}} = f(\overline{x}) + \sum_{i=1}^{4} f_i(\overline{x})\, CM_i \tag{4.22}$$

The vector $\overline{x}$ and the vector fields f_0, f_1, f_2, f_3 and f_4 have the form as in (4.23-4.28), where the parameters δ englobe the terms multiplying the state variables

in the equations of motion.

$$\overline{x}^T = \{x_1, ..., \overline{x}_{20}\} = \{X, \dot{X}, Y, \dot{Y}, Z, \dot{Z}, \theta, \dot{\theta}, \phi, \dot{\phi}, \psi, \dot{\psi}, \gamma_1, \overline{\Omega}_1, \gamma_2, \overline{\Omega}_2, \gamma_3, \overline{\Omega}_3, \gamma_4, \overline{\Omega}_4\} \tag{4.23}$$

$$f_0 = \left\{ \begin{array}{c} x_2 \\ g\sin(x_9) + x_{12}x_4 - x_8x_6 + \delta_1 x_{10}x_{12} \\ +\delta_2 x_{10}x_{12}(\overline{x}_{14}^2 - \overline{x}_{18}^2) - \delta_3 x_2 \\ x_4 \\ -g\sin(x_7)\cos(x_9) - x_2x_{12} + x_6x_{10} \\ -\delta_4 x_8x_{12} + \delta_5 x_8x_{12}(\overline{x}_{16}^2 - \overline{x}_{20}^2) - \delta_6 x_4 \\ x_6 \\ g - g\cos(x_7)\cos(x_9) - x_4x_{10} + x_2x_8 \\ +\delta_7(\overline{x}_{14}^2 + \overline{x}_{16}^2 + \overline{x}_{18}^2 + \overline{x}_{20}^2) + \delta_8(x_8^2 + x_{10}^2) - \delta_9 x_6 \\ x_8 \\ \delta_{10}(\overline{x}_{18}^2 - \overline{x}_{14}^2) + \delta_{11}x_{10}x_{12} \\ -\delta_{12}x_{10}(\overline{x}_{14} + \overline{x}_{16} + \overline{x}_{18} + \overline{x}_{20}) - \delta_{13}x2 \\ x_{10} \\ \delta_{14}(\overline{x}_{20}^2 - \overline{x}_{16}^2) + \delta_{15}x_8x_{12} \\ +\delta_{16}x_8(\overline{x}_{14} + \overline{x}_{16} + \overline{x}_{18} + \overline{x}_{20}) - \delta_{17}x_4 \\ x_{12} \\ \delta_{18}x_8x_{10} \\ \overline{x}_{14} \\ \delta_{19}\overline{x}_{14}^2 \\ \overline{x}_{16} \\ -\delta_{20}\overline{x}_{16}^2 \\ \overline{x}_{18} \\ \delta_{21}\overline{x}_{18}^2 \\ \overline{x}_{20} \\ -\delta_{22}\overline{x}_{20}^2 \end{array} \right\} \tag{4.24}$$

$$f_1^T = \{0,0,0,0,0,0,0,0,0,0,0,0,-\frac{1}{I_z''},0,-\frac{1}{J_r},0,0,0,0,0,0\} \tag{4.25}$$

$$f_2^T = \{0,0,0,0,0,0,0,0,0,0,0,0,-\frac{1}{I_z''},0,0,0,-\frac{1}{J_r},0,0,0,0\} \tag{4.26}$$

$$f_3^T = \{0,0,0,0,0,0,0,0,0,0,0,0,-\frac{1}{I_z''},0,0,0,0,0,-\frac{1}{J_r},0,0\} \tag{4.27}$$

$$f_4^T = \{0,0,0,0,0,0,0,0,0,0,0,0,-\frac{1}{I_z''},0,0,0,0,0,0,0,-\frac{1}{J_r}\} \tag{4.28}$$

With the equations of motion now described as a nonlinear affine in control system, its *Lie bracket* algebra, also called accessibility distribution C, is constructed:

$$C = \left[f_0, f_1, ...f_4, [f_0, f_i], ..., \left[ad_{f_0}^k, f_i\right], ..., [f_4, f_i], ..., \left[ad_{f_4}^k, f_i\right], ..\right] \tag{4.29}$$

The accessibility distribution matrix has been constructed with the *Lie brackets* of the system up to order 4 ($k = 4$), obtaining that the rank of the matrix is 20, which is the number of states. Therefore, the nonlinear equations that represent the system of the quadrotor are locally controllable around hover.

If the translations along the linear axes are carried out at low speed, the roll and pitch angles and rates are small and can be considered as perturbations around hover. Therefore, the system is also locally controllable for smooth trajectories and slow translations.

4.3 Control method

Once the system has been proven to be controllable, next the control system is designed. Quadrotor's control is achieved by varying the rotational speed of the rotors since the aerodynamic forces depend on the blades' squared speed and the rotation is the main contribution to this velocity. In order to modify the rotor's rotational speed, a moment needs to be applied from the structure. This torque

varies the angular acceleration, increasing or decreasing in this way, the rotational speed of the rotors.

To simplify the control design process, the rigid simple aerodynamic model with aerodynamic forces as function of rotational speed (Section 3.4.1) has been used and afterwards, once the control method has been designed, it has been applied to the system when the more complex aerodynamic models were implemented: the rigid complete model (Section 3.4.2) and the elastic complete model (Section 3.4.3). In this case, it will be shown in the simulations section that the control strategy works well.

4.3.1 Description of the algorithm

The control method designed to stabilize and control the quadrotor's trajectory is a PVA method (Position-Velocity-Acceleration) which consists on the feedback of a control action proportional to the position error, $e_p(t)$, the velocity error, $e_v(t)$, and the acceleration error, $e_a(t)$, as shown in (4.30).

$$U = \left\{ \begin{array}{ccc} K_1 & K_2 & K_3 \end{array} \right\} \left\{ \begin{array}{ccc} e_p(t) & e_v(t) & e_a(t) \end{array} \right\}^T \tag{4.30}$$

This method has been chosen from a large choice of options due to two main reasons:

i. This particular method is widely used for the control of positioning devices in which the overshoot needs to be suppressed [155]. It has also been used recently as a base for a quadrotor's control implementation with experimental results that validate the use of this method [79].

ii. One of the most interesting features of this method is the low computational load it represents, which is considerably lower than other more sofisticated methods. It translates in a faster control process.

The control actions required to achieve quadrotor's adequate manoeuvring are the moments the electrical motors generate and apply to each rotor. Those moments have different components that depend on the variable they are intending to modify:

- Height control, $Z_{STR}(t)$. The moments applied to each rotor for height control have the same magnitude, therefore, they produce the same angular speed variation at each of the four rotors and consequently, the same Thrust variation. The only special consideration to be made is the different direction of rotation of the rotors; moments applied to rotors 1 and 3 are positive and moments applied to rotors 2 and 4 are negative to increase the rotational speed.

$$(CM_i)_z = (-1)^{i+1}\left[(k_1)_z\left(Z^{ref}_{STR}(t) - Z_{STR}(t)\right) + (k_2)_z\left(\dot{Z}^{ref}_{STR}(t) - \dot{Z}_{STR}(t)\right) + (k_3)_z\left(\ddot{Z}^{ref}_{STR}(t) - \ddot{Z}_{STR}(t)\right)\right] \tag{4.31}$$

- Roll control, $\phi_{STR}(t)$. The control moments for roll control are only applied to rotors 2 and 4 since this degree of freedom is mainly governed by these two rotors.

$$(CM_2)_\phi = (k_1)_\phi\left(\phi^{ref}_{STR}(t) - \phi_{STR}(t)\right) + \left(k_2)_\phi(\dot{\phi}^{ref}_{STR}(t) - \dot{\phi}_{STR}(t)\right) + \left(k_3)_\phi(\ddot{\phi}^{ref}_{STR}(t) - \ddot{\phi}_{STR}(t)\right) \tag{4.32}$$

$$(CM_4)_\phi = -\frac{|\Omega_2|}{\sqrt{\frac{mg}{2a_1} - (\Omega_2)^2}}(CM_2)_\phi \tag{4.33}$$

- Pitch control, $\theta_{STR}(t)$. Similarly to the roll control, the pitch dynamics are mainly governed by two rotors; therefore, pitch control moments are applied to rotors 1 and 3.

$$(CM_3)_\theta = (k_1)_\theta \left(\theta^{ref}_{STR}(t) - \theta_{STR}(t)\right) + (k_2)_\theta \left(\dot{\theta}^{ref}_{STR}(t) - \dot{\theta}_{STR}(t)\right) + (k_3)_\theta \left(\ddot{\theta}^{ref}_{STR}(t) - \ddot{\theta}_{STR}(t)\right) \quad (4.34)$$

$$(CM_1)_\theta = -\frac{|\Omega_3|}{\sqrt{\frac{mg}{2a_1} - (\Omega_3)^2}}(CM_3)_\theta \quad (4.35)$$

- Yaw control, $\psi_{STR}(t)$. In order to keep constant the moments balance around $\mathtt{X_{STR}}$ and $\mathtt{Y_{STR}}$ axes constant, the moments applied to opposite rotors have equal magnitude; and therefore, roll and pitch moments are cancelled.

$$(CM_{1,3})_\psi = (k_1)_\psi \left(\psi^{ref}_{STR}(t) - \psi_{STR}(t)\right) + (k_2)_\psi \left(\dot{\psi}^{ref}_{STR}(t) - \dot{\psi}_{STR}(t)\right) + (k_3)_\psi \left(\ddot{\psi}^{ref}_{STR}(t) - \ddot{\psi}_{STR}(t)\right) \quad (4.36)$$

$$(CM_{2,4})_\psi = -\frac{|\Omega_{1,3}|}{\sqrt{\frac{mg}{2a_1} - (\Omega_{1,3})^2}}(CM_{1,3})_\psi \quad (4.37)$$

Expressions (4.33), (4.35) and (4.37) have been calculated such that the roll, pitch and yaw control actions do not interfere with the vertical displacement, $Z_{STR}(t)$; i.e. the total Thrust remains constant. The relation between the moments that guarantees this balance along the vertical axis has been derived in this work and is included in Appendix E.

As mentioned in section 3.1.1, lateral and longitudinal positions ($Y_{STR}(t)$, $X_{STR}(t)$) are determined by the quadrotor's inclination ($\phi_{STR}(t)$, $\theta_{STR}(t)$) and the total Thrust ($\mathbf{T}$).

In order to take this interaction into account, lateral and longitudinal references have been included in the roll and pitch references, and this is done by equations (4.38) to (4.43)

$$\phi_{STR}^{ref}(t) = -\Big[(k_1)_y\left(Y_{STR}^{ref}(t) - Y_{STR}(t)\right) + (k_2)_y\left(\dot{Y}_{STR}^{ref}(t) - \dot{Y}_{STR}(t)\right) + (k_3)_y\left(\ddot{Y}_{STR}^{ref}(t) - \ddot{Y}_{STR}(t)\right)\Big] \quad (4.38)$$

$$\theta_{STR}^{ref}(t) = \Big[(k_1)_x\left(X_{STR}^{ref}(t) - X_{STR}(t)\right) + (k_2)_x\left(\dot{X}_{STR}^{ref}(t) - \dot{X}_{STR}(t)\right) + (k_3)_x\left(\ddot{X}_{STR}^{ref}(t) - \ddot{X}_{STR}(t)\right)\Big] \quad (4.39)$$

$$\dot{\phi}_{STR}^{ref}(t) = -\Big[(k_{d1})_y\left(\dot{Y}_{STR}^{ref}(t) - \dot{Y}_{STR}(t)\right) + (k_{d2})_y\left(\ddot{Y}_{STR}^{ref}(t) - \ddot{Y}_{STR}(t)\right) + (k_{d3})_y\left(\dddot{Y}_{STR}^{ref}(t) - \dddot{Y}_{STR}(t)\right)\Big] \quad (4.40)$$

$$\dot{\theta}_{STR}^{ref}(t) = \Big[(k_{d1})_x\left(\dot{X}_{STR}^{ref}(t) - \dot{X}_{STR}(t)\right) + (k_{d2})_x\left(\ddot{X}_{STR}^{ref}(t) - \ddot{X}_{STR}(t)\right) + (k_{d3})_x\left(\dddot{X}_{STR}^{ref}(t) - \dddot{X}_{STR}(t)\right)\Big] \quad (4.41)$$

$$\ddot{\phi}_{STR}^{ref}(t) = -\Big[(k_{dd1})_y\left(\ddot{Y}_{STR}^{ref}(t) - \ddot{Y}_{STR}(t)\right) + (k_{dd2})_y\left(\dddot{Y}_{STR}^{ref}(t) - \dddot{Y}_{STR}(t)\right) + (k_{dd3})_y\left(Y^{IV}{}_{STR}^{ref}(t) - Y^{IV}{}_{STR}(t)\right)\Big] \quad (4.42)$$

$$\ddot{\theta}_{STR}^{ref}(t) = \Big[(k_{dd1})_x\left(\ddot{X}_{STR}^{ref}(t) - \ddot{X}_{STR}(t)\right) + (k_{dd2})_x\left(\dddot{X}_{STR}^{ref}(t) - \dddot{X}_{STR}(t)\right) + (k_{dd3})_x\left(X^{IV}{}_{STR}^{ref}(t) - X^{IV}{}_{STR}(t)\right)\Big] \quad (4.43)$$

This way roll and pitch profiles can be calculated in such a way that they provide the desired lateral and longitudinal positioning, providing a successful trajectory tracking through an adequate angular orientation.

The values of all the control parameters that appear in expressions (4.31-4.43) that have been used in this work can be found in Table 4.2.

The control moment applied to each of the rotors is calculated as the addition of the moments derived to control each one of the variables they affect:

$$
\begin{aligned}
CM_1 &= (CM_1)_z + (CM_1)_\theta + (CM_1)_\psi \\
CM_2 &= (CM_2)_z + (CM_2)_\phi + (CM_2)_\psi \\
CM_3 &= (CM_3)_z + (CM_3)_\theta + (CM_3)_\psi \\
CM_4 &= (CM_4)_z + (CM_4)_\phi + (CM_4)_\psi
\end{aligned}
\tag{4.44}
$$

The VS-Lisp code corresponding to the application of the control moments is:

```
(add-moment CMi :name "CMi"
                :direction [Siz]
                :magnitude "@CMi_yw + @CMi_p + @CMi_r + @CMi_z"
                :body1 Si
                :body2 str)
```

being the variables `@CMi_yw`, `@CMi_p`, `@CMi_r` and `@CMi_z` defined by expressions (4.31-4.37) and the moment applied from the vehicle's main body, STR, to each rotor, S_i.

Table 4.2: Control parameters.

Parameter	Value	Parameter	Value	Parameter	Value
$(k_1)_z$	0.15	$(k_2)_z$	-0.1	$(k_3)_z$	-0.01
$(k_1)_\phi$	0.5	$(k_2)_\phi$	-0.3	$(k_3)_\phi$	-0.01
$(k_1)_\theta$	0.5	$(k_2)_\theta$	-0.3	$(k_3)_\theta$	-0.01
$(k_1)_\psi$	0.08	$(k_2)_\psi$	-0.1	$(k_3)_\psi$	-0.001
$(k_1)_x$	0.05	$(k_2)_x$	-1.0	$(k_3)_x$	-0.1
$(k_1)_y$	0.05	$(k_2)_y$	-1.0	$(k_3)_y$	-0.1
$(k_1)_{dx}$	1.0	$(k_2)_{dx}$	-0.1	$(k_3)_{dx}$	0.0
$(k_1)_{dy}$	1.0	$(k_2)_{dy}$	-0.1	$(k_3)_{dy}$	0.0
$(k_1)_{ddx}$	0.0	$(k_2)_{ddx}$	0.0	$(k_3)_{ddx}$	0.0
$(k_1)_{ddy}$	0.0	$(k_2)_{ddy}$	0.0	$(k_3)_{ddy}$	0.0

4.3.2 Control of Drag Moments

As it was discussed at the beginning of Section 3.4, the effect of the Drag Forces on the vehicle has been modelled as moments applied from the air to the rotors, resulting in a rotational speed slowdown. In order to reduce the effect of these moments in the quadrotor's behaviour and control, an additional term needs to be added to the control actions which counteracts the Drag Moments; this is the Counter Drag Moment.

The Counter Drag Moment is opposite to the aerodynamic Drag Moment and, depending on the model it is applied to, it has different expressions although all of them are based on the stationary flight rotational speed, Ω_0. In the Counter Drag Moment's calculations, the stationary flight rotational speed, Ω_0, is used instead of each shaft real rotational speed, Ω_i, in order to not cancel completely the effect of drag in the dynamic behaviour of the quadrotor and to introduce in the model the uncertainty usually present in the drag characterization. In this way, the control system is allowed to demonstrate its robustness to uncertainties in the drag characterization.

The Counter Drag Moment helps to reduce the effect of the Drag Moment due to the rotational speed of the rotor. It acts even when there is no displacement, in order to maintain the hover speed of the rotors, Ω_0. This implies that even for hover condition there will always be a torque acting on the rotors, CDM_0.

A standard rule for quadrotor design is that the combined Thrust forces must generate around the double of the hover Thrust force, meaning that hovering conditions should be achieved at 40-50% of maximum thrust [156]. This standard is quite intuitive: hovering at less than this value will cause the vehicle to become too responsive to changes in thrust, which will reduce the vehicle's stability and increase the vibrations. At a higher value, the motors will consume more power than needed to create the necessary thrust, causing a greatly reduced flight time

and making the vehicle sluggish and unresponsive.

This rule implies that the maximum torque that the rotors could produce is between 200% and 250% the value of the Counter Drag Moment for hover conditions, Maximum Torque = 200-250% CDM_0.

4.3.2.1 Counter Drag Moment as a function of the rotational speed.

For the simple aerodynamic model, that only considers the contribution of the rotational speed to the aerodynamic forces calculus, the expression of the Drag Moment on each shaft is modelled as:

$$TQR_{ij}(\alpha_{ij}) = D_{ij}(\alpha_{ij}) = \frac{1}{2}\rho_\infty S C_D(\alpha_{ij}) \left[r_{rep_0}\Omega_i\right]^2$$

$$MD_i(\alpha_{ij}) = \sum_{j=1}^{2} r_{cp_0} TQR_{ij}(\alpha_{ij})$$

Therefore, the Counter Drag Moment expression is similar:

$$CDM_i(\alpha_{ij}) = -\sum_{j=1}^{2} r_{cp_0} TQR_{0_{ij}}(\alpha_{ij}) = -\frac{1}{2}\rho_\infty S \sum_{j=1}^{2} r_{cp_0} C_D(\alpha_{ij}) \left[r_{rep_0}\Omega_0\right]^2 \quad (4.45)$$

The application of the Counter Drag Moment leads to a reduction of the Drag Moment effect on the shafts' rotational speed, helping in this way to maintain the rotational speed of the rotors.

The VS-Lisp code implemented to define the Counter Drag Moment in this model adopts the form of (4.45) as follows:

```
(setsym   @TQR0ij   "0.5*rho*R*(1-e)*chord*@CDa_ij*(prep0*OMo)^2
          @CDMi     "-cp0*(@TQR0i1 + @TQR0i2)")
```

4.3.2.2 Counter Drag Moment as a function of the rotational and translational speed.

In this case, the Counter Drag Moments have been calculated similarly to the previous case, making use of the stationary flight rotational speed and including also the translational speed in this case, V_t.

For the aerodynamic model considering the translational speed, the Drag Moment was modelled as:

$$DM_i(\alpha_{ij}) = \sum_{j=1}^{2} r_{cp_{ij}} TQR_{ij}$$

where TQR_{ij} is given by expression (3.54), and L_{ij} and D_{ij} are given by expressions (3.64) and (3.65) respectively.

Therefore the Counter Drag Moments can now be expressed as:

$$CDM_i(\alpha_{ij}) = -\sum_{j=1}^{2} r_{cp_{ij}} TQR_{0_{ij}} \tag{4.46}$$

where $TQR_{0_{ij}}$ responds to expression:

$$TQR_{0_{ij}} = D_{0_{ij}} \cos \alpha_{in_{ij}} - L_{0_{ij}} \sin \alpha_{in_{ij}} \tag{4.47}$$

and Lift and Drag forces in stationary conditions are:

$$L_{0_{ij}} = \frac{1}{2} \rho S C_L(\alpha_{ij}) \left[V_{t_{ij}} + r_{rep_{ij}} \Omega_0 \right]^2 \tag{4.48}$$

$$D_{0_{ij}} = \frac{1}{2} \rho S C_D(\alpha_{ij}) \left[V_{t_{ij}} + r_{rep_{ij}} \Omega_0 \right]^2 \tag{4.49}$$

The VS-Lisp code used to define the Counter Drag Moment in this model is presented below:

```
(setsym   @L0ij     "0.5*rho*chord*R*(1-e)*CLa*(alphas +
                    + @alpha_ij)*(@Vt_ij + @prep_ij*OMo)^2"
          @D0ij     "0.5*rho*chord*R*(1-e)*@CDa_ij*(@Vt_ij +
                    + @prep_ij*OMo)^2"
          @TQR0ij   "@D0ij cos(@alpha_in_ij) - @L0ij sin(@alpha_in_ij)"
          @CDMi     "@cp_i1*@TQR0i1 + @cp_i2*TQR0i2"
```

In this case only expressions and the code for the non stationary pressure centre and the representative point have been given. In order to consider the simplified aerodynamic model, the parameters r_{cp_j} (`@cp_ij`) and r_{rep_j} (`@prep_ij`) should be substituted by their corresponding stationary values, r_{cp_0} (`cp0`) and r_{rep_0} (`prep0`), in both equations.

4.3.2.3 Counter Drag Moment for elastic blades.

The previous sections considered the Counter Drag Moment for rigid blades in which the moment has only two components, one for each rigid blade. When the elastic blades are included in the model, the blades are discretized in n elements, and the Counter Drag Moment has $2n$ components, one for each blade segment.

Considering only the most complete aerodynamic model, that considers translational speed and the real values of the representative point and pressure centre, the effect of the Drag Moment was modelled as:

$$DM_i(\alpha_{ij}) = \sum_{j=1}^{2} \left(\sum_{k=1}^{n} r_{cp_{ijk}} TQR_{ijk} \right)$$

where $TQR_{ijk}(\alpha_{ijk})$ is given by expression (3.54) and $L_{ijk}(\alpha_{ijk})$ and $D_{ijk}(\alpha_{ijk})$ are given by expressions (3.67) and (3.68) respectively.

Therefore the Counter Drag Moments can be expressed as:

$$CDM_i(\alpha_{ij}) = -\sum_{j=1}^{2}\left(\sum_{k=1}^{n} r_{cp_{ijk}} TQR_{0_{ijk}}\right) \tag{4.50}$$

where $TQR_{0_{ijk}}(\alpha_{ijk})$ responds to the expression:

$$TQR_{0_{ijk}} = D_{0_{ijk}} \cos\alpha_{in_{ij}} - L_{0_{ijk}} \sin\alpha_{in_{ij}} \tag{4.51}$$

and Lift and Drag forces in stationary conditions on each segment are:

$$L_{0_{ijk}} = \frac{1}{2}\rho S_k C_L(\alpha_{ijk}) \left[V_{t_{ij}} + r_{rep_{ijk}}\Omega_0\right]^2 \tag{4.52}$$

$$D_{0_{ijk}} = \frac{1}{2}\rho S_k C_D(\alpha_{ij}) \left[V_{t_{ij}} + r_{rep_{ijk}}\Omega_0\right]^2 \tag{4.53}$$

The VS-Lisp code used to define the Counter Drag Moment in the discretized blade elastic model is as follows:

```
(setsym   @L0ijk     "0.5*rho*chord*(x_k-x_k-1)*R*(1-e)*CLa*(alphas +
                     + @alpha_ij)*(@Vt_ij + @prep_ijk*OMo)^2"
          @D0ijk     "0.5*rho*chord*(x_k-x_k-1)*R*(1-e)*@CDa_ij*
                     *(@Vt_ij + @prep_ijk*OMo)^2"
          @TQR0ijk   "@D0ijk*cos(@alpha_in_ij) -
                     - @L0ijk*sin(@alpha_in_ij)"
          @CDMi      "@cp_i11*@TQR0i11 + @cp_i21*TQR0i21 +
                     ...
                     + @cp_i1(k-1)*@TQR0i1(k-1) +
                     + @cp_i2(k-1)*TQR0i2(k-1) +
                     + @cp_i1k*@TQR0i1k+ @cp_i2k*TQR0i2k")
```

4.3.3 Predefined smooth references

In most trajectory and guidance control applications, the reference signals represent the desired position that the vehicle should reach. One of the most common

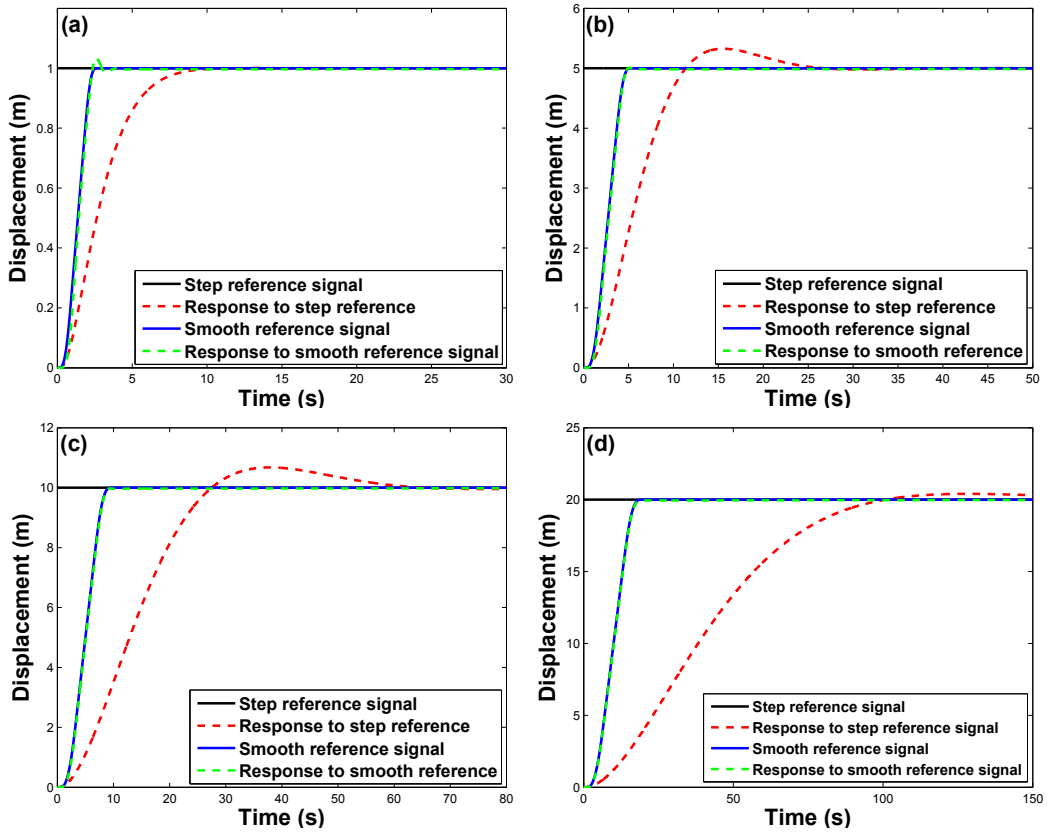

Figure 4.1: Comparison of responses to step and smooth reference signals for different longitudinal displacements on the $\mathtt{X_n}$ axis. (a) 1 meter translation. (b) 5 meters translation. (c) 10 meters translation. (d) 20 meters translation.

reference signal is the step input, known in this way because of its shape, which is squared. Taking into account the control law, which is proportional to the position error, $e_p(t)$, a step reference implies a high and abrupt initial control action, therefore, different control parameters are needed to stabilise the quadrotor's response when different amplitudes of steps' references are applied in order not to saturate the control actions: the larger the reference amplitude, the smaller the values of the parameters needed, otherwise, the rotor reaches its maximum torque or destabilizes the vehicle. This leads to a slow response for high values of the reference as it is shown in Figure 4.1.

This is the reason why predefined smooth references are very convenient to be used instead of a stepping reference signals. By defining the position, velocity, acceleration and acceleration derivatives references as smooth signals, smaller and smoother control actions are expected, which actually happens. Figure 4.2 repre-

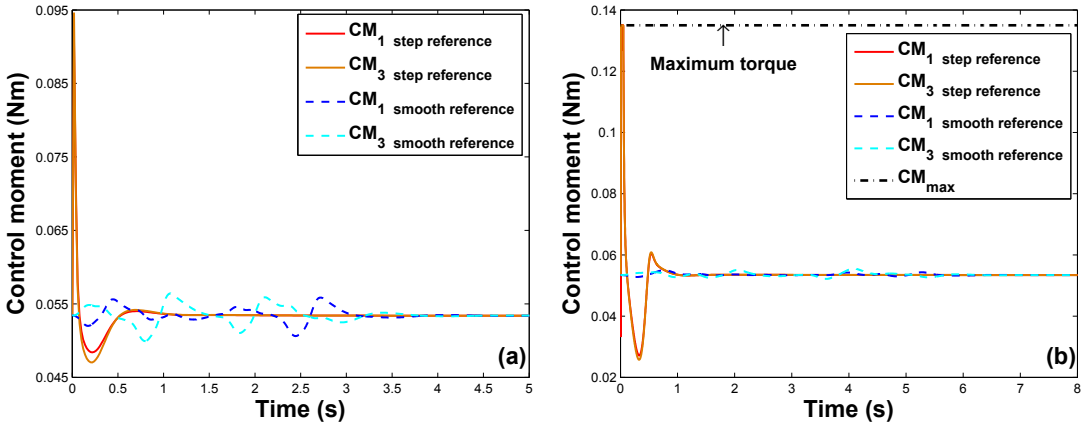

Figure 4.2: Comparison between the control actions that lead to 1 (a) and 5 (b) meters of longitudinal displacement. Smooth reference inputs (- - -), step reference inputs (—).

sents the control action necessary for the rigid simple model to follow some of the trajectories shown in Figure 4.1. It can be seen that when the step references are applied to the vehicle, the control actions present an initial high peak due to the instantaneous error of position that produces control action saturation. However, for smooth predefined trajectories, the position error is not instantaneous, therefore, the control actions are smoother and far from reaching the saturation limits ($CM_{max} = 0.135$ Nm), calculated as the 250% of the hover condition Counter Drag Moment ($CDM_0 = 0.05339$ Nm).

The use of smooth trajectories as reference signals presents several advantages; constant control parameters for the indirectly controlled variables instead of variable functions, the possibility to define the maximum acceleration and speed values and smaller and smoother control actions; all these lead towards a better performance of the quadrotor, minimizing the presence of vibrations introduced by the control system, so the structural vibrations produced by the mobile components can be analysed.

Fifth order trajectories have been selected for this work. It implies quadratic curves for the acceleration derivative, third order curves for the acceleration, fourth order curves for the speed and fifth order curves for the position reference signals, as shown in Figure 4.3.

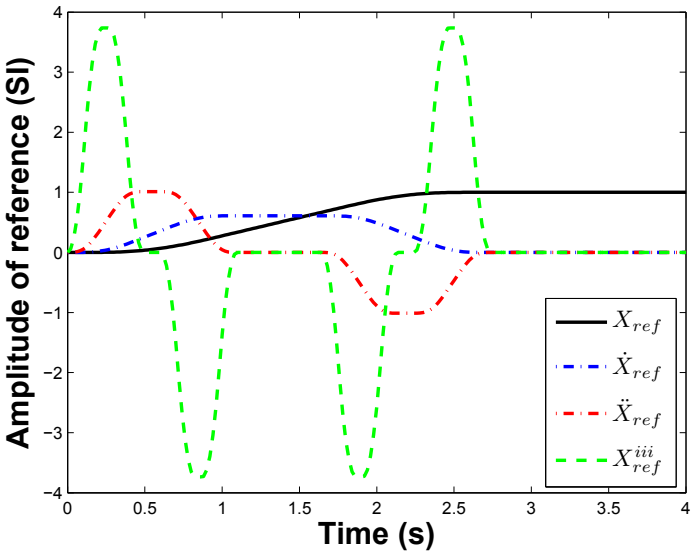

Figure 4.3: Example of fifth order trajectory signals generated by Matlab and applied to the quadrotor.

4.4 Trajectory tracking results

With the equations of motion presented (4.1-4.10), including the control system and the trajectories generator, several simulations have been carried out in order to study the behaviour of the quadrotor's controlled models developed in this work.

The simulations here presented include both the rigid simple aerodynamic model and the rigid complete aerodynamic model, excluding the intermediate rigid aerodynamic model since the results are similar to those obtained from the rigid complete model.

Figures 4.4 shows a comparison of the trajectory tracking error for the two models when motions in all the axes are required simultaneously. Figure 4.5 shows a comparison of the control actions applied to achieved these trajectories for the simple and the complete aerodynamic model.

As it can be appreciated, the trajectory tracking is similar for both models; however the control actions that lead to these displacements are very different. When considering the complete aerodynamic model, oscillations in the control

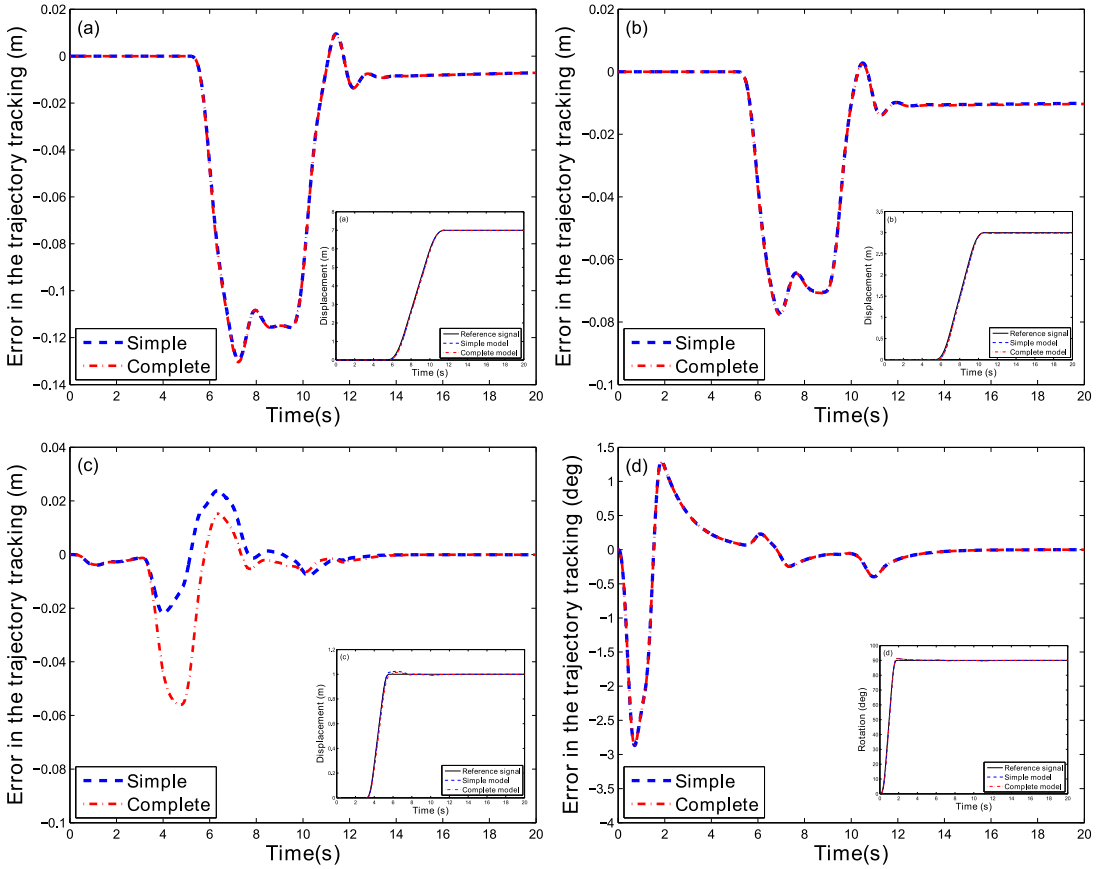

Figure 4.4: Example of quadrotor trajectories tracking and errors for different models: reference signals (—), rigid simple model (- - -), rigid complete model (- · -). (a) Translation error on the X_n axis. Inset: 7 m translation on the X_n axis. (b) Translation error on the Y_n axis. Inset: 3 m translation on the Y_n axis. (c) Translation error on the Z_n axis. Inset: 1 m translation on the Z_n axis. (d) Yaw rotation error around the Z_n axis. Inset: 90 yaw rotation around the Z_n axis.

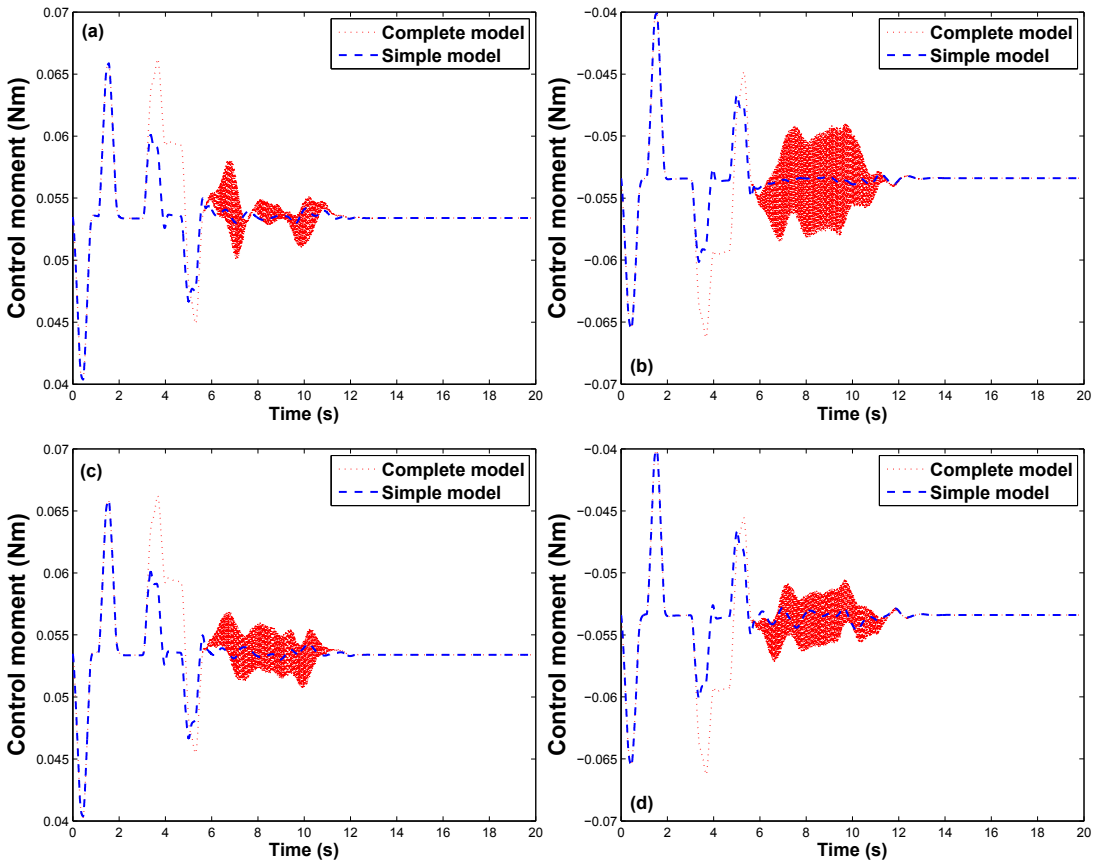

Figure 4.5: Comparison of the control actions that lead in the movements shown in Figure 4.4 for different models: rigid simple model (- - -), rigid complete model (···). (a) Control moment applied to rotor 1. (b) Control moment applied to rotor 2. (c) Control moment applied to rotor 3. (d) Control moment applied to rotor 4.

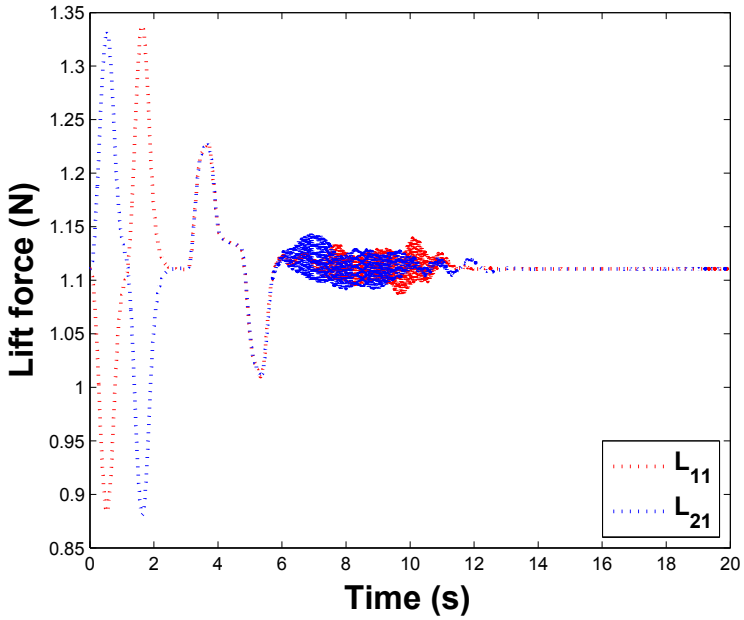

Figure 4.6: Example of the oscillations appearing in the Lift generated by blades B_{11} and B_{21} when the lateral and longitudinal trajectories shown in Figure 4.4 are followed.

actions can be seen. These fluctuations are necessary in order to counteract the oscillations in the aerodynamic forces, since the aerodynamic forces depend on the translational speed and this speed oscillates from positive to negative at the blades' rotational frequency when there is lateral or longitudinal displacement. These oscillations in the Lift forces are shown in Figure 4.6.

Using the controlled model presented in (4.1-4.10) and the complete aerodynamic model, three-dimensional trajectories have been applied to the quadrotor. Figures 4.7 and 4.8 represent the simulation of an helical trajectory of 3 meters radius and 50 meters height and the tracking of a rectangular trajectory of 10 meters side and 3 meters height respectively. As it can be seen, in both cases, the quadrotor follows the prescribed trajectory satisfactorily.

Figures 4.9 and 4.10 show the control moments needed to achieve the motions represented in Figures 4.7 and 4.8 respectively. As in the previous simulation shown in this chapter, the control moments that produce the motion when the complete aerodynamic model is used, are of oscillating nature, but due to the smooth predefined trajectories they have a small amplitude, quite far from the

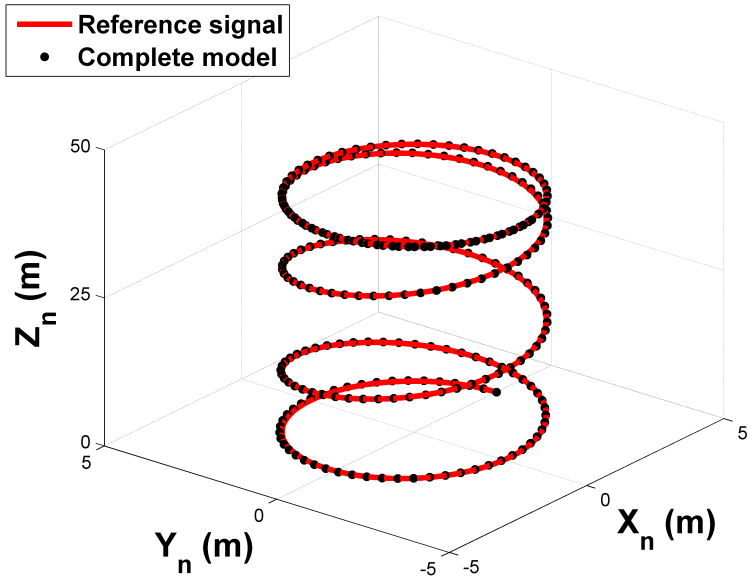

Figure 4.7: Three-dimensional helical trajectory tracking using the rigid complete aerodynamic model. (—) is the reference signal and (·) is the rigid complete model trajectory.

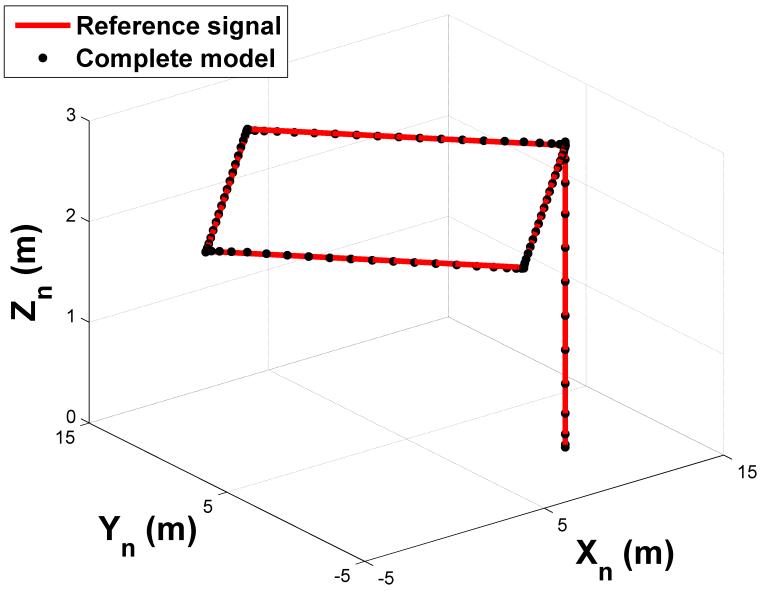

Figure 4.8: Three-dimensional rectangular trajectory tracking using the rigid complete aerodynamic model. (—) is the reference signal and (·) is the rigid complete model trajectory.

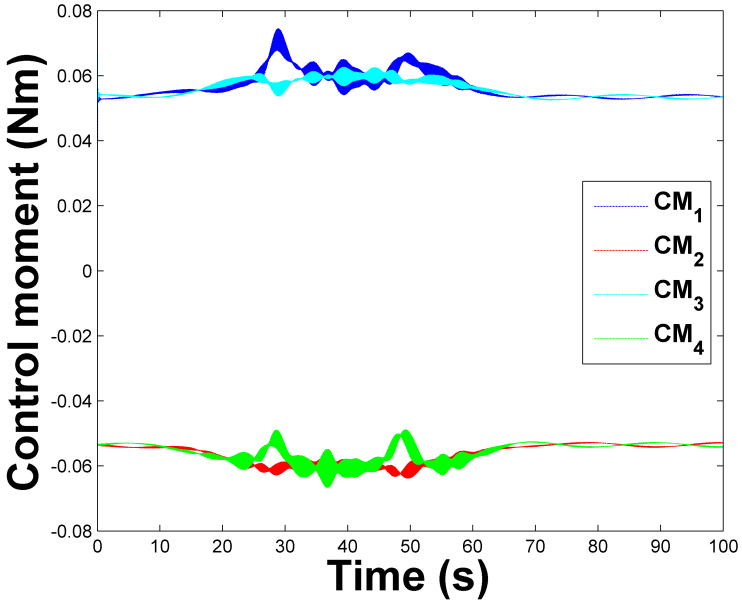

Figure 4.9: Control moments applied to obtain the three-dimensional helical trajectory shown in Figure 4.7.

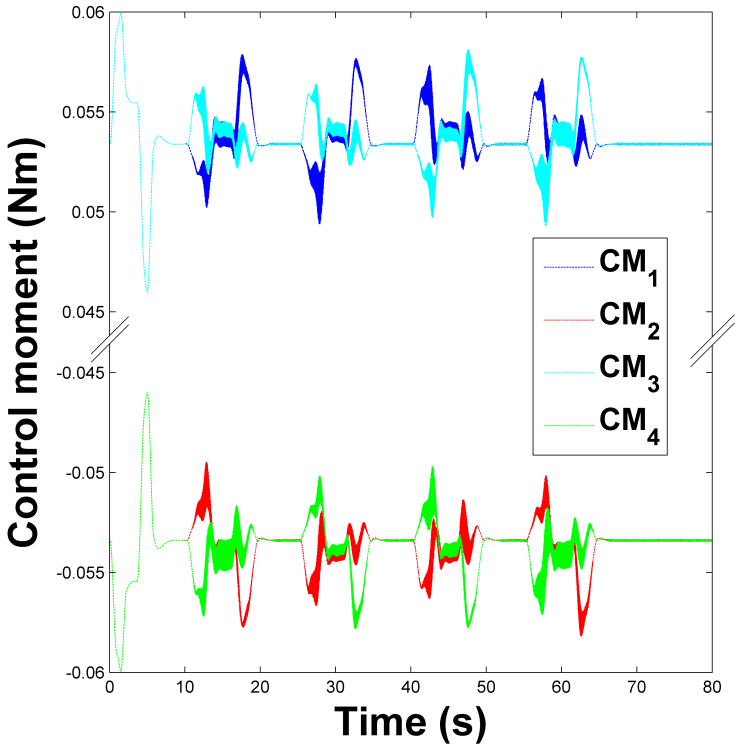

Figure 4.10: Control moments applied to obtain the three-dimensional rectangular trajectory shown in Figure 4.8.

maximum torque. These oscillations are produced by the consideration of the translational speed in the aerodynamic forces and the frequency at which oscillate lays between 40-53 Hz, which is the range of rotational speed of the rotors for the trajectories.

4.5 Summary of the chapter

In this chapter the nonlinear equations of motion obtained from VehicleSim have been written according to the notation used in this work.

The basics of nonlinear systems controllability have been introduced and a controllability test has been performed on the vehicle's equations of motion.

The PVA control method used for the stabilization and trajectory tracking of the quadrotor has been presented. The relation between the moments applied to opposite rotors has been derived in order to maintain the height constant.

The Counter Drag Moment has also been introduced in the model in order to control the effects of the aerodynamic Drag and a standard design rule has been given for a maximum rotor torque, related to the Counter Drag Moment for hover condition.

Fifth order smooth reference signals have been included in the control system. It has been shown that the use of smooth reference signals produces a reduction in the control actions demand and in the settling time when compared to step reference signals.

Successful trajectory tracking using various aerodynamic models has been proved and some complex three-dimensional trajectories have been applied to the vehicle, presenting a good tracking performance. The control actions for all the trajectories have been shown. It was observed that the control actions for the complete

aerodynamic model presents an oscillating pattern with a frequency between 40-53 Hz, which is the range of the rotational speed of the rotors.

Chapter 5

Vibrations

Quadrotors are autonomous vehicles usually employed in hazardous environments, most of the times in reconnaissance activities in hostile territory, therefore a good performance of the vehicle is a basic requirement. It is necessary to keep the structural vibrations of the vehicle to the minimum since these can affect the measurement systems and/or image acquisition systems.

In this work, a thorough characterization of the vibrations appearing in the vehicle has been performed, based on the materials usually employed in the manufacture of quadrotor blades, pointing out which are the main sources of these vibrations and trying to avoid their effects on the control system.

Due to the advantages quadrotors present - relatively low price, hover capability and high manoeuvrability -, it is a very good choice for unsafe missions in hostile terrain. That is why the vehicle may be subjected to structural damage, accidental or deliberate, which can endanger its integrity and that of the sensible information it carries.

In order to face this possibility, several approaches to structural damage are presented, software and hardware based, which would allow the vehicle to return to base after suffering from severe structural damage, like a complete blade loss.

5.1 Vibrational analysis

When dealing with autonomous vehicles, their performance is a vital aspect to consider whilst the design process takes place. In order to fully understand the dynamics involved in quadrotors motion, it is important to have a complete model that captures the behaviour of the same. Therefore, it is essential to know which is the behaviour of the elastic blades and how they could affect the overall quadrotor's behaviour.

In this section, the vibrational characterization of the quadrotor and its elastic components is shown. The natural frequencies and motion of the elastic blades have been obtained for non rotational motion and for rotational motion too. The vibrational behaviour of the blades when the quadrotor is in motion has also been studied, as well as how this behaviour is translated to the overall performance of the vehicle.

5.1.1 Static and dynamic characterization of elastic blades

As seen in Chapter 3, at this point in the research, only the blades are modelled as elastic bodies. For the vibrational analysis of the blades, these have been discretized as shown in Figure 5.1, with a rigid shorter segment near the root of length r_1, since usually the root section has considerably higher stiffness than the rest of the blade [157], and two equal double length segments, $2r_1$, with flap degree of freedom.

The elastic part of the blade has not been modelled in more segments for three main reasons:

- When discretizing an elastic beam or blade with rotational springs and dampers, the equivalent solution is a chaotic system for high number of elements; for the static solution is better to discretize in more segments,

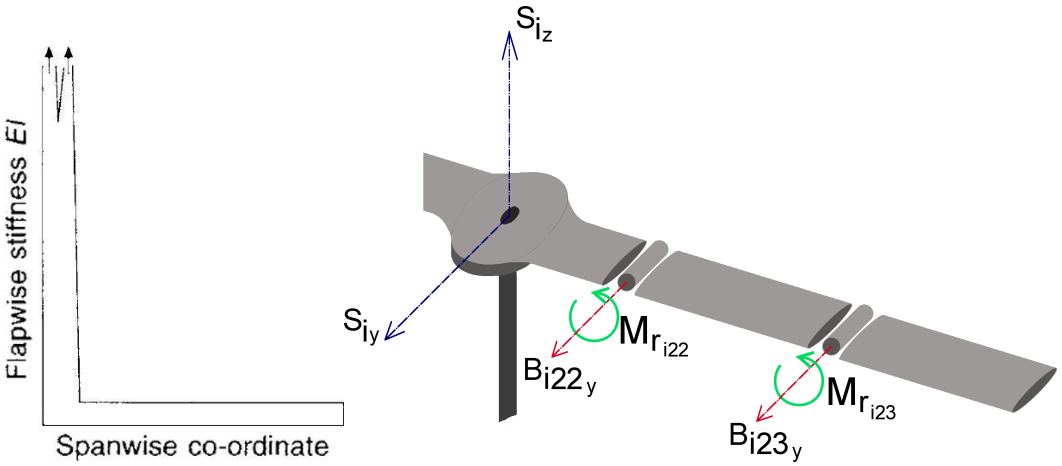

Figure 5.1: Left: Usual stiffness distribution in a helicopter blade, credits to [157]. Right: Elastice blade modelled with a rigid segment close to the root and two elastic double length segments with flap degree of freedom.

however when simulating the dynamic behaviour this is chaotic for more than one element.

- With a discretization of a rigid element near the root and two moving elements is enough to reproduce the static behaviour - as will be seen along this chapter.

- Discretizing the blade in two moving elements, the flap equations can be obtained from VehicleSim and can be presented in handy manner, which could be then used in conjunction with the vehicle's motion equation to reproduce the effect of the elastic blades, without the need of the software.

Since the blade is now discretized in different length segments, the value of the parameter $b(n)$ is slightly different as that given by equation (3.51). The value of the elastic equivalent now corresponds to expression (5.1), where n_t is the total equivalent number of segments if they were considered of the same length - in this case would be 5 segments of length r_1 -, and n_f is the equivalent number of segments which are free to move - 4 in this case, because only 4 equivalent segments are allowed to move - as can be seen in Figure 5.2.

$$b(n_t, n_f) = \frac{3EI}{R}\left(\frac{1}{2} + \frac{{}^1/_2}{n_t}\right)\frac{n_f}{n_t} \tag{5.1}$$

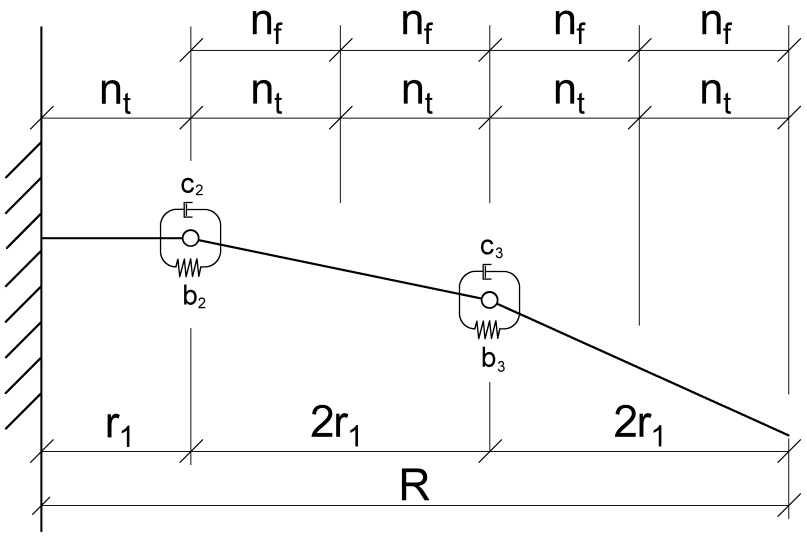

Figure 5.2: Representation of the blade discretization in a rigid segment next to the root of length r_1 and two equal double length segment with flap degree of freedom of length $2r_1$. Equivalent number of segments of equal length r_1, $n_t = 5$, equivalent number of segments with flap degree of freedom of equal length r_1, $n_f = 4$.

The values of the parameters $c(n_t, n_f)$ are obtained such that the tip motion decay of the discretized blade matches the decay of the elastic blade, as in Section 3.3.2.

With this discretization, different materials frequently used for the manufacture of quadrotor blades have been modelled - ABS plastic, balsa wood, aluminium and carbon fiber. The elastic and structural properties of these materials [144, 158–163] and also their discrete equivalents can be found in Table 5.1.

Table 5.1: Elastic and structural properties of materials and equivalents for blade discretization.

Material	E (GPa)	ξ	$b(5,4)$ (Nm/rad)	$c(5,4)$[1] (Nms/rad)
ABS	1.5	0.065 - 0.13	0.0865	0.0009
Balsa wood	4	0.02-0.04	0.23136	0.0005
Aluminium	70	0.02 - 0.04	4.05	0.0015
Carbon fibre	150	0.05 - 0.15	8.65	0.015

[1]Only the average value of the damping ratio for each material is used to calculate this discrete parameter

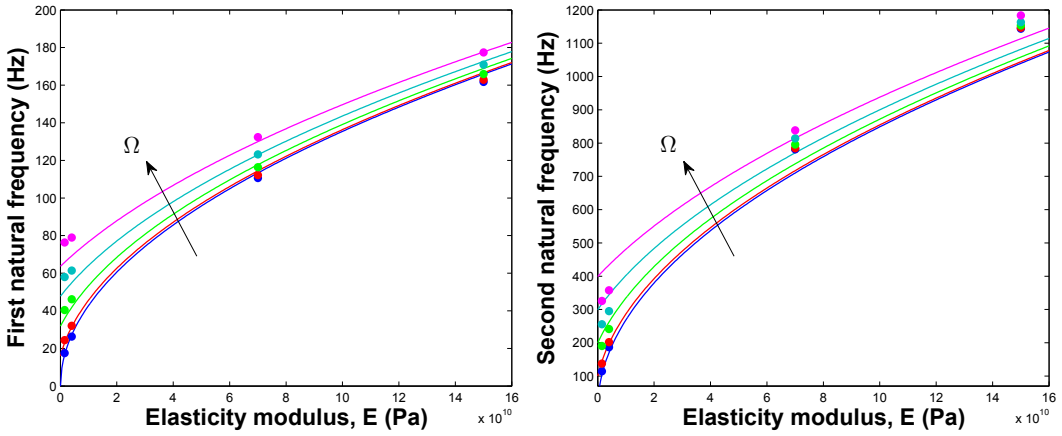

Figure 5.3: Blade's first and second natural frequencies' variation with elasticity and rotational speed. Continuous lines represent the theoretical frequencies (5.2-5.3); the dots represent the frequencies obtained with the VehicleSim simulation for different materials; and the different colors represent the different rotational speeds ($\Omega = 0$ (blue), 100 (red), 200 (green), 300 (cyan), 400 (magenta) rad/s).

With these values of the spring parameters b - calculated with expression (5.1) - and the damper parameters values c - adjusted to have a similar decay as seen in Section 3.3.2 - the static and dynamic properties of the equivalent elastic blades are completely depicted.

The first natural frequency of the blade can be expressed as (5.2) being Ω the rotational speed and I_{y_b} represents the second moment of inertia of the blade around the flapping axis [164]. Assuming that the relation between the second and first rotating natural frequencies is equal to the non rotational case (3.47), the second rotational natural frequency would be expressed by (5.3).

$$\omega_{n_{1_r}} = \sqrt{\Omega^2 + \frac{3EI/R}{I_{y_b}}} \tag{5.2}$$

$$\omega_{n_{2_r}} = \frac{4.694^2}{1.875^2}\sqrt{\Omega^2 + \frac{3EI/R}{I_{y_b}}} \tag{5.3}$$

The first and second natural frequencies have been obtained for the discretized blade model for the different materials by taking the system out of equilibrium and

analysing its oscillatory response with no damping. The results are presented in Figure 5.3 along with the theoretical natural frequencies (5.2- 5.3). It can be seen that the discretized system can reproduce the first and second natural frequencies with an acceptable error ranging from 5% to 15% for the first frequency and from 10% to 20% for the second frequency, the higher errors corresponding to the higher rotational speeds.

The deflection and damping of the discretized system match the elastic blades' - the values of the parameters b and c have been selected to obtain this agreement - and the natural frequencies also approximate the theoretical expected frequencies. Therefore, it can be stated that blade discretization with a rigid segment and two segments with flap degree of freedom is a good approximation to an elastic blade.

The equations that describe the motion of the elastic segments, they can be found below, where the notation has been modified for simplicity: β_2 represents the flap displacement of the second segment, β_{ij2}; L_2 represents the Lift force generated by the second segment, L_{ij2}, applied at the pressure centre of the second segment cp_2, $r_{cp_{ij2}}$; M_{r_2} is the restoring moment acting at the second segment, $M_{r_{ij2}}$, which responds to expression (5.4). The same modifications in the notation also apply to the third segment.

$$M_{r_{ijk}} = b(5,4)\beta_{ijk} - c(5,4)\dot{\beta}_{ijk} \tag{5.4}$$

$$\begin{aligned}
\ddot{\beta}_3 = &-\frac{L_3\left[2r_1(1+\cos\beta_3+\cos 2\beta_3) - cp_3(5+2\cos\beta_3)\right]}{M_b r_1^2(4\cos{\beta_3}^2-5)} \\
&-\frac{L_2 cp_2(1+2\cos\beta_3) - M_{r_2}(1+2\cos\beta_3) + M_{r_3}(6+4\cos\beta_3)}{M_b r_1^2(4\cos{\beta_3}^2-5)} \\
&+\frac{r_1^2\dot{\beta}_2^2(12\sin\beta_3+4\sin 2\beta_3) + r_1^2\dot{\beta}_3^2(2\sin\beta_3+2\sin\beta_3)}{r_1^2(4\cos{\beta_3}^2-5)} \\
&+\frac{4r_1^2\dot{\beta}_2\dot{\beta}_3(\sin\beta_3+\sin 2\beta_3) + 2gr_1\cos\beta_2 - 6gr_1\cos\beta_2\sin\beta_3}{r_1^2(4\cos{\beta_3}^2-5)}
\end{aligned} \tag{5.5}$$

$$\ddot{\beta}_2 = \frac{L_2 cp_2 + L_3 \cos\beta_3 (2r_1 - 2cp_3) - M_{r_2} + M_{r_3}(1 + 2\cos\beta_3)}{M_b r_1^2 (4\cos{\beta_3}^2 - 5)}$$
$$- \frac{2r_1^2 \dot{\beta}_2^2 \sin\beta_3 (1 + 2\cos\beta_3) + 2r_1^2 \dot{\beta}_3^2}{r_1^2 (4\cos{\beta_3}^2 - 5)}$$
$$+ \frac{2r_1 g \cos\beta_2 - g r_1 (\cos\beta_2 + 2\cos\beta_3) + 4r_1^2 \dot{\beta}_2 \dot{\beta}_3 \sin\beta_3}{r_1^2 (4\cos{\beta_3}^2 - 5)} \tag{5.6}$$

By solving these equations simultaneously with the quadrotor equations of motion (4.1)-(4.4), taking into account that the Lift forces are acting now perpendicular to the blade's segment surface, it would be possible to obtain an approximation of the vehicle's motion when elastic blades are considered, without the necessity of using VehicleSim in this case.

5.1.2 Effect of elastic blades in the quadrotor motion

The natural frequencies of the discretized model have been found to be close to the theoretical ones for different materials, and the structural damping has been adjusted to present a similar dynamic behaviour to the continuous blade.

Now that the discretized system has been fully characterized, the elastic blades model is introduced in the quadrotor model in order to analyse the effect of the blades' elasticity in the overall performance.

When the variation of the aerodynamic forces with the translational speed is considered, the aerodynamic forces are oscillating, as shown in previous chapters (Figure 4.6). Elastic blades behaviour will be then dominated by the non-vanishing external force, the Lift force, which oscillates at the rotational frequency which lays between 40.8 and 53.4 Hz (256.5-335.5 rad/s) for a common tridimensional trajectory ($X_n^{ref} = 7$ m, $Y_n^{ref} = 3$ m, $Z_n^{ref} = 1$ m).

A comparison of the pitch angle position when different blade materials are con-

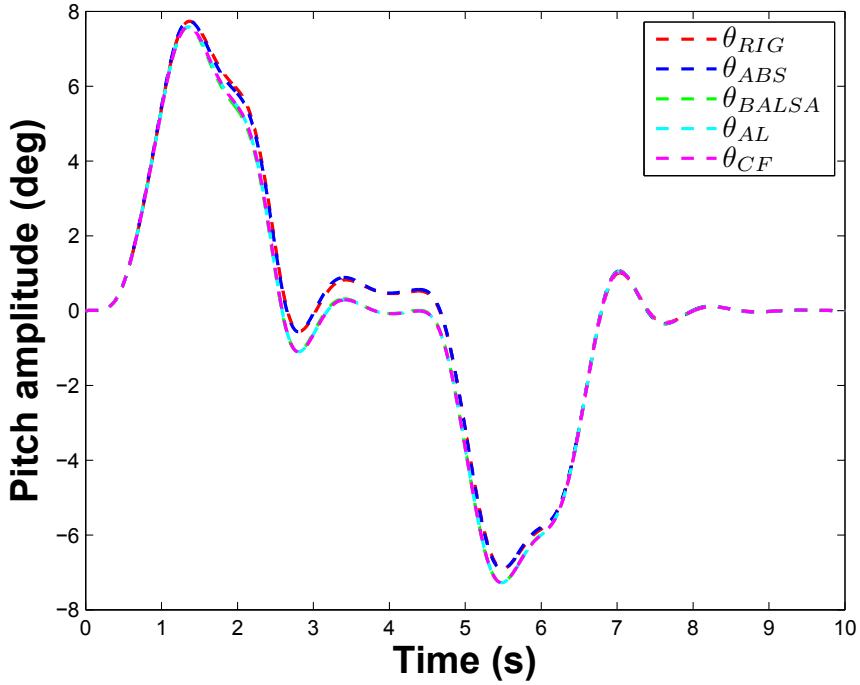

Figure 5.4: Comparison of the pitch amplitude for a usual tridimensional trajectory ($X_n^{ref} = 7$ m, $Y_n^{ref} = 3$ m, $Z_n^{ref} = 1$ m) when rigid and elastic blades of different materials are considered.

sidered can be found in Figure 5.4. The rigid model has also been included as reference. It shows that for all the materials, the vehicle presents a similar pitch profile - the same can be said about the roll angle - where no oscillations can be appreciated.

In the case of the angular acceleration, the oscillations caused by the aerodynamic oscillating forces are more evident, as shown in Figure 5.5 for pitch acceleration. The figure shows that for the materials considered, the pitch acceleration presents the same profile, with basically the same amplitude, than the rigid blade case. It also includes details of the pitch acceleration for different blades materials at different simulation times.

The spectrum of the pitch acceleration for the usual trajectory can be found in Figure 5.6 for the different materials and the rigid case. It can be seen that for ABS plastic, balsa wood and carbon fiber the only vibrations appearing in the structure have a frequency twice the rotational frequency and that the amplitude of the vibration is smaller than the rigid model vibration amplitude. This is

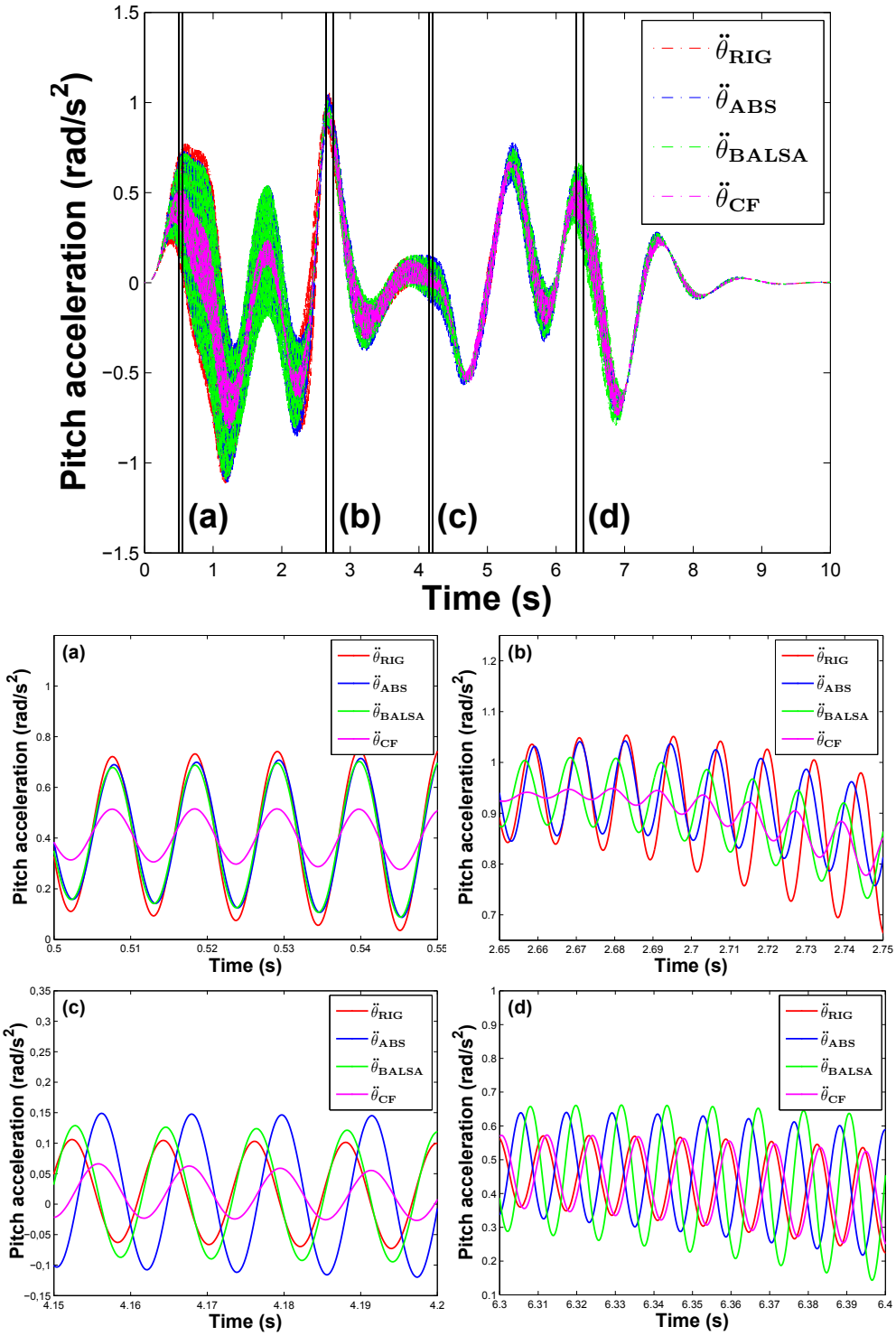

Figure 5.5: Comparison of the vehicle's pitch acceleration amplitude for a usual tridimensional trajectory ($X_n^{ref} = 7$ m, $Y_n^{ref} = 3$ m, $Z_n^{ref} = 1$ m) when rigid and elastic blades of different materials are considered and details at different times. (a) Detail of acceleration between 0.50 and 0.55 s time. (b) Detail of acceleration between 2.65 and 2.75 s time. (c) Detail of acceleration between 4.15 and 4.20 s time. (d) Detail of acceleration between 6.30 and 6.40 s time.

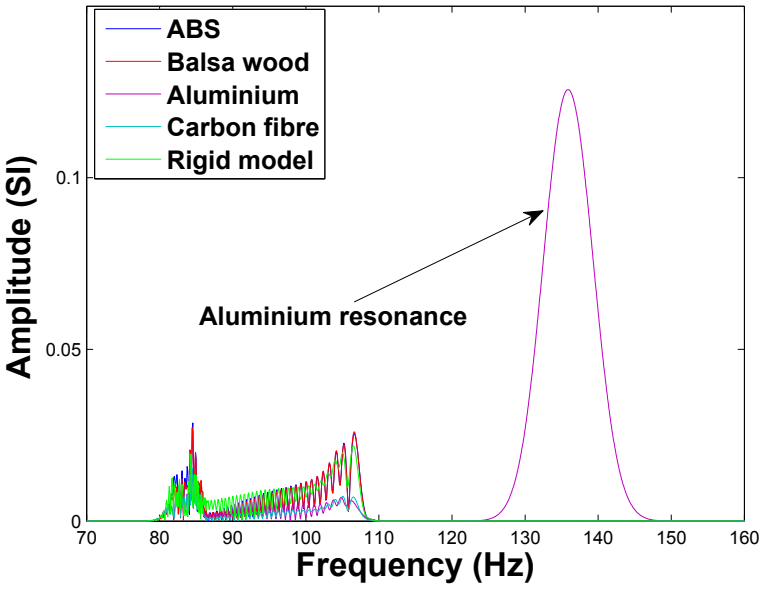

Figure 5.6: Comparison of the vehicle's pitch acceleration's frequency spectra for the usual trajectory and different materials, including the aluminium, which is prone to resonance for the given flight conditions.

because these oscillations in the structure are not caused by the elasticity of the blade but from having the oscillating external forces (aerodynamic forces) applied at the moving pressure centre of each blade instead of being applied at the rotor centre; therefore, whenever the complete aerodynamic model will be considered, these oscillations are expected to appear.

For the aluminium case, a high peak arises at its natural frequency. This indicates that for the specific flight conditions, an aluminium blade would prone to resonate, therefore, an aluminium blade would be out of question in the manufacturing of this particular vehicle. However, resonance phenomenon could be avoided by changing the morphology of the blade, this is, changing its mass and inertia properties would modify its natural frequency.

Based on the response of the vehicle when elastic blades or rigid blades are considered for the same trajectory, it can be seen that the effect of the elastic blades on the overall performance of the quadrotor is not noticeable: the oscillations that appear in the angular acceleration are mainly produced by the fact of applying the aerodynamic forces at the pressure centre of each blade, which translates in

oscillating forces with rotating application points. Blades elasticity slightly increases the oscillations of the angular acceleration for the more elastic materials - ABS and balsa wood blades - and decreases the amplitude of the oscillations for rigid materials - carbon fiber blades.

It can be then said that blades elasticity does not show significant influence on the overall performance of the quadrotor, specially when the complete aerodynamic model is considered, as its effects overtake the elastic blades', except for the aluminium blades case, which shows a resonant behaviour for the specific flight conditions of the quadrotor modelled in here. The problems that the oscillatory angular acceleration may have in the control system will be discussed in next section.

5.2 Oscillations appearing in the angular acceleration.

During the evaluation of the vehicle's response in the case of elastic blades, it was shown the little influence elasticity had on the overall performance. However, other considerations should be taken into account when analysing vibrations transmitted to the vehicle's structure.

As could be seen in the previous section (Figure 5.5), the angular acceleration of the structure has a high vibrational response that is usually not found in other quadrotor models due to the application point of the aerodynamic forces. Other models consider the lift force produced by one rotor as a singular force applied in the centre of the rotor [82] and also most of them don't consider the lift variation with the translational speed [103].

As seen in Sections 3.4.2 and 3.4.3, the aerodynamics modelled during this research include the effect of the translational speed and consider the aerodynamic

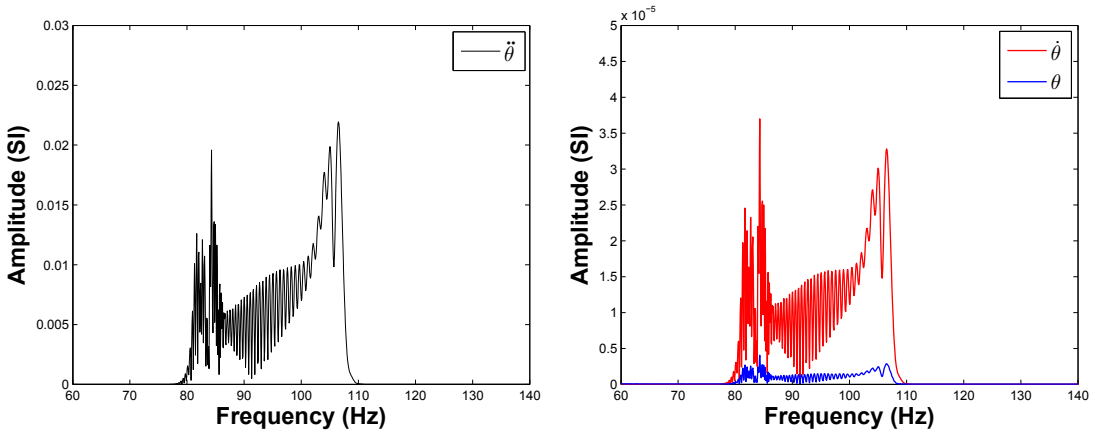

Figure 5.7: Vibrational spectrum of the pitch speed and position compared to the magnitude of the vibrational spectrum of the pitch acceleration for a usual tridimensional trajectory ($X_n^{ref} = 7$ m, $Y_n^{ref} = 3$ m, $Z_n^{ref} = 1$ m).

forces produced by the blades separately, applying them in the pressure centre of each blade. This consideration produces a rotating application point of the force, which translates in oscillating roll and pitch moments. These high vibrational roll and pitch moments mean that also the roll and pitch accelerations present a vibrational character that, when introduced in the control system as feedback, lead to large vibrational control actions. Also there is to consider the numeric derivative calculation that the VehicleSim software uses to calculate accelerations from speeds, this may not be optimized, and because of the characteristics of the software the method cannot be modified. This would mean that any small oscillations in the angular speed could be magnified in the numeric derivative process.

Although the roll and pitch angles show a smooth shape, the angular accelerations present high vibrational characteristics (as shown in Figure 5.5 even for the blades rigid model). Figure 5.7 represents the frequency spectra for the pitch position, speed and acceleration for the conventional trajectory tracking ($X_n^{ref} = 7$ m, $Y_n^{ref} = 3$ m, $Z_n^{ref} = 1$ m). It shows that the magnitude of the vibrations on the angular position and speed are negligible when compared to the accelerations. As the figure suggests, the acceleration oscillations do not affect the general quadrotor's response since the oscillations are not translated into an oscillatory pitch speed

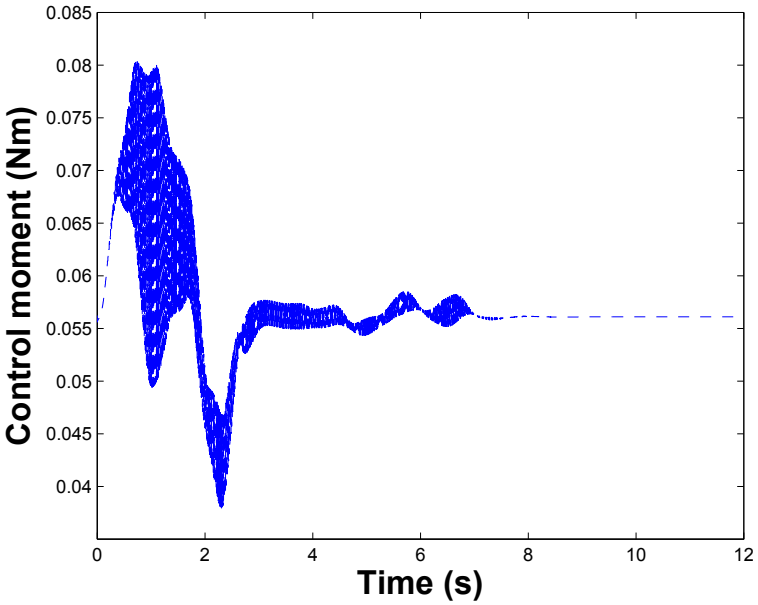

Figure 5.8: Total control moment applied to rotor 1 in order to follow the trajectory $X_n^{ref} = 7$ m, $Y_n^{ref} = 3$ m, $Z_n^{ref} = 1$ m when the complete aerodynamic model is considered.

or position. However, the feedback control contains positions, speeds and more important, accelerations. This means that the oscillations of the acceleration are in fact introduced in the control system, generating oscillating control actions (as can be seen in Figure 5.8).

These oscillations appearing in the control system could lead to saturation and the destabilization of the platform, therefore it is required to avoid their feedback into the system; however, an oscillatory control action is necessary to overcome the vibrational nature of the aerodynamic forces and their application point displacement. The vibrations in the control action cannot be avoided completely, nonetheless, their amplitude can be reduced by a predictor-corrector process.

5.2.1 Predictor-corrector process for angular acceleration oscillations.

The oscillations on the angular accelerations can not be reduced since their origin is mainly aerodynamic, increased by the numerical derivations as the software

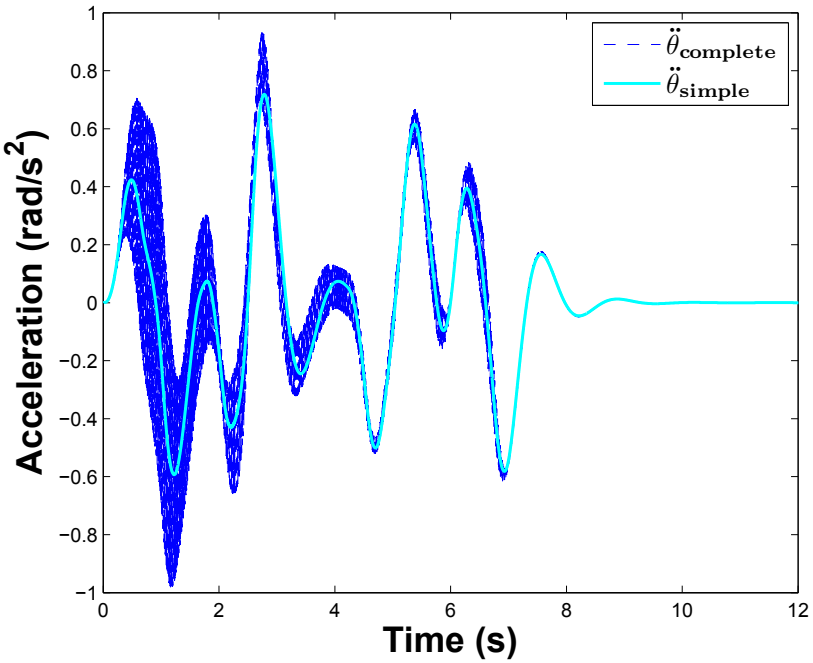

Figure 5.9: Comparison of the pitch acceleration when the aerodynamic complete and aerodynamic simple models are considered for the conventional trajectory tracking ($X_n^{ref} = 7$ m, $Y_n^{ref} = 3$ m, $Z_n^{ref} = 1$ m).

used in this research does not allow to modify the way numeric derivatives are calculated. However, the amplitude of the acceleration being fedback to the control system can be reduced notably, therefore the control action can be reduced by applying a predictor-corrector process.

The predictor-corrector process consists on using a corrected acceleration instead of the actual measured acceleration for the calculation of the control action - see equation (5.7) for pitch example.

$$(CM_3)_\theta = (k_1)_\theta(\theta_{STR}^{ref} - \theta_{STR}) + (k_2)_\theta(\dot{\theta}_{STR}^{ref} - \dot{\theta}_{STR}) + (k_3)_\theta(\ddot{\theta}_{STR}^{ref} - \ddot{\theta}_{CORR}) \quad (5.7)$$

For this calculation, the predictor-corrector process takes advantage of the fact that the angular acceleration average value of both the simple and the complete aerodynamic models are equal, as shown in Figure 5.9. Lets take the pitch acceleration as example. The complete model angular acceleration follows the same profile as the simple model plus the oscillations produced by the moving pressure

centre of the blades.

$$\ddot{\theta}_{CORR} = \ddot{\theta}_S + \frac{\ddot{\theta}_C - \ddot{\theta}_S}{k_a} \tag{5.8}$$

The corrected angular acceleration is calculated as in expression (5.8), where the subscript C refers to the aerodynamic complete model with the aerodynamic forces applied at the pressure centre of each blade and S refers to the aerodynamic simple model in which the effect of the aerodynamic forces applied to the pressure centre of the blade is cancelled as the forces are equal for both blades in a given rotor. The value of the parameter k_a varies from 1 to 8 depending on the difference between the response of the aerodynamic complete model being controlled and the supposed response it should have as predicted by the aerodynamic simple model.

In this way, if the complete model response diverges from the response of the simple model, the parameter k_a has value 1, so the corrected acceleration takes the value of the measured complete acceleration. But if the response of the complete model is similar to the simplified model response, the parameter k_a can take values from 4 to 8, occurring in this case that the corrected acceleration shares the same profile as the complete model acceleration but with a smaller amplitude, as seen in Figure 5.10.

By feeding back the corrected acceleration to the control system a smaller control action, but with the same profile, is achieved (as shown in Figure 5.11), obtaining a successful trajectory tracking with lower control actions.

The predictor-corrector process here explained can also be applied to angular speeds if necessary and could be extended to the rest of the variables. It could also be applied to measured variables that present a noise component, comparing the variables mesaured with a suitable but simplified model performance.

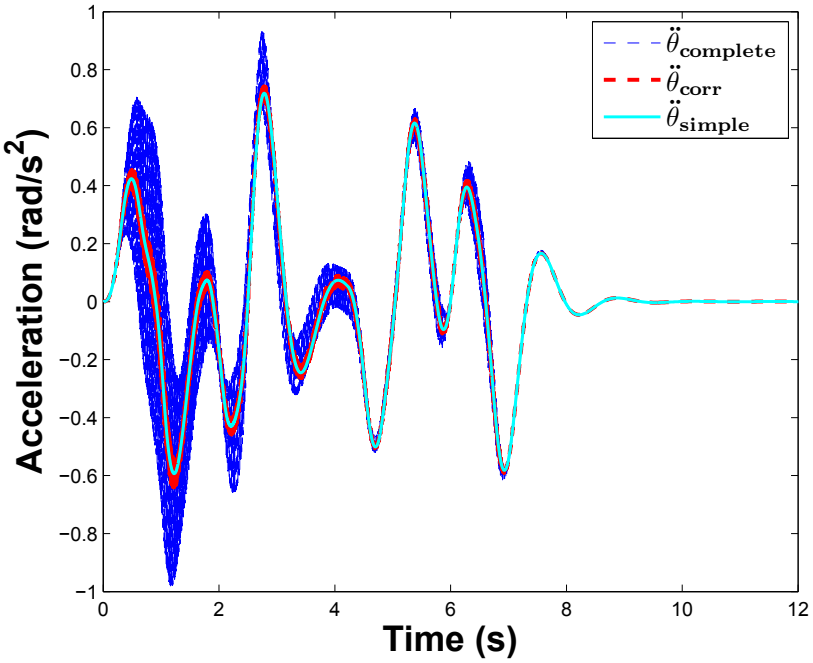

Figure 5.10: Comparison between the pitch acceleration when the same trajectory is applied ($X_n^{ref} = 7$ m, $Y_n^{ref} = 3$ m, $Z_n^{ref} = 1$ m) to different aerodynamic models: complete model, corrected model and simple model.

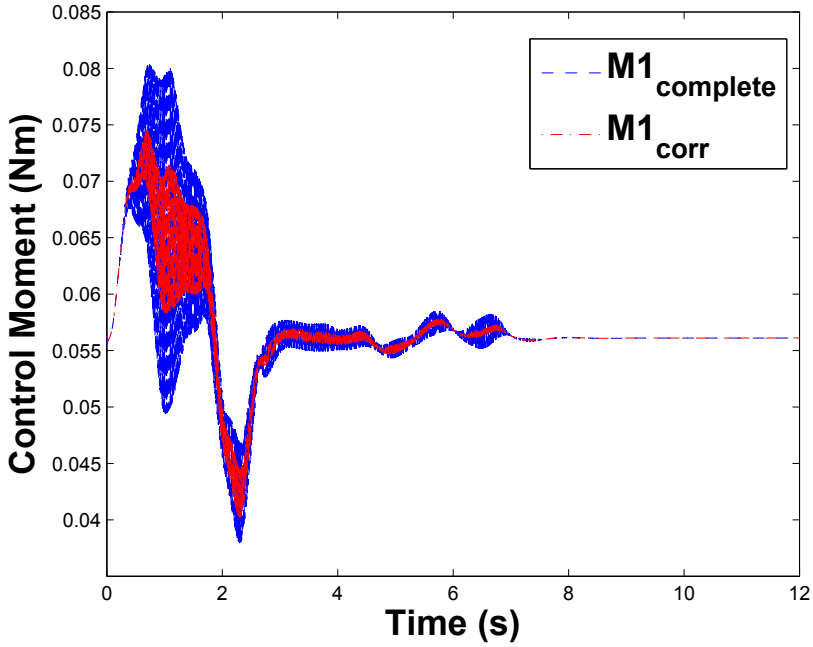

Figure 5.11: Comparison between the complete model and the corrected model control actions, for the same trajectory ($X_n^{ref} = 7$ m, $Y_n^{ref} = 3$ m, $Z_n^{ref} = 1$ m).

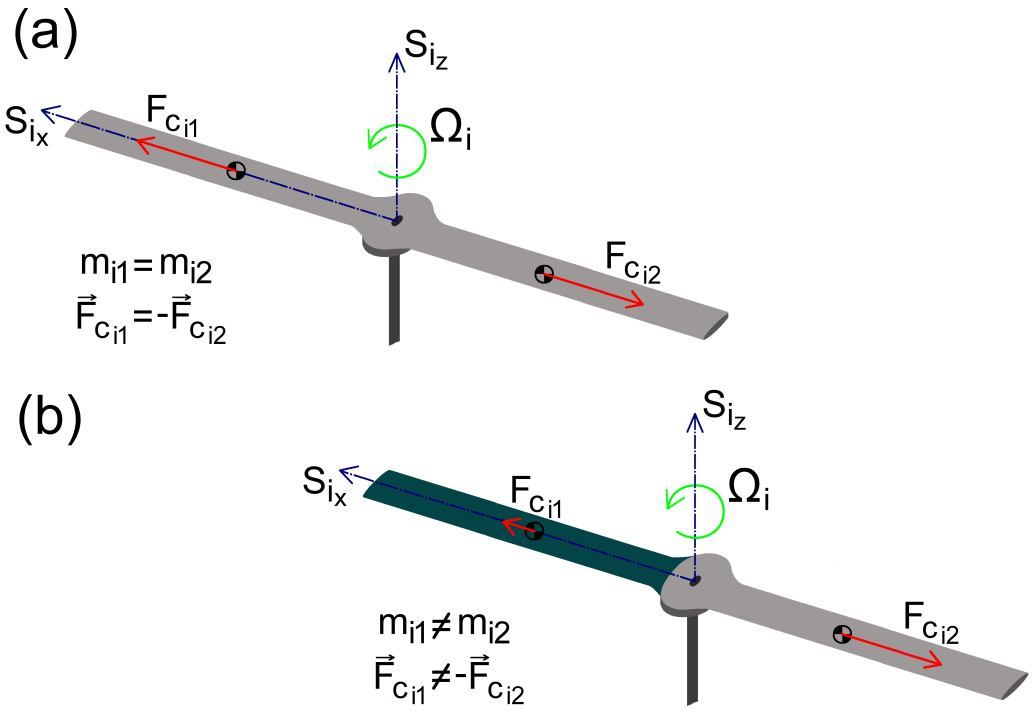

Figure 5.12: (a) Centrifugal forces acting on the two rotating blades of a compensated rotor. (b) Centrifugal force decompensation appearing in the rotor when a rotating blade with different mass is considered.

5.3 Different blade mass and blade fracture

In previous sections it has been possible to observe that the effect of the elastic blades on the overall performance of the quadrotor was not vital. However, being the blades rotating bodies they are a possible source of vibrations.

As rotating bodies, the blades experience a centrifugal force. When the two blades on one rotor have the same structural properties - mass, length, inertia, ... - the centrifugal force they experience has the same magnitude since they are rotating at the same speed, and therefore their total magnitude is balanced and the effect on the platform is cancelled. However, if any of the previous properties is different, as a different mass or length, the centrifugal force the blades experience is not the same anymore (see Figure 5.12). Therefore, the total centrifugal force is different from zero, pulling the platform in the blade's direction, which could affect the performance of the vehicle. Figure 5.13 shows

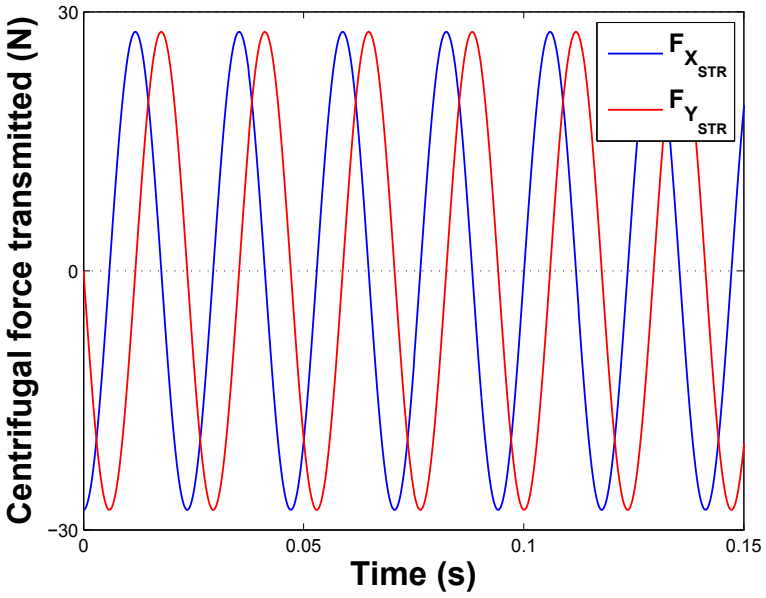

Figure 5.13: Centrifugal force transmitted to the vehicle along the $\mathtt{X}_{\mathtt{STR}}$ and $\mathtt{Y}_{\mathtt{STR}}$ axis when a complete blade is missing in rotor 1, prescribed trajectories $X_n^{ref} = 0$ m, $Y_n^{ref} = 0$ m, $Z_n^{ref} = 0$ m.

the total centrifugal force transmitted to the vehicle's structure along $\mathtt{X}_{\mathtt{STR}}$ and $\mathtt{Y}_{\mathtt{STR}}$ axes when a complete blade is missing from rotor 1. The projections of the total centrifugal force transmitted along the axes present an oscillating behaviour, which therefore produce oscillating accelerations along both axes at the rotor's rotational speed that are hardly manageable by the control system.

Since the quadrotors may be object of accidents or attacks when performing their missions, the chances of structural damage are high and need to be considered. The consequence of having a different mass blade in one of the rotors is here explored, studying how this affects the controllability of the vehicle and the overall performance. Also the study of severe differences in the blades has been addressed, as broken or complete missing blades.

5.3.1 Controllability of a different mass blade system.

Similarly to the original quadrotor system, a controllability study has been carried out for a different blade mass system. The equations of the motion when a faulty

blade is considered in rotor 1 have been obtained. Since the symbolic equations are extremely complex, they have been obtained numerically; i.e., the values of the vehicle parameters have been substituted by their numerical values, remaining only as symbolic expressions the variables and the external forces: $\phi_{STR}(t)$, $\theta_{STR}(t)$, $\psi_{STR}(t)$, $X_{STR}(\mathrm{t})$, $Y_{STR}(\mathrm{t})$, $Z_{STR}(\mathrm{t})$ - which have been redesignated as ϕ, θ, ψ, X, Y, Z in the next equations for simplicity -, rotational positions and speeds of the rotors (γ_i and Ω_i respectively), Thrust forces (T_i), Drag Moments (DM_i) and Control Moments (CM_i).

The faulty blade is in this case 5 grams instead of 6 grams (the usual weight of the blades). In order to derive the equations, a simplification has been made: the small terms bounded by sines and cosines of angles have been neglected when the constant part was at least 2 orders of magnitude higher, for example:

$$\mathcal{O}(-2) + \mathcal{O}(-4)\sin\Omega_1 + \mathcal{O}(-5)\sin\Omega_1\cos\Omega_1 \approx \mathcal{O}(-2) \tag{5.9}$$

The equations in this case are as follows:

$$\begin{aligned}\ddot{X} = {} & 9.80665\sin\theta + \dot{Y}\dot{\psi} - \dot{Z}\dot{\theta} \\ & +0.167323T_1 - 0.166953T_3 + 0.627159(CM_1 + DM_1)\sin\gamma_1 \\ & -0.000113598\cos\gamma_1\dot{\psi}\Omega_1 - 0.0000567991\cos\gamma_1\Omega_1^2\end{aligned} \tag{5.10}$$

$$\begin{aligned}\ddot{Y} = {} & -9.80665\cos\phi\sin\theta - \dot{X}\dot{\psi} + \dot{Z}\dot{\theta} \\ & +(0.0208759 - 0.630893\cos\gamma_1)CM_1 + \sum_{i=2}^{4} 0.0208759CM_i \\ & -0.165889T_2 + 0.165889T_4 - 0.630893\cos\gamma_1 DM_1 \\ & -0.000114275\sin\gamma_1\dot{\psi}\Omega_1 - 0.0000571373\sin\gamma_1\Omega_1^2\end{aligned} \tag{5.11}$$

$$\begin{aligned}\ddot{Z} = {} & 1.11145T_1 + 1.10498T_2 + 1.09851T_3 + 1.10498T_4 \\ & -9.80665\cos\theta\cos\phi + \dot{X}\dot{\phi} - \dot{Y}\dot{\theta} \\ & +0.000116476\sin\gamma_1\dot{\phi}\Omega_1 + 0.000116476\cos\gamma_1\dot{\theta}\Omega_1\end{aligned} \tag{5.12}$$

$$\ddot{\psi} = (64.3113 - 11.1974\cos\gamma_1)CM_1 + \sum_{i=2}^{4} 64.3091 CM_i$$
$$+0.0154866(T_2 - T_4) - 11.1974\cos\gamma_1 DM_1$$
$$-0.0020282\sin\gamma_1\dot{\psi}\Omega_1 - 0.0010141\sin\gamma_1\Omega_1^2 \quad (5.13)$$

$$\ddot{\phi} = -19.539T_1 + 19.4958T_3 + 1.56276\sin\gamma_1 DM_1$$
$$+(-0.00204763\sin\gamma_1 + 0.00391093\cos\gamma_1\sin\gamma_1)\dot{\phi}\Omega_1$$
$$-0.000283056\cos\gamma_1\dot{\psi}\Omega_1 + \sum_{i=2}^{4} 0.00426927\cos\gamma_i\sin\gamma_i\dot{\phi}\Omega_i$$
$$+(0.00393275 - 0.00205159\cos\gamma_1 + 0.00391853\cos{\gamma_1}^2)\dot{\theta}\Omega_1$$
$$+\sum_{i=2}^{4}(0.00393275 + 0.00427756\cos{\gamma_i}^2)\dot{\theta}\Omega_i - 0.000141528\cos\gamma_1\Omega_1^2 \quad (5.14)$$

$$\ddot{\theta} = 19.3722(T_4 - T_2) - \sum_{i=2}^{4} 0.0516219 CM_i$$
$$+(-0.0531948 + 1.56007\cos\gamma_1)CM_1 + 1.56007\cos\gamma_1 DM_1$$
$$+\left(-0.0338639 + 0.00194147\cos{\gamma_1}^2 + \sum_{i=2}^{4} 0.00212287\cos{\gamma_i}^2\right)\dot{\psi}\dot{\theta}$$
$$+0.000282578\sin\gamma_1\dot{\psi}\Omega_1 + 0.000141289\sin\gamma_1\Omega_1^2$$
$$+\sum_{i=2}^{4}(-0.00387444 - 0.0042748\sin{\gamma_i}^2)\dot{\phi}\Omega_i$$
$$-(0.00387444 + 0.00391635)\dot{\phi}\Omega_1$$
$$-0.00387969\cos\gamma_1\sin\gamma_1\dot{\theta}\Omega_1 - \sum_{i=2}^{4} 0.00423745\cos\gamma_i\sin\gamma_i\dot{\theta}\Omega_i \quad (5.15)$$

As it can be seen, the equations of the system contain similar terms to those presented in Section 4.1 for the full vehicle case and there are as well other terms that appear as the system contains a different blade mass.

The system (5.10)-(5.15) can be written as an affine control system:

$$\dot{x} = f_{0_{dif}}(x) + \sum_{i=1}^{m} u_i f_{i_{dif}}(x) \quad (5.16)$$

where the vector fields $f_{0_{dif}}$ and $f_{i_{dif}}$ can be obtained from expressions (5.10)-

(5.15) similarly to done in Section 4.2.

Composing the *Lie bracket* algebra:

$$C_{dif} = \Big[f_{0_{dif}}, f_{1_{dif}}, ...f_{4_{dif}}, \left[f_{0_{dif}}, f_{i_{dif}}\right], ..., \left[ad^k_{f_{0_{dif}}}, f_{i_{dif}}\right], \\ ..., \left[f_{4_{dif}}, f_{i_{dif}}\right], ..., \left[ad^k_{f_{4_{dif}}}, f_{i_{dif}}\right], ..\Big] \tag{5.17}$$

and calculating the rank of the accessibility distribution C_{dif}, it yields to a rank of 20, which means that the the system containing a fault (different blade mass) is still locally accessible.

5.3.2 Behaviour of a mass defective blade or fractured blade quadrotor

It has been shown that a quadrotor in which one blade has a different mass than the rest, is in theory a controllable system. However, the necessary control actions for trajectory tracking are divergent - producing a diversion in the solving method short after a second - and far higher than the maximum allowed by the rotor's specifications (Figure 5.14).

Even for the simple task of hover flight, there exits a drift in all the variables that the control system can not compensate for (Figure 5.15.b), with control actions reaching saturation and showing an oscillating nature, which is not a desirable condition (Figure 5.15.a).

Figures 5.14-5.15 correspond to a 5% mass difference on one of blades. When the blade is broken, this is, a section of the blade is missing, the tip, the Lift force produced by the rotor is reduced and the pressure centre of the blade is shifted towards the root. This, added to the centrifugal force unbalance caused by the blades' mass difference, causes an imbalance hardly manageable by the control system (Figure 5.16).

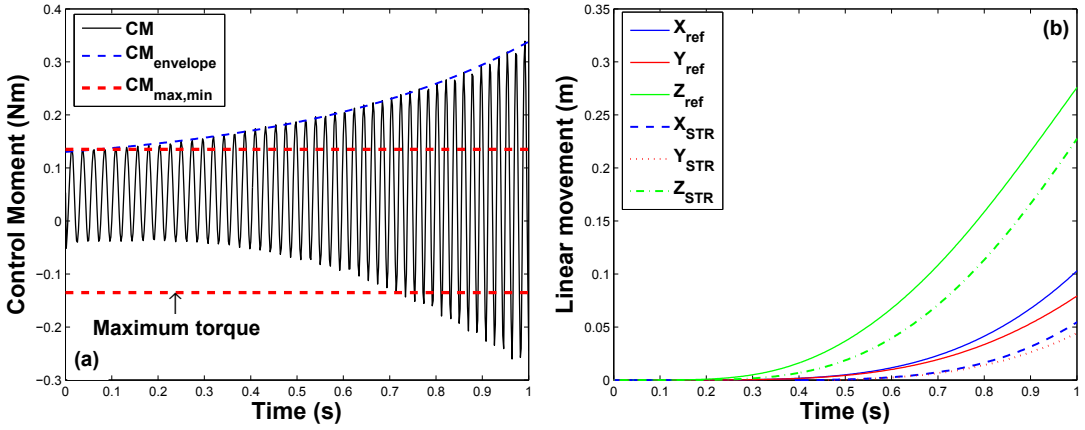

Figure 5.14: (a) Unsaturated control actions (CM) required to follow the prescribed trajectories with a 5 % defective mass blade, showing the exponential envelope of the curve (CM envelope) and the rotor's working limits (CM_{max}, CM_{min}). (b) Prescribed trajectories $X_n^{ref} = 7$ m, $Y_n^{ref} = 3$ m, $Z_n^{ref} = 1$ m) and vehicle tracking.

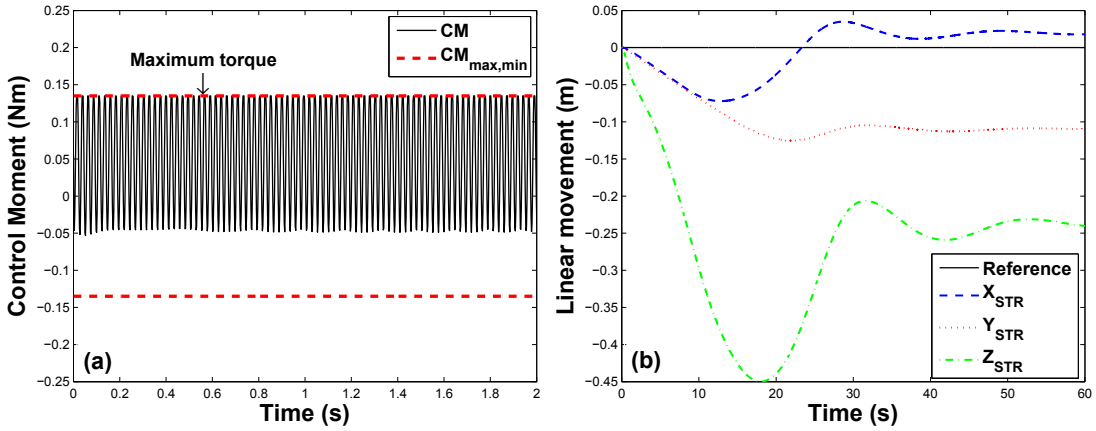

Figure 5.15: (a) Saturated control actions (CM) required to follow the prescribed trajectories with a 5 % defective mass blade, showing the rotor's working limits (CM_{max}, CM_{min}). (b) Prescribed trajectories and vehicle tracking ($X_n^{ref} = 0$ m, $Y_n^{ref} = 0$ m, $Z_n^{ref} = 0$ m).

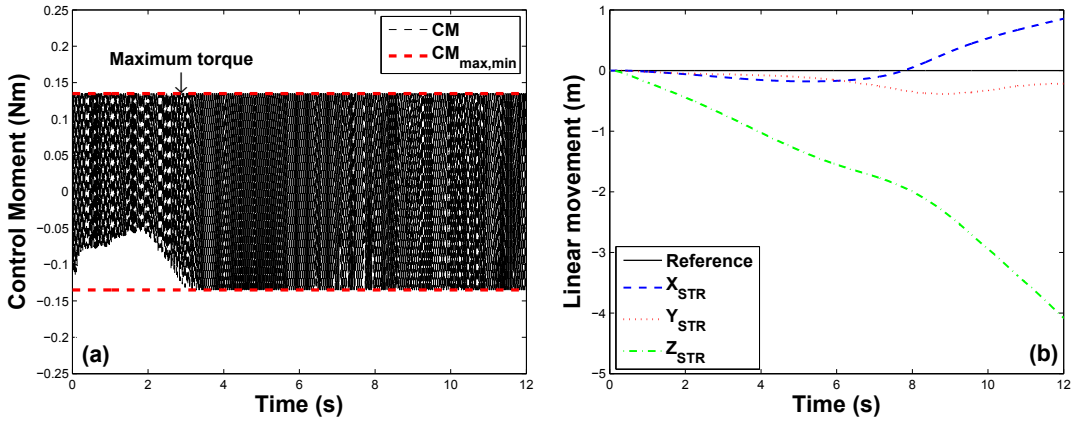

Figure 5.16: (a) Saturated control actions (CM) required to follow the prescribed trajectories with a 5 % length broken blade, showing the rotor's working limits (CM_{max}, CM_{min}). (b) Prescribed trajectories and vehicle tracking ($X_n^{ref} = 0$ m, $Y_n^{ref} = 0$ m, $Z_n^{ref} = 0$ m).

In order for the quadrotor to survive after moderate structural damage is caused, the control system can be adapted to the operative conditions to improve the general response of the vehicle.

5.3.3 Adaptive control for moderate structural damage

As could be seen in previous sections, the response of the vehicle when a faulty blade with a 5% less mass than the original one is in theory controllable. However, the system has resulted to be uncontrollable for hover and trajectory tracking.

The main problem when there is a fault on the blades is the centrifugal force unbalance appearing on the rotor, that is transmitted to the rest of the structure, reducing the overall performance of the vehicle. The oscillating centrifugal force is translated to an oscillating acceleration in both $\mathtt{X}_{\mathtt{STR}}$ and $\mathtt{Y}_{\mathtt{STR}}$ axes.

When this acceleration is included in the control system - in the PVA control method the feedback includes the acceleration of the system - the control actions increase and have a high oscillatory nature that result in the uncontrollability of the system. A solution would be to suppress the feedback of the linear acceleration of the system when a failure on the blade is detected. This can be done by

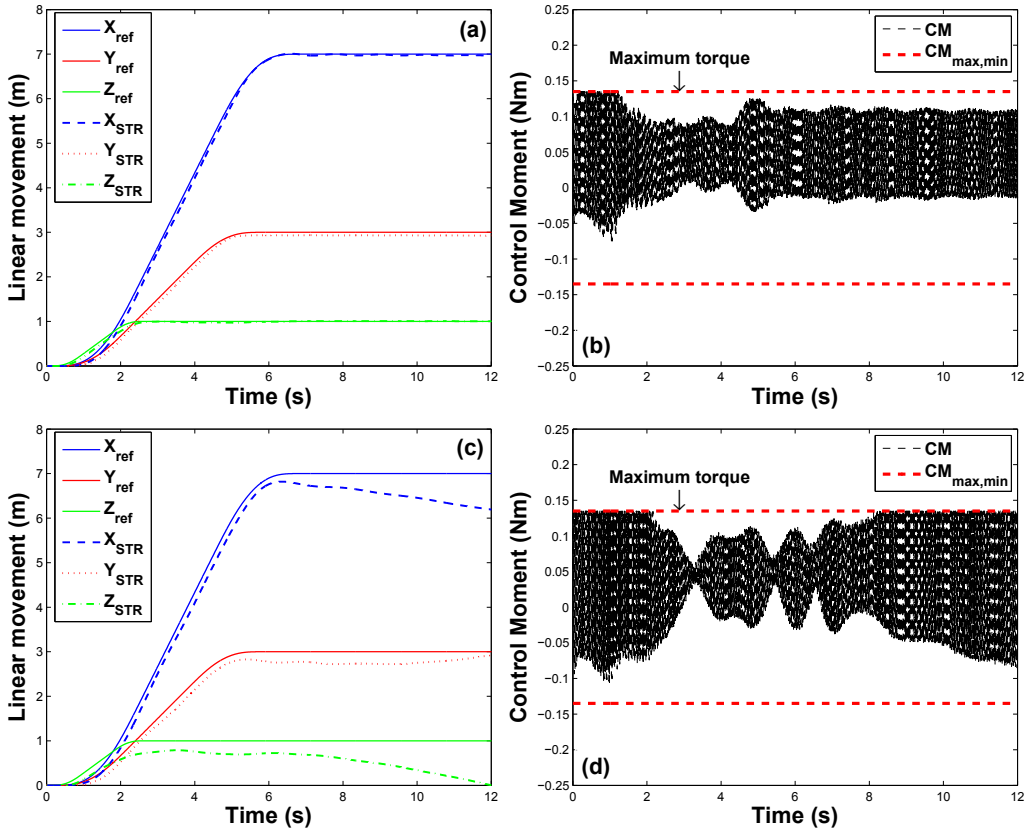

Figure 5.17: Response of the platform and control action leading to it when the modified adaptive PVA control system is applied to the vehicle for different length of broken blade: (a) Trajectory tracking with 15% of blade length broken. (b) Control moment applied to rotor 1 that lead to trajectories shown in (a). (c) Trajectory tracking with 25% blade length broken. (d) Control moment applied to rotor 1 that lead to trajectories shown in (c).

checking the acceleration, since there is a high peak of acceleration in roll or pitch when a blade breaks for the sudden decompensation of the aerodynamic forces forces, followed by a high oscillatory acceleration. By adapting the control system to the environmental and working conditions of the vehicle an improvement is achieved compared to the PVA control system.

Some simulations for different lengths of broken blade and the acceleration adaptive control system have been carried out in order to test the vehicle's behaviour when these changes are introduced.

Figure 5.17 shows the responses of the vehicle and corresponding the control action leading to it for different lengths of broken blade in rotor 1 when the

adaptive PVA control system is applied to the quadrotor. Figures 5.17.a and 5.17.b correspond to the case of 15% of the length missing, representing the trajectory tracking and the control actions necessary respectively, and the Figures 5.17.c and 5.17.d correspond to the case of 25% of the blade length missing, representing the trajectory tracking and the control actions necessary respectively, which represents a larger fault than that produced by a 5% deffective mass blade shown in Figure 5.14.

This figure shows that by adapting the control system to the changing conditions, the vehicle's performance improves such that it can fly safely with a 15% of one of the blades missing. However, for larger parts of the blade missing, the adaptive control system is not able to overcome the oscillating centrifugal force that appears and is transmitted to the structure, and that can be appreciated in the divergent control action of Figure 5.17.d.

5.3.4 Isolating control device for severe structural damage

It has been shown in the previous section that differences on the blades mass or length would affect the behaviour of the entire vehicle due to the centrifugal force that it induces, besides the decompensation the different lift forces and pressure centre location can cause. When the length of the missing section of the blade is less than 15% of the total length, the instability that the centrifugal force causes in the vehicle can be compensated by the modified adaptive control. However, when a larger section of the blade is missing, the presented adaptive control is not an effective solution and other approaches may be required.

In order to address navigation difficulties when severe structural damage has been caused to the blades, a hardware modification is necessary. An isolating control device located between the motor and the quadrotor's arm is included in order to avoid the transmission of the centrifugal force to the vehicle's structure.

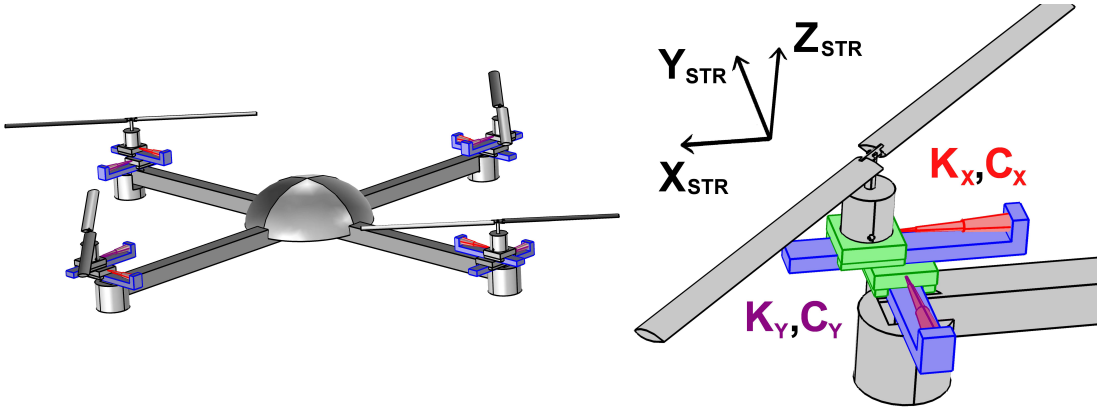

Figure 5.18: Sketch of the isolating control device located between each arm and rotor and detail of the isolating control device located in rotor S_1, with spring and damper parameters $K_{x,y}$ and $C_{x,y}$ respectively.

5.3.4.1 Description of the isolating control device

The designed isolation control device (ICD) is a mechanism attached to the end of the structure's arm, being the motor mounted on it. It allows the stator of the motor to move in a combination of two degrees of freedom - along the X_{STR} axis and the Y_{STR} axis - between some predefined values determined by its structure.

The motor motion with respect to the arm is restricted by a mechanism composed at this point by a spring and damper system (represented in red and purple in Figure 5.18). This way, allowing a small looseness between the motor and the structure, the centrifugal force is not transmitted to the structure. There exists however a reaction force transmitted from the spring and damper system to the structure. By performing an adequate choice of the spring and damping parameters, the force transmitted to the structure is minimized so that it can be managed by the control system.

5.3.4.2 Preliminary study of the isolating control device

A preliminary study of the ICD has been carried out in order to obtain adequate values for the spring and damper coefficients.

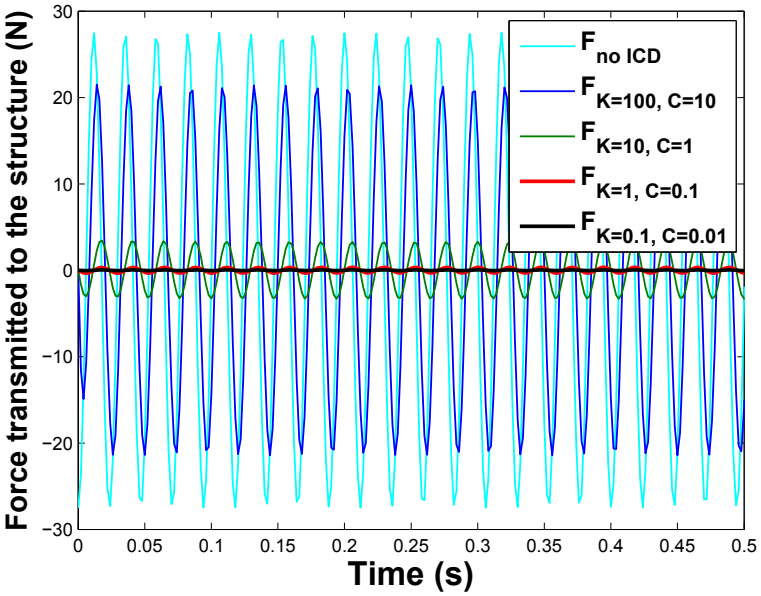

Figure 5.19: Different oscillating force transmitted to the X_{STR} axis of the structure due to the missing blade when no ICD or different ICDs are applied.

A simplified quadrotor model has been implemented for this study. It includes a main structure and four motors with their respective blades, but only one translational degree of freedom has been allowed to the structure - along its X_{STR} axis - and one translational degree of freedom has been allowed to the ICD - also along the X_{STR} axis.

In order to fully appreciate the role of the ICD a complete blade has been removed from rotor 1, and different simulations have been carried out, first, without the ICD and after including the ICD with different parameters for the spring and damper system. The aim is to obtain a pair of parameters for the spring-damper system that produces a small reaction force on the structure but simultaneously maintains a stable movement of the platform between the specific limits.

In Figure 5.19 the total force transmitted to the structure when a blade from rotor 1 is missing is represented. It shows that the force transmitted is larger when no ICD is applied, also, the lower the parameters of the spring-damper system, the smaller the force transmitted. However, when the parameters are too small, the motion of the rotor over the ICD platform is not stable enough, as

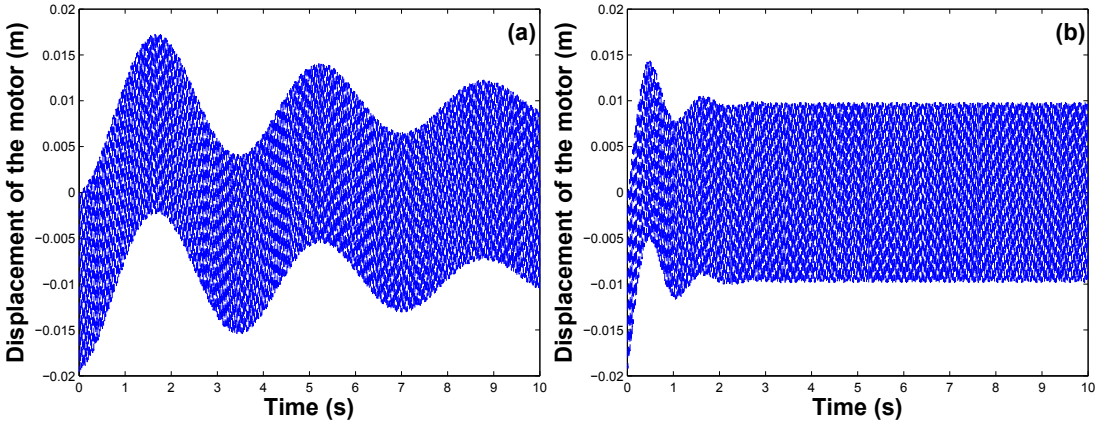

Figure 5.20: Movement of the motor over the ICD platform alog $\mathtt{X}_{\mathtt{STR}}$ axis with different spring-damper parameter values. (a) Spring and damper parameter values $K = 0.1$ N/m, $C = 0.01$ Ns/m respectively. (b) Spring and damper parameter values $K = 1$ N/m, $C = 0.1$ Ns/m respectively.

shown in Figure 5.20.

In order to adequately choose the spring-damper parameters a compromise between the force transmitted to the structure and the motion of the motor relative to the structure is needed: the lower the values of the spring-damper parameters, the lower the centrifugal force transmitted, however, the motion of the rotor with respect to the structure becomes unstable when the parameters are to small. Therefore, the parameters need to be as small as possible in order to reduce the transmission of the force, but not to low as to produce an uncontrolled rotor motion over the ICD platform.

5.3.4.3 Application of the isolating control device

After carrying out the search for the best parameters for the spring-damper system, simulations of the complete model with and without the isolating device have been carried out. Because the angular references are calculated based on lateral and longitudinal motions (4.38-4.43), the oscillations appearing in the lateral and longitudinal motion are transmitted to the angular references. In order to avoid this, a predictor-corrector method as described in Section 5.2.1 for the acceleration has been applied to the angular accelerations and angular rates ref-

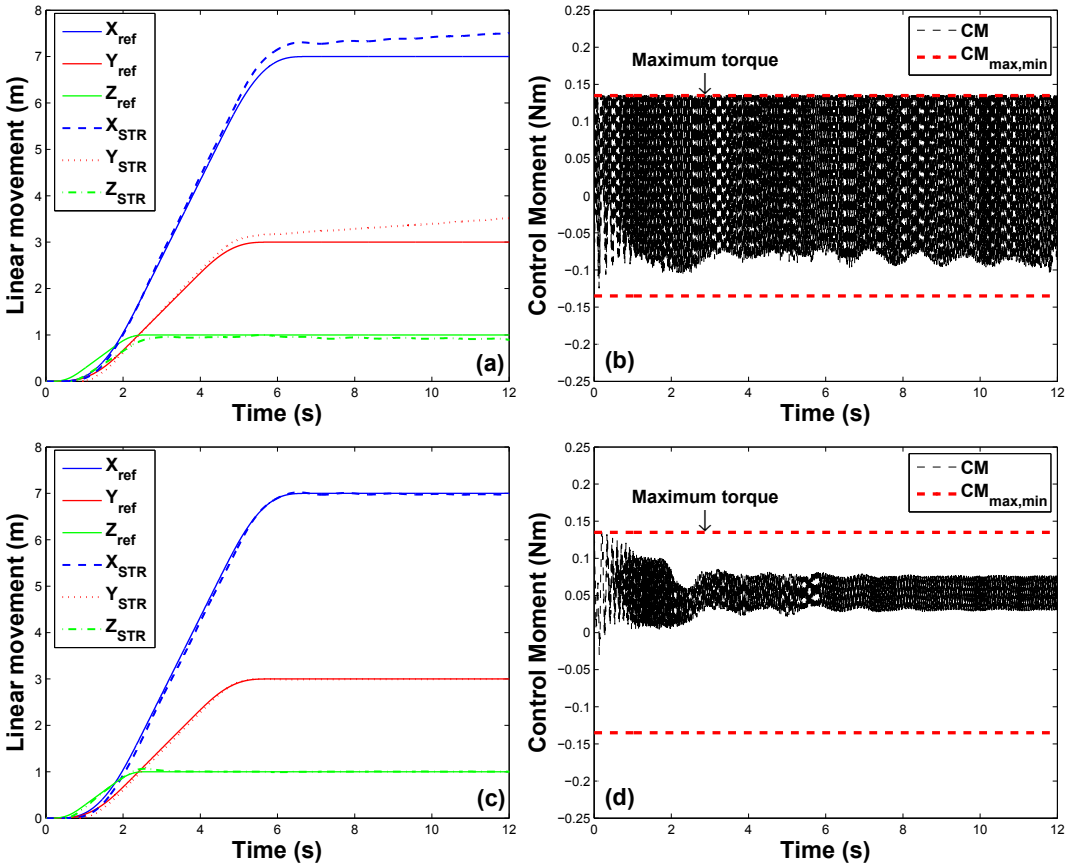

Figure 5.21: Comparison of the response of the platform with and without ICD applied when a 35% of the blade length is broken: (a) Trajectory tracking without the ICD implemented. (b) Control action applied to rotor 1 for the trajectories shown in (a). (c) Trajectory tracking with the ICD implemented. (d) Control action applied to rotor 1 for the trajectories shown in (c).

erences and also the PVA adaptive control system described in Section 5.3.3 has been implemented.

Some simulations for a 35% blade length broken have been carried out. As can be seen in Figure 5.21, the translational response with the system with no ICD could be considered acceptable. However, the control actions necessary for this show unacceptable saturation. On the other hand, the response of the trajectory tracking with the ICD fitted in the system is better and the control actions necessary for it are more acceptable, not reaching the saturation limit at any point.

Clearly the performance of the vehicle when a blade is broken is better when the

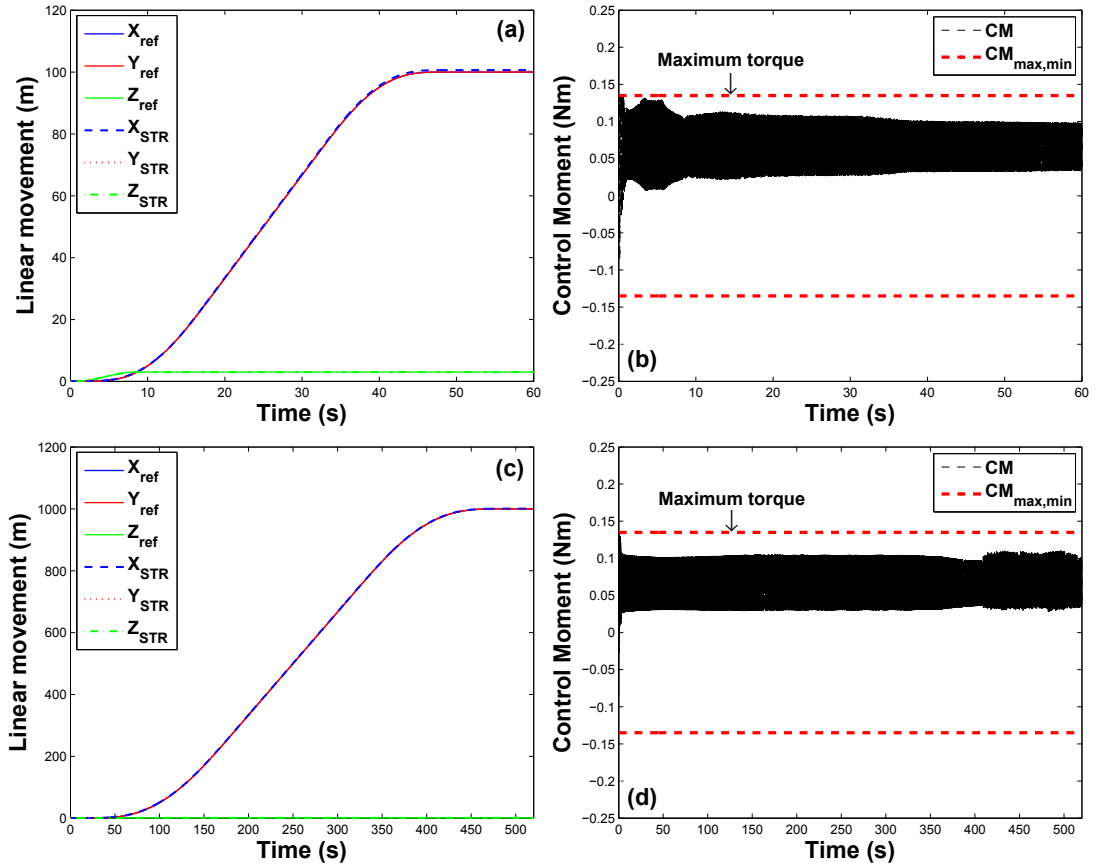

Figure 5.22: Response of the platform with the ICD installed when a complete blade is missing in rotor 1: (a) References ($X_n^{ref} = 100$ m, $Y_n^{ref} = 100$ m, $Z_n^{ref} = 3$ m) and trajectory tracking. (b) Control action applied to rotor 1 for trajectories shown in (a). (c) References ($X_n^{ref} = 1000$ m, $Y_n^{ref} = 1000$ m, $Z_n^{ref} = 3$ m) and trajectory tracking. (d) Control action applied to rotor 1 for trajectories shown in (c)

ICD is installed.

Since the main objective when a part of the vehicle is damaged is to recover it, such that it can be repaired and used in future missions, it is necessary to check that the vehicle is able to travel longer distances than those that have been simulated in here. Is for that reason that simulations with longer distances travelled and more severe structural damage have been carried out.

Figure 5.22 shows the trajectory tracking and the corresponding control action necessary when a complete blade is missing from rotor 1. The prescribed trajectory now are 100 (Figure 5.22.a) and 1000 (Figure 5.22.c) meters long in a combination of lateral and longitudinal motion, and 3 meters height. The results

in this case, show that the vehicle is capable of travelling longer distances with a complete blade missing and in spite of the control actions showing an oscillatory nature, they remain within the working limits of the motors.

It can be concluded then that an ICD could an effective method for ensuring safe flight when a sensitive part, such as a blade, is missing due to an accident or damage.

5.4 Summary of the chapter

In this chapter elastic blades have been modelled and their vibrational characterization has been carried out for different materials usually employed in quadrotors blades' manufacture.

The first and second natural frequencies of the modelled blades have been obtained for the non rotation case and for different rotational speeds, finding out that they match the expected theoretical frequencies for each material. Since the maximum deflection, the hysteretic damping and the natural frequencies of a discretized blade are found to agree with those for the continuous elastic blade for different materials, the discretization proposed is accepted as valid.

The effects of the elastic blades consideration on the overall performance of the quadrotor have been studied. It was observed that the behaviour in this case was basically the same as when rigid blades were considered, except when aluminium elastic blades were considered since they presented resonance for the flight conditions simulated.

Oscillations induced by blades' elasticity has been shown to be negligible when compared to the oscillations produced by the aerodynamic forces and their moving application points. A predictor-corrector process has been presented in order to reduce the amplitude of the oscillations - produced by the aerodynamic forces -

being fedback into the control system. It has proved to reduce the control actions amplitude, maintaining their shape and successful trajectory tracking.

The elasticity of the blades has shown not to be a principal source of vibrations, however, as they are rotating bodies, a difference in the blades properties may induce strong destabilizations on the platform. A study of the controllability for a quadrotor in which one of the blades had a different mass has been carried out. The vehicle in this case is still controllable, but it has been shown that the control actions needed to stabilize the platform are larger than the working limits of the rotors.

Different approaches have been addressed in order to tackle the destabilization produced either by a difference of blade mass, moderate or severe structural damage of the blades: a modification in the control system has shown to successfully overcome the effect of the centrifugal force unbalance induced by different mass blades and moderate structural damage (up to 25 % of broken blade); for larger parts of blade missing, a hardware modification is shown to be necessary. An isolating control device has been designed and implemented in the quadrotor model in order to reduce the transmission of the centrifugal force to the vehicle when a blade is severely damaged. An initial study of the device, which at present consists on a basic spring and damper system, has been carried out. This device has shown to effectively isolate the centrifugal force unbalance enough to allow long distances safe flight in the case of a complete blade missing.

Chapter 6

Conclusions and future work

6.1 Summary

A review of the history of unmanned and rotary-wing vehicles has been presented for the better understanding of the reader about the origins of unmanned rotorcrafts. Also a revision of the state of the art of the quadrotors study has been carried out, pointing out the areas still in need of further research in order to produce effective autonomous quadrotor platforms free of vibrations.

A rough description of the quadrotor layout and operation is provided, with an overview of the aerodynamic forces governing its behaviour. The dynamic modelling software has been introduced, pointing out its strengths and describing the methodology used for obtaining the motion equations and the integration methods included in the software.

The structural layout of the bodies composing the multibody system of the vehicle has been presented, both for rigid and elastic blades and also the equivalence between the discretized and the continuous elastic blade is shown.

Different aerodynamic models were derived: a simple one used for control system design purposes, this model that neglects the translational speed and its effects,

and a complete one needed in order to simulate a more realistic platform for the study of the vibrations propagated to the structure.

The nonlinear equations of motion have been obtained from the multibody modelling process, equivalent to the equations obtained by other methodologies, and a controllability test has been conducted on them, which showed that the system is locally reachable. A PVA control method has been implemented on the vehicle's model, including the Counter Drag Moment and smooth predefined trajectories, in order to avoid rotors' speed slowdown and discontinuous control actions. The controlled system has shown to be able to perform satisfactory trajectory tracking for different maneuvers.

The elastic blades characterization has been carried out, and it has been shown that the proposed discretization is a good representation of the static and dynamic behaviour of elastic continuous blades. The influence of blades elasticity on the overall behaviour of the vehicle has been studied, showing that its effect is negligible when compared to some aerodynamic effects. A predictor-corrector process has been designed in order to reduce some of the aerodynamic effects producing structural vibrations, which reduces the magnitude of the control actions necessary to perform a successful trajectory tracking.

The elasticity of the blades has shown not to be a major source of vibrations, however, as rotating bodies they may still induce strong destabilizations on the platform. A study of the effects of different mass blades and lengths has been carried out, showing that these conditions produce high oscillatory centrifugal forces that destabilize the vehicle. Different approaches have been addressed in order to control the destabilization produced either by a difference of blades mass, moderate or severe structural damage on the blades. A modification in the control system has shown to successfully overcome the effect of the different mass blade and moderate structural damage and an isolating control device, introduced between the structure and the rotors, has shown to efficiently isolate the centrifugal

force enough to allow the safe flight of the vehicle in spite of severe structural damage, as a full blade missing.

6.2 Conclusions

- During the development of this work a quadrotor structural multibody model was obtained. The equations representing the motion of the vehicle, obtained using VehicleSim by means of Kane's method, are equivalent to those obtained by means of other formulations, such as Newton-Euler and Lagrange methodologies. This proves the convenience of VehicleSim and Kane's equations for the modelling of multibody dynamic systems, as it is a faster and reliable method.

- Various aerodynamic models were implemented. The most complete aerodynamic model developed here considers the variation of the aerodynamic forces with the translational speed, both in magnitude and distribution. The aerodynamic force variation and the moving pressure centre on the lifting surfaces includes an oscillating generation process in the model, usually not considered in the vast majority of quadrotor models; that implies oscillating angular accelerations and therefore, the oscillating control actions necessary to control the vehicle motion.

- A new predictor-corrector method was designed and implemented for the reduction of oscillations in the angular acceleration - produced by the vehicle aerodynamics - being fedback to the control system, thus reducing the amplitude of the oscillations present in the control actions.

- The elasticity of the blades was included in the vehicle's model. The discretization used for the elastic blades modelling has shown to be valid for the static and dynamic properties representation, reaching an agreement

between the theoretical and the simulated displacements, frequencies and damping.

- With the model provided by VehicleSim and the blades elasticity included, it has been possible to study the transmitted vibrations produced by the elastic blades. It has been shown that the vibrations produced by elastic blades are negligible when compared to vibrations produced by the aerodynamic effects. However, the blades have yet shown to be an important source of vibrations, not due to their elasticity but for the centrifugal force they are submitted to as rotating bodies: it has been found that even a small difference on the blades masses in one of the rotors is enough to produce an unbalanced rotating centrifugal force that transmitted to the structure destabilizes the vehicle.

- The centrifugal force produced by a blades masses difference (or moderate structural damage) in one of the blades can be overcome by the adaptive control algorithm designed and implemented for this purpose. For the stabilization and control of the vehicle under severe structural damage, a hardware modification has shown to be necessary. An isolating control device has been designed and introduced in the vehicle's model, this highly reducing the transmission of the centrifugal force to the structure and allowing the satisfactory flying and trajectory tracking of the damaged vehicle.

6.3 Future work guidelines

Some future research paths related to the work here developed are presented in the following lines:

- The vibrations introduced by the elasticity of the blades on small scale quadrotors have shown to be negligible. However, having shown that the

software is efficient in modelling and studying the vibrations in dynamic systems, larger vehicles - in which the blades would induce higher oscillations - can be modelled for a better study and understanding of vibrations transmission in rotary-wing vehicles.

- The quadrotor modelled for this research has been considered to contain no imperfections, structurally speaking. Some of the imperfections usually present in the rotors and the joints between them and the structure could be considered in future works, since these defects could be an additional source of vibrations.

- The isolating control device presented has shown to be efficient to avoid the transmission of the oscillating centrifugal force to the structure. A possible research path would include a study of the extensive use of the ICD device and its implementation with more sophisticated elements, as adaptive or active systems, similarly to those used in advanced automotive suspension systems, which can further reduce the transmission of centrifugal forces.

6.4 List of contributions

As a result of the research carried out during these years, some contributions have been presented at symposiums, conferences and specialized journals:

- PVA control applied to a quadrotor validated through a multibody simulation model. Research Symposium 2012, City University London, UK. Poster presentation

- Control PVA aplicado a un quadrotor validado a través de un modelo de simulación multicuerpo. XXXIII Jornadas de Automática, 5^{th}-7^{th} September 2012, Vigo, Spain, pp. 393-398.

- Seguimiento de trayectorias tridimensionales de un quadrotor mediante control PVA. Revista Iberoamericana de Automática Industrial, 2014, vol. 11(1), pp. 54-67.

- Quadrotor Multibody Modelling by VehicleSim: Adaptive Technique for Oscillations in a PVA Control System. Under edition at Journal of Vibrations and Control.

- Enclosed form of elastic blades model for quadrotor applications. Under preparation.

- Quadrotors centrifugal forces isolating control devices. Under preparation.

Appendix A

Calculus of the representative point of the blade

Considering an untwisted blade of lenght R with offset eR, rotating at Ω speed and advancing at V_a speed the resultant Lift force generated by the ij blade is

$$L_{ij} = \frac{a_1}{r_{rep}^2}\left(V_{t_{ij}} + r_{rep_{ij}}\Omega_i\right)^2 = \frac{a_1/2}{r_{rep}^2}\left(V_{t_{ij}}^2 + r_{rep_{ij}}^2\Omega_i^2 + 2r_{rep_{ij}}V_{t_{ij}}\Omega_i\right) \tag{A.1}$$

where $V_{t_{ij}}$ is the projection of translational speed on the $\mathtt{Y}_{\mathtt{B}_{ij}}$ axis of the blade.

However, this Lift force is not uniformly distributed, it is depedant on the longitudinal position along the blade span. Considering the blade composed by bidimensional airfoils, the differential of lift corresponding to each section is given by expression A.2.

$$dL_{ij}(r) = \frac{a_1/2}{Rr_{rep_{ij}}^2(1-e)}V_{t_{ij}}^2 + \frac{3a_1/2}{R^3(1-e^3)}\Omega_i^2 r^2 + \frac{4a_1/2}{r_{rep_{ij}}R^2(1-e^2)}V_{t_{ij}}\Omega_i r \tag{A.2}$$

Then, the total Lift force along the blade span is just the following integral:

$$L_{ij} = \int_{eR}^{R} dL_{ij}(r)dr \tag{A.3}$$

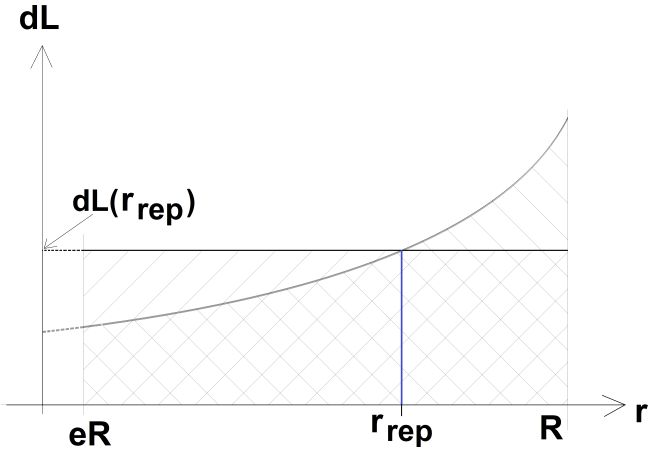

Figure A.1: Correlation between the assumed lift distribution dL(r) and an uniformly distributed lift.

The representative point is located in such a position that considering a uniform distribution of Lift force with value $dL(r_{rep})$ along the blade lenght, the total Lift force is equal to this obtained by considering the variable Lift distribution in expression A.2, as shown in Figure A.1:

$$dL_{ij}(r_{rep_{ij}})(R - eR) = \int_{eR}^{R} dL_{ij}(r)dr \tag{A.4}$$

By manipulating expression A.4 and solving for $r_{rep_{ij}}$, three solutions are obtained. Two of them are of imaginary nature, and only the third one is considered in this case for the representative point position:

$$r_{rep_{ij}} = A + \frac{\Omega_i R^2 (1+3)^3 + 2\Omega_i R^2 e(1+e) - 4V_{t_{ij}} R (1+e+e^2)}{3 (3\Omega_i + 3e\Omega_i) A} \tag{A.5}$$

where A is given by

$$A = \left[\frac{2V_{t_{ij}} R^2 e^3 + 4V_{t_{ij}} R^2 e^2 + 4V_{t_{ij}} R^2 e + 2V_{t_{ij}} R^2}{2 (3\Omega_i + 3e\Omega_i)} + \right.$$
$$+ \left(\frac{\left[2V_{t_{ij}} R^2 (1+e)^3 + 4V_{t_{ij}} R^2 e(1+e)\right]^2}{4 (3\Omega_i + 3e\Omega_i)^2} - \right.$$
$$\left. \left. - \frac{\left[\Omega_i R^2 (1+3)^3 + 2\Omega_i R^2 e(1+e) - 4V_{t_{ij}} R (1+e+e^2)\right]^3}{27 (3\Omega_i + 3e\Omega_i)^3} \right)^{\frac{1}{2}} \right]^{\frac{1}{3}} \tag{A.6}$$

By calculating the total Lift using the speed of the representative point, the Lift force would be the same as the Lift generated by the lift distribution along the blade length.

The stationary value of the representative point is calculated when the vehicle is in stationary or hover conditions; i.e. no translational velocity, $V_{t_{ij}} = 0$, and the rotational speed is the hover rotational speed $\Omega_i = \Omega_0$.

Appendix B

Calculus of the representative point of the blade's segment for elastic blades

For discretized blades, there is the need to calculate the representative point for each segment. Since the position of the representatives points do not vary significantly with the translational speed, the derivation of the points is made for stationary conditions.

Therefore, considering stationary conditions and a blade discretized in three segments of arbitrary length (x_1R, x_2R, and x_3R), the Lift distribution would be:

$$dL_{ij}(r) = \frac{3a_1/2}{R^3(1-e^3)}\Omega_i^2 r^2 \tag{B.1}$$

As before, the representative points are located in such positions that considering a uniform distribution of Lift force on each segment with value $dL(r_{rep_{ijk}})$, the total Lift force would be equal to the one obtained by considering the variable

Lift distribution in expression B.1.

$$dL_{ijk}(r_{rep_{ijk}})(r_k - r_{k-1}) = \int_{r_k}^{r_{k-1}} dL_{ijk}(r)dr \tag{B.2}$$

Solving expression B.2 for each $r_{rep_{ijk}}$ the location of the representative points are obtained for each segment:

$$r_{rep_1} = \left(\frac{1}{3}\frac{x_1^3 - e^3}{x_1 - e}\right)^{\frac{1}{2}} R \tag{B.3}$$

$$r_{rep_2} = \left(\frac{1}{3}\frac{x_2^3 - x_1^3}{x_2 - x_1}\right)^{\frac{1}{2}} R \tag{B.4}$$

$$r_{rep_3} = \left(\frac{1}{3}\frac{x_3^3 - x_2^3}{x_3 - x_2}\right)^{\frac{1}{2}} R \tag{B.5}$$

Appendix C

Calculus of the pressure centre of the blade

The pressure centre of a blade is the point where the resultant aerodynamic force acts. The position of this point varies with the pressure distribution over the blade's surface, which is dependant on the relative velocity between the blade and the air.

For incompressible regime, the pressure centre is usually located at 25 % of an airfoil blade's chord. In here, this point will be aligned with the centre of the rotor, so only the longitudinal position of the pressure centre needs to be calculated.

The position of the pressure centre is located in such a position that the moment generated by the Lift force acting at this point around the rotor centre would be the same as considering the quadratic Lift distribution along the span given by expression (A.2):

$$L_{ij} r_{cp_{ij}} = \int_{eR}^{R} dL(r) r dr \tag{C.1}$$

Therefore, the longitudinal position of the pressure centre can be calculated as:

$$r_{cp_{ij}} = \frac{\int_{eR}^{R} dL(r) r dr}{L_{ij}} \tag{C.2}$$

The numerator of equation C.2 is calculated below.

$$\int_{eR}^{R} rdL(r)dr =$$

$$\int_{eR}^{R} \left(\frac{a_1}{r_{rep_{ij}}^2 R(1-e)} V_{t_{ij}}^2 r + \frac{3a_1}{R^3(1-e^3)} \Omega_i^2 r^3 + \frac{4a_1}{r_{rep_{ij}} R^2(1-e^2)} V_{t_{ij}} \Omega_i r^2 \right) dr =$$

$$= \left[\frac{a_1 V_{t_{ij}}^2}{r_{rep_{ij}}^2 R(1-e)} \frac{1}{2} r^2 + \frac{3a_1 \Omega_i^2}{4R^3(1-e^3)} r^4 + \frac{4a_1 V_{t_{ij}} \Omega_i}{3r_{rep_{ij}} R^2(1-e^2)} r^3 \right]_{eR}^{R} =$$

$$= \frac{a_1 V_{t_{ij}}^2 R(1-e^2)}{2r_{rep_{ij}}^2(1-e)} + \frac{3a_1 R \Omega_i^2 (1-e)}{4(1-e^3)} + \frac{4a_1 V_{t_{ij}} \Omega_i R(1-e^3)}{3r_{rep_{ij}}(1-e^2)} \quad \text{(C.3)}$$

By rearranging the previous expression:

$$\int_{eR}^{R} rdL(r)dr = a_1 R \left[\frac{1}{2} \frac{V_{t_{ij}}^2}{r_{rep_{ij}}^2} \frac{1-e^2}{1-e} + \frac{4}{3} \Omega_i^2 \frac{1-e^4}{1-e^3} + \frac{4}{3} \frac{V_{t_{ij}} \Omega_i}{r_{rep_{ij}}} \frac{1-e^3}{1-e^2} \right] \quad \text{(C.4)}$$

By including equation C.4 into equation C.2, and considering the total lift, L_{ij}, given by equation A.1, the expression of the longitudinal position of the pressure centre can obtained:

$$r_{cp_{ij}} = \frac{R \left[\frac{V_{t_{ij}}^2}{2} \frac{1-e^2}{1-e} + \frac{3}{4} r_{rep_{ij}}^2 \Omega^2 \frac{1-e^4}{1-e^3} + \frac{4}{3} V_{t_{ij}} \Omega r_{rep_{ij}} \frac{1-e^3}{1-e^2} \right]}{\left[V_{t_{ij}}^2 + r_{rep_{ij}}^2 \Omega^2 + 2V_{t_{ij}} \Omega r_{rep_{ij}} \right]} \quad \text{(C.5)}$$

This is the expression derived for the pressure centre longitudinal position.

The stationary pressure centre position is calculated when the vehicle is in stationary or hover conditions; i.e. non translational velocity, $V_{t_{ij}} = 0$, and the rotational is the hover rotational speed $\Omega_i = \Omega_0$, like the in the stationary representative point case.

Appendix D

Calculus of the pressure centre of the blade's segment for elastic blades.

For discretized blades the pressure centre needs calculated for each segment, and again, the pressure centre positions are considered in such a way that the moment generated by the Lift forces applied at these points around the rotor centre is the same than considering the quadratic Lift distribution along the span.

$$dL_{ijk}(r_{rep_{ijk}})(r_k - r_{k-1})r_{cp_{ijk}} = \int_{r_{k-1}}^{r_k} dL(r)rdr \tag{D.1}$$

The longitudinal positions of the pressure centres can be calculated as:

$$r_{cp_{ijk}} = \frac{\int_{r_{k-1}}^{r_k} dL(r)rdr}{dL_{ijk}(r_k - r_{k-1})} \tag{D.2}$$

Particularizing for a three segment discretization of arbitrary length (x_1R, x_2R and x_3R) and stationary conditions, the positions of the pressure centres are:

$$r_{cp_{ij1}} = \frac{3}{4}\frac{x_1^4 - e^4}{x_1^3 - e^3}R \tag{D.3}$$

$$r_{cp_{ij2}} = \frac{3}{4}\frac{x_2^4 - x_1^4}{x_2^3 - x_1^3}R \tag{D.4}$$

$$r_{cp_{ij3}} = \frac{3}{4}\frac{x_3^4 - x_2^4}{x_3^3 - x_2^3}R \tag{D.5}$$

Appendix E

Moments' relation to maintain the forces balance

In order to maintain the quadrotor height as constant as possible when controlling roll, pitch and yaw, the increase of one rotor Thrust needs to be equal to the decrease of Thrust in the opposite rotor. To maintain the total Thrust constant, the relation of moments expressed in equations 4.33, 4.35 and 4.37 must be satisfied.

The derivation of these expressions is found in the following. The roll expression derivation is shown, and is similar to those of pitch and yaw.

As the control system was designed for the simple aerodynamic model, only rotational speed is considered in the Lift generation, and also the notation of equation 3.70 is used since it is more compact.

The necessary Thrust force in order to maintain the vehicle on hover is:

$$\mathbf{T} = \mathbf{L} = mg$$

$$a_1(\Omega_2^2 + \Omega_4^2 + 2\Omega_0^2) = mg \tag{E.1}$$

Ω_0 is the stationary rotational speed, i.e. the rotational speed necessary to maintain hover. Its magnitude is given by:

$$\Omega_0 = \sqrt{\frac{mg}{4a_1}} \tag{E.2}$$

The angular acceleration of the rotor is related to the moment applied through the rotatory inertia of the rotor by means of:

$$M_i = J_r \dot{\Omega}_i \tag{E.3}$$

By integrating equation E.3, the angular speed of the rotor can be found as:

$$\Omega_i = \int \frac{M_i}{J_r} dt \tag{E.4}$$

By substituting the expression of angular speed given by equation E.4 into equation E.1, a different expression for the hover condition can be obtained, now this is a expression dependent on the applied moments:

$$a_1 \left(\left(\int \frac{M_2}{J_r} dt \right)^2 + \left(\int \frac{M_4}{J_r} dt \right)^2 + 2\Omega_0^2 \right) = mg \tag{E.5}$$

Substituting the value of Ω_0 into the equation E.5 and rearranging, gives:

$$\int \left(\frac{M_4}{J_r} \right) dt = \sqrt{\frac{mg}{2a_1} - \left(\int \frac{M_2}{J_r} dt \right)^2} \tag{E.6}$$

By deriving equation E.6 with respect to time yields:

$$\frac{d}{dt} \left(\int \left(\frac{M_4}{J_r} \right) dt \right) = -2 \frac{1}{2} \frac{\int \left(\frac{M_2}{J_r} \right) dt}{\sqrt{\frac{mg}{2a_1} - \left(\int \frac{M_2}{J_r} dt \right)^2}} \frac{d}{dt} \left(\int \left(\frac{M_2}{J_r} \right) dt \right) \tag{E.7}$$

Considering the Fundamental Theorem of Calculus E.0.1 [165], and taking into account that the angular acceleration is continuous in the interval $[0, t]$, E.7 can

be rewritten as:

$$\left(\frac{M_4}{J_r}\right) = -\frac{\int\left(\frac{M_2}{J_r}\right)dt}{\sqrt{\frac{mg}{2a_1} - \left(\int \frac{M_2}{J_r}dt\right)^2}}\left(\frac{M_2}{J_r}\right) \tag{E.8}$$

Finally, introducing expression E.4 into equation E.8, the the next relation is obtained:

$$\frac{M_4}{J_r} = -\frac{\Omega_2}{\sqrt{\frac{mg}{2a_1} - (\Omega_2)^2}}\frac{M_2}{J_r} \tag{E.9}$$

This relation between the control moments applied decreases the height control effort, since this relation helps to keep a constant total Lift force during maneuvers.

Fundamental Theorem of Calculus. E.0.1 *If $f(x)$ is a continuous and derivable function in the interval $I \subseteq \mathbb{R}$ y $a \in I$, then the function G defined by:*

$$G(x) = \int_a^x f(x)dx$$

is derivable in int(I) and also $G'(x) = f(x)$ in int(I).

Bibliography

[1] K. Nonami, "Prospect and recent research & development for civil use autonomous unmanned aircraft as uav and mav," *Journal of System Design and Dynamics*, vol. 1, no. 2, pp. 120–128, 2007.

[2] Yamaha, *http://rmax.yamaha-motor.com.au/*. Last visited 28^{th} August 2015, 2015.

[3] Draganfly, *http://www.draganfly.com/*. Last visited 28^{th} August 2015, 2015.

[4] L. Martin, *http://www.lockheedmartin.com/us/products/lighter-than-air-vehicles/haa.html*. Last visited 28^{th} August 2015, 2015.

[5] M. L. of the Delft University of Technology, *http://mavlab.lr.tudelft.nl/*. Last visited 28^{th} August 2015, 2015.

[6] Visiongain, "Unmanned aerial vehicles (auv) market 2009-2019," 2009.

[7] L. Dickerson, "Uavs on the rise," *Aviation Week & Space Technology*, vol. 166, no. 3, pp. 114 – 116, 2007.

[8] "Unmanned aerial vehicles roadmap, 2002-2027," *Office of the U.S. Secretary of Defense*, 2002.

[9] D. Weatherington and U. Deputy, "Unmanned aircraft systems roadmap, 2005-2030," *Deputy, UAV Planning Task Force, OUSD (AT&L)*, 2005.

[10] K. Nonami, F. Kendoul, S. Suzuki, W. Wang, and D. Nakazawa, *Autonomous Flying Robots*. Springer Japan, 2010.

[11] A. C. Gellius, *Noctes Atticae*. Perseus Digital Library, 1927.

[12] K. Dalamagkidis, "Aviation history and unmanned flight," in *Handbook of Unmanned Aerial Vehicles* (K. P. Valavanis and G. J. Vachtsevanos, eds.), pp. 57–81, Springer Netherlands, 2015.

[13] A. Gessow and G. C. Myers, *Aerodynamics of the Helicopter*. Frederick Ungar, 1952.

[14] S. S. McGowen, *Helicopters: an illustrated history of their impact*. ABC-CLIO, 2005.

[15] J. G. Leishman, *Principles of Helicopter Aerodynamics*. Cambridge university press, 2006.

[16] *http://www.aviastar.org/*. Last visited 26^{th} June 2013, 2013.

[17] B. W. McCormick, B. W. McCormick, and B. W. McCormick, *Aerodynamics, aeronautics, and flight mechanics*, vol. 2. Wiley New York, 1995.

[18] M. Béjar and A. Ollero, "Modelado y control de helicópteros autónomos. revisión del estado de la técnica," *Revista Iberoamericana de Automática e Informática Industrial {RIAI}*, vol. 5, no. 4, pp. 5 – 16, 2008.

[19] A. Ollero and I. Maza, *Multiple Heterogeneous Unmanned Aerial Vehicles*. Heidelberg: Springer Berlin, 2007.

[20] M. Achtelik, A. Bachrach, R. He, S. Prentice, and N. Roy, "Autonomous navigation and exploration of a quadrotor helicopter in gps-denied indoor environments," in *First Symposium on Indoor Flight*, no. 2009, 2009.

[21] M. Orsag and S. Bogdan, "Hybrid control of quadrotor," in *Control and Automation, 2009. MED '09. 17th Mediterranean Conference on*, pp. 1239–1244, June 2009.

[22] N. Kottenstette and J. Porter, "Digital passive attitude and altitude control schemes for quadrotor aircraft," in *Control and Automation, 2009. ICCA 2009. IEEE International Conference on*, pp. 1761–1768, Dec 2009.

[23] P.-J. Bristeau, P. Martin, E. Salaun, and N. Petit, "The role of propeller aerodynamics in the model of a quadrotor uav," in *Control Conference (ECC), 2009 European*, pp. 683–688, Aug 2009.

[24] A. Rodic and G. Mester, "Modeling and simulation of quad-rotor dynamics and spatial navigation," in *Intelligent Systems and Informatics (SISY), 2011 IEEE 9th International Symposium on*, pp. 23–28, Sept 2011.

[25] A. Rodić and G. Mester, "The modeling and simulation of an autonomous quad-rotor microcopter in a virtual outdoor scenario," *Acta Polytechnica Hungarica*, vol. 8, no. 4, pp. 107–122, 2011.

[26] R. Zhang, X. Wang, and K.-Y. Cai, "Quadrotor aircraft control without velocity measurements," in *Decision and Control, 2009 held jointly with the 2009 28th Chinese Control Conference. CDC/CCC 2009. Proceedings of the 48th IEEE Conference on*, pp. 5213–5218, Dec 2009.

[27] S. González-Vázquez and J. Moreno-Valenzuela, "A new nonlinear pipid controller for quadrotor posture regulation," in *Electronics, Robotics and Automotive Mechanics Conference (CERMA), 2010*, pp. 642–647, Sept 2010.

[28] E. Stingu and F. Lewis, "Design and implementation of a structured flight controller for a 6dof quadrotor using quaternions," in *Control and Automation, 2009. MED '09. 17th Mediterranean Conference on*, pp. 1233–1238, June 2009.

[29] S. Lesecq, S. Gentil, and N. Daraoui, "Quadrotor attitude estimation with data losses," in *Control Conference (ECC), 2009 European*, pp. 3851–3856, Aug 2009.

[30] J. Guerrero-Castellanos, N. Marchand, A. Hably, S. Lesecq, and J. Delamare, "Bounded attitude control of rigid bodies: Real-time experimentation to a quadrotor mini-helicopter," *Control Engineering Practice*, vol. 19, no. 8, pp. 790 – 797, 2011.

[31] J. Guerrero-Castellanos, J. Tállez-Guzmán, S. Durand, N. Marchand, J. Alvarez-Munoz, and V. González-Díaz, "Attitude stabilization of a quadrotor by means of event-triggered nonlinear control," *Journal of Intelligent & Robotic Systems*, vol. 73, no. 1-4, pp. 123–135, 2014.

[32] T. Lee, "Robust adaptive attitude tracking on so(3) with an application to a quadrotor uav," *Control Systems Technology, IEEE Transactions on*, vol. 21, pp. 1924–1930, Sept 2013.

[33] B. S. M. Henriques, *Estimation and control of a quadrotor attitude*. PhD thesis, Master's thesis, Instituto Superior Técnico, 2011.

[34] S. Seghour, M. Bouchoucha, and H. Osmani, "From integral backstepping to integral sliding mode attitude stabilization of a quadrotor system: Real time implementation on an embedded control system based on a dspic μc," in *Mechatronics (ICM), 2011 IEEE International Conference on*, pp. 154–161, April 2011.

[35] R. Czyba, "Design of attitude control system for an uav type-quadrotor based on dynamic contraction method," in *Advanced Intelligent Mechatronics, 2009. AIM 2009. IEEE/ASME International Conference on*, pp. 644–649, July 2009.

[36] J. Kim, M.-S. Kang, and S. Park, "Accurate modeling and robust hovering control for a quad-rotor vtol aircraft," in *Selected papers from the 2nd International Symposium on UAVs, Reno, Nevada, USA June 8–10, 2009*, pp. 9–26, Springer, 2010.

[37] I. González, S. Salazar, J. Torres, R. Lozano, and H. Romero, "Real-time attitude stabilization of a mini-uav quad-rotor using motor speed feedback," *Journal of Intelligent & Robotic Systems*, vol. 70, no. 1-4, pp. 93–106, 2013.

[38] A. Salih, M. Moghavvemi, H. Mohamed, and K. Gaeid, "Modelling and pid controller design for a quadrotor unmanned air vehicle," in *Automation Quality and Testing Robotics (AQTR), 2010 IEEE International Conference on*, vol. 1, pp. 1–5, May 2010.

[39] K. T. Öner, E. Çetinsoy, M. Ünel, M. F. Akşit, I. Kandemir, and K. Gülez, "Dynamic model and control of a new quadrotor unmanned aerial vehicle with tilt-wing mechanism," 2008.

[40] D. Snyder, "The quad tiltrotor: its beginning and evolution," in *Proceedings of the 56th Annual Forum, American Helicopter Society, Virginia Beach, Virginia*, 2000.

[41] M. Ryll, H. Bulthoff, and P. Giordano, "Modeling and control of a quadrotor uav with tilting propellers," in *Robotics and Automation (ICRA), 2012 IEEE International Conference on*, pp. 4606–4613, May 2012.

[42] J. Escareño, S. Salazar, H. Romero, and R. Lozano, "Trajectory control of a quadrotor subject to 2d wind disturbances," *Journal of Intelligent & Robotic Systems*, vol. 70, no. 1-4, pp. 51–63, 2013.

[43] D. Lara, G. Romero, A. Sanchez, R. Lozano, and A. Guerrero, "Robustness margin for attitude control of a four rotor mini-rotorcraft: Case of study," *Mechatronics*, vol. 20, no. 1, pp. 143 – 152, 2010. Special Issue on Servo Control for Data Storage and Precision Systems, from 17th {IFAC} World Congress 2008.

[44] S.-H. Jeong and S. Jung, "Experimental studies of a disturbance observer for attitude control of a quad-rotor system," in *Control, Automation and*

Systems (ICCAS), 2012 12th International Conference on, pp. 579–583, Oct 2012.

[45] A. Azzam and X. Wang, "Quad rotor arial robot dynamic modeling and configuration stabilization," in *Informatics in Control, Automation and Robotics (CAR), 2010 2nd International Asia Conference on*, vol. 1, pp. 438–444, March 2010.

[46] Y. Bouktir, M. Haddad, and T. Chettibi, "Trajectory planning for a quadrotor helicopter," in *Control and Automation, 2008 16th Mediterranean Conference on*, pp. 1258–1263, June 2008.

[47] J. Li and Y. Li, "Dynamic analysis and pid control for a quadrotor," in *Mechatronics and Automation (ICMA), 2011 International Conference on*, pp. 573–578, Aug 2011.

[48] G. M. Hoffmann, H. Huang, S. L. Waslander, and C. J. Tomlin, "Quadrotor helicopter flight dynamics and control: Theory and experiment," in *Proc. of the AIAA Guidance, Navigation, and Control Conference*, vol. 2, 2007.

[49] S. Bouabdallah, P. Murrieri, and R. Siegwart, "Design and control of an indoor micro quadrotor," in *Robotics and Automation, 2004. Proceedings. ICRA '04. 2004 IEEE International Conference on*, vol. 5, pp. 4393–4398 Vol.5, April 2004.

[50] K. Alexis, C. Papachristos, G. Nikolakopoulos, and A. Tzes, "Model predictive quadrotor indoor position control," in *Control Automation (MED), 2011 19th Mediterranean Conference on*, pp. 1247–1252, June 2011.

[51] H. Voos, "Nonlinear control of a quadrotor micro-uav using feedback-linearization," in *Mechatronics, 2009. ICM 2009. IEEE International Conference on*, pp. 1–6, April 2009.

[52] C. Berbra, S. Lesecq, and J. Martinez, "A multi-observer switching strategy for fault-tolerant control of a quadrotor helicopter," in *Control and*

Automation, 2008 16th Mediterranean Conference on, pp. 1094–1099, June 2008.

[53] S. Bouabdallah and R. Siegwart, "Full control of a quadrotor," in *Intelligent Robots and Systems, 2007. IROS 2007. IEEE/RSJ International Conference on*, pp. 153–158, Oct 2007.

[54] S. hyun Lee, S. H. Kang, and Y. Kim, "Trajectory tracking control of quadrotor uav," in *Control, Automation and Systems (ICCAS), 2011 11th International Conference on*, pp. 281–285, Oct 2011.

[55] A. A. Mian and W. Daobo, "Modeling and backstepping-based nonlinear control strategy for a 6 {DOF} quadrotor helicopter," *Chinese Journal of Aeronautics*, vol. 21, no. 3, pp. 261 – 268, 2008.

[56] M. Bouchoucha, M. Tadjine, A. Tayebi, and P. Mullhaupt, "Step by step robust nonlinear pi for attitude stabilisation of a four-rotor mini-aircraft," in *Control and Automation, 2008 16th Mediterranean Conference on*, pp. 1276–1283, June 2008.

[57] A. Benallegue, A. Mokhtari, and L. Fridman, "Feedback linearization and high order sliding mode observer for a quadrotor uav," in *Variable Structure Systems, 2006. VSS'06. International Workshop on*, pp. 365–372, June 2006.

[58] Q.-L. Zhou, Y. Zhang, C. Rabbath, and D. Theilliol, "Design of feedback linearization control and reconfigurable control allocation with application to a quadrotor uav," in *Control and Fault-Tolerant Systems (SysTol), 2010 Conference on*, pp. 371–376, Oct 2010.

[59] T. Madani and A. Benallegue, "Sliding mode observer and backstepping control for a quadrotor unmanned aerial vehicles," in *American Control Conference, 2007. ACC '07*, pp. 5887–5892, July 2007.

[60] M. V. P. Giraldo, E. C. V. Gonzales, and C. I. R. Feliciano, "Modelamiento dinámico y control lqr de un quadrotor," *Avances: Investigacion en Ingeniería*, no. 13, pp. 71–86, 2010.

[61] S. Jeong, S. Jung, and M. Tomizuka, "Attitude control of a quad-rotor system using an acceleration-based disturbance observer: An empirical approach," in *Advanced Intelligent Mechatronics (AIM), 2012 IEEE/ASME International Conference on*, pp. 916–921, July 2012.

[62] Y. Naidoo, R. Stopforth, and G. Bright, "Quad-rotor unmanned aerial vehicle helicopter modelling & control," *International Journal of Advanced Robotic Systems*, vol. 8, no. 4, pp. 139–149, 2011.

[63] S. Bouabdallah, A. Noth, and R. Siegwart, "Pid vs lq control techniques applied to an indoor micro quadrotor," in *Intelligent Robots and Systems, 2004. (IROS 2004). Proceedings. 2004 IEEE/RSJ International Conference on*, vol. 3, pp. 2451–2456 vol.3, Sept 2004.

[64] A. Patel, M. Patel, and D. Vyas, "Modeling and analysis of quadrotor using sliding mode control," in *System Theory (SSST), 2012 44th Southeastern Symposium on*, pp. 111–114, March 2012.

[65] R. Xu and U. Ozguner, "Sliding mode control of a quadrotor helicopter," in *Decision and Control, 2006 45th IEEE Conference on*, pp. 4957–4962, Dec 2006.

[66] A. Das, F. Lewis, and K. Subbarao, "Backstepping approach for controlling a quadrotor using lagrange form dynamics," *Journal of Intelligent and Robotic Systems*, vol. 56, no. 1-2, pp. 127–151, 2009.

[67] G. V. Raffo, M. G. Ortega, and F. R. Rubio, "An integral predictivenonlinear control structure for a quadrotor helicopter," *Automatica*, vol. 46, no. 1, pp. 29 – 39, 2010.

[68] J. M. B. Domingues, "Quadrotor prototype," *Uneversidade Tecnica de Lisboa. Dissertacão*, 2009.

[69] E. Fresk and G. Nikolakopoulos, "Full quaternion based attitude control for a quadrotor," in *Control Conference (ECC), 2013 European*, pp. 3864–3869, July 2013.

[70] R. Zhang, Q. Quan, and K.-Y. Cai, "Attitude control of a quadrotor aircraft subject to a class of time-varying disturbances," *Control Theory Applications, IET*, vol. 5, pp. 1140–1146, June 2011.

[71] A. Honglei, L. Jie, W. Jian, and W. J. M. Hongxu, "Backstepping-based inverse optimal attitude control of quadrotor," *International Journal of Advanced Robotic Systems*, vol. 10, 2013.

[72] A. Tayebi and S. McGilvray, "Attitude stabilization of a vtol quadrotor aircraft," *Control Systems Technology, IEEE Transactions on*, vol. 14, pp. 562–571, May 2006.

[73] A. Tayebi and S. McGilvray, "Attitude stabilization of a four-rotor aerial robot," in *Decision and Control, 2004. CDC. 43rd IEEE Conference on*, vol. 2, pp. 1216–1221 Vol.2, Dec 2004.

[74] J.-Y. Wen and K. Kreutz-Delgado, "The attitude control problem," *Automatic Control, IEEE Transactions on*, vol. 36, pp. 1148–1162, Oct 1991.

[75] B. L. Stevens and F. L. Lewis, *Aircraft control and simulation*. John Wiley & Sons, 2003.

[76] A. Sanchez, L. García Carrillo, E. Rondon, R. Lozano, and O. Garcia, "Hovering flight improvement of a quad-rotor mini uav using brushless dc motors," *Journal of Intelligent & Robotic Systems*, vol. 61, no. 1-4, pp. 85–101, 2011.

[77] A.-L. Chan, S.-L. Tan, and C.-L. Kwek, "Sensor data fusion for attitude stabilization in a low cost quadrotor system," in *Consumer Electronics (ISCE), 2011 IEEE 15th International Symposium on*, pp. 34–39, June 2011.

[78] P. Pounds, R. Mahony, and P. Corke, "Modelling and control of a large quadrotor robot," *Control Engineering Practice*, vol. 18, no. 7, pp. 691 – 699, 2010. Special Issue on Aerial Robotics.

[79] H. Huang, G. Hoffmann, S. Waslander, and C. Tomlin, "Aerodynamics and control of autonomous quadrotor helicopters in aggressive maneuvering," in *Robotics and Automation, 2009. ICRA '09. IEEE International Conference on*, pp. 3277–3282, May 2009.

[80] Y. Al-Younes, M. Al-Jarrah, and A. Jhemi, "Linear vs. nonlinear control techniques for a quadrotor vehicle," in *Mechatronics and its Applications (ISMA), 2010 7th International Symposium on*, pp. 1–10, April 2010.

[81] S. Park, D. Won, M. Kang, T. Kim, H. Lee, and S. Kwon, "Ric (robust internal-loop compensator) based flight control of a quad-rotor type uav," in *Intelligent Robots and Systems, 2005. (IROS 2005). 2005 IEEE/RSJ International Conference on*, pp. 3542–3547, Aug 2005.

[82] B. Erginer and E. Altug, "Modeling and pd control of a quadrotor vtol vehicle," in *Intelligent Vehicles Symposium, 2007 IEEE*, pp. 894–899, June 2007.

[83] K. Alexis, G. Nikolakopoulos, and A. Tzes, "Constrained optimal attitude control of a quadrotor helicopter subject to wind-gusts: Experimental studies," in *American Control Conference (ACC), 2010*, pp. 4451–4455, June 2010.

[84] G. Lee, D. Y. Jeong, N. D. Khoi, and T. Kang, "Attitude control system design for a quadrotor flying robot," in *Ubiquitous Robots and Ambient*

Intelligence (URAI), 2011 8th International Conference on, pp. 74–78, Nov 2011.

[85] H. Voos, "Nonlinear and neural network-based control of a small four-rotor aerial robot," in *Advanced intelligent mechatronics, 2007 IEEE/ASME international conference on*, pp. 1–6, Sept 2007.

[86] H. Voos, "Nonlinear state-dependent riccati equation control of a quadrotor uav," in *Computer Aided Control System Design, 2006 IEEE International Conference on Control Applications, 2006 IEEE International Symposium on Intelligent Control, 2006 IEEE*, pp. 2547–2552, Oct 2006.

[87] A. Mokhtari and A. Benallegue, "Dynamic feedback controller of euler angles and wind parameters estimation for a quadrotor unmanned aerial vehicle," in *Robotics and Automation, 2004. Proceedings. ICRA '04. 2004 IEEE International Conference on*, vol. 3, pp. 2359–2366 Vol.3, April 2004.

[88] A. Khalifa, M. Fanni, A. Ramadan, and A. Abo-Ismail, "Modeling and control of a new quadrotor manipulation system," in *Innovative Engineering Systems (ICIES), 2012 First International Conference on*, pp. 109–114, Dec 2012.

[89] A. Mian and W. Daobo, "Nonlinear flight control strategy for an underactuated quadrotor aerial robot," in *Networking, Sensing and Control, 2008. ICNSC 2008. IEEE International Conference on*, pp. 938–942, 2008.

[90] I. Palunko and R. Fierro, "Adaptive feedback controller design and quadrotor modelin with dynamic changes of center of gravity," in *18th IFAC World Congress*, August-September 2011.

[91] D. Lee, H. Jin Kim, and S. Sastry, "Feedback linearization vs. adaptive sliding mode control for a quadrotor helicopter," *International Journal of Control, Automation, and Systems*, vol. 7, pp. 419–428, 06 2009.

[92] L. Derafa, A. Benallegue, and L. Fridman, "Super twisting control algorithm for the attitude tracking of a four rotors {UAV}," *Journal of the Franklin Institute*, vol. 349, no. 2, pp. 685 – 699, 2012. Advances in Guidance and Control of Aerospace Vehicles using Sliding Mode Control and Observation Techniques.

[93] C. T. Ton and W. MacKunis, "Robust attitude tracking control of a quadrotor helicopter in the presence of uncertainty," in *Decision and Control (CDC), 2012 IEEE 51st Annual Conference on*, pp. 937–942, Dec 2012.

[94] H. Bouadi, S. Simoes Cunha, A. Drouin, and F. Mora-Camino, "Adaptive sliding mode control for quadrotor attitude stabilization and altitude tracking," in *Computational Intelligence and Informatics (CINTI), 2011 IEEE 12th International Symposium on*, pp. 449–455, Nov 2011.

[95] Z. Fang and W. Gao, "Adaptive integral backstepping control of a micro-quadrotor," in *Intelligent Control and Information Processing (ICICIP), 2011 2nd International Conference on*, vol. 2, pp. 910–915, July 2011.

[96] F. Hoffmann, N. Goddemeier, and T. Bertram, "Attitude estimation and control of a quadrocopter," in *Intelligent Robots and Systems (IROS), 2010 IEEE/RSJ International Conference on*, pp. 1072–1077, Oct 2010.

[97] L. Kis, G. Regula, and B. Lantos, "Design and hardware-in-the-loop test of the embedded control system of an indoor quadrotor helicopter," in *Intelligent Solutions in Embedded Systems, 2008 International Workshop on*, pp. 1–10, July 2008.

[98] Z. Zuo, "Trajectory tracking control design with command-filtered compensation for a quadrotor," *Control Theory Applications, IET*, vol. 4, pp. 2343–2355, November 2010.

[99] P. Castillo, P. Albertos, P. Garcia, and R. Lozano, "Simple real-time attitude stabilization of a quad-rotor aircraft with bounded signals," in *De-*

cision and Control, 2006 45th IEEE Conference on, pp. 1533–1538, Dec 2006.

[100] G. Antonelli, F. Arrichiello, S. Chiaverini, and P. Giordano, "Adaptive trajectory tracking for quadrotor mavs in presence of parameter uncertainties and external disturbances," in *Advanced Intelligent Mechatronics (AIM), 2013 IEEE/ASME International Conference on*, pp. 1337–1342, July 2013.

[101] I. Sadeghzadeh, A. Mehta, Y. Zhang, and C.-A. Rabbath, "Fault-tolerant trajectory tracking control of a quadrotor helicopter using gain-scheduled pid and model reference adaptive control," in *Annual Conference of the Prognostics and Health Management Society*, vol. 2, 2011.

[102] Z. T. Dydek, A. M. Annaswamy, and E. Lavretsky, "Adaptive control of quadrotor uavs in the presence of actuator uncertainties," *AIAA Infotech@ Aerospace*, pp. 20–22, 2010.

[103] K. Alexis, G. Nikolakopoulos, and A. Tzes, "Model predictive quadrotor control: attitude, altitude and position experimental studies," *Control Theory Applications, IET*, vol. 6, pp. 1812–1827, Aug 2012.

[104] K. Alexis, G. Nikolakopoulos, and A. Tzes, "Switching model predictive attitude control for a quadrotor helicopter subject to atmospheric disturbances," *Control Engineering Practice*, vol. 19, no. 10, pp. 1195 – 1207, 2011.

[105] K. Alexis, G. Nikolakopoulos, and A. Tzes, "Experimental model predictive attitude tracking control of a quadrotor helicopter subject to wind-gusts," in *Control Automation (MED), 2010 18th Mediterranean Conference on*, pp. 1461–1466, June 2010.

[106] T. Dierks and S. Jagannathan, "Output feedback control of a quadrotor uav using neural networks," *Neural Networks, IEEE Transactions on*, vol. 21, pp. 50–66, Jan 2010.

[107] D. Honegger, L. Meier, P. Tanskanen, and M. Pollefeys, "An open source and open hardware embedded metric optical flow cmos camera for indoor and outdoor applications," in *Robotics and Automation (ICRA), 2013 IEEE International Conference on*, pp. 1736–1741, May 2013.

[108] B. Herisse, T. Hamel, R. Mahony, and F.-X. Russotto, "A nonlinear terrain-following controller for a vtol unmanned aerial vehicle using translational optical flow," in *Robotics and Automation, 2009. ICRA '09. IEEE International Conference on*, pp. 3251–3257, May 2009.

[109] S. Zingg, D. Scaramuzza, S. Weiss, and R. Siegwart, "Mav navigation through indoor corridors using optical flow," in *Robotics and Automation (ICRA), 2010 IEEE International Conference on*, pp. 3361–3368, May 2010.

[110] J. Conroy, G. Gremillion, B. Ranganathan, and J. Humbert, "Implementation of wide-field integration of optic flow for autonomous quadrotor navigation," *Autonomous Robots*, vol. 27, no. 3, pp. 189–198, 2009.

[111] L. Besnard, Y. Shtessel, and B. Landrum, "Control of a quadrotor vehicle using sliding mode disturbance observer," in *American Control Conference, 2007. ACC '07*, pp. 5230–5235, July 2007.

[112] K. Alexis, G. Nikolakopoulos, and A. Tzes, "Design and experimental verification of a constrained finite time optimal control scheme for the attitude control of a quadrotor helicopter subject to wind gusts," in *Robotics and Automation (ICRA), 2010 IEEE International Conference on*, pp. 1636–1641, May 2010.

[113] G. Raffo, M. Ortega, and F. Rubio, "Backstepping/nonlinear h_∞; control for path tracking of a quadrotor unmanned aerial vehicle," in *American Control Conference, 2008*, pp. 3356–3361, June 2008.

[114] J. Colorado, A. Barrientos, A. Martinez, B. Lafaverges, and J. Valente, "Mini-quadrotor attitude control based on hybrid backstepping amp; frenet-serret theory," in *Robotics and Automation (ICRA), 2010 IEEE International Conference on*, pp. 1617–1622, May 2010.

[115] M. Elsamanty, A. Khalifa, M. Fanni, A. Ramadan, and A. Abo-Ismail, "Methodology for identifying quadrotor parameters, attitude estimation and control," in *Advanced Intelligent Mechatronics (AIM), 2013 IEEE/ASME International Conference on*, pp. 1343–1348, July 2013.

[116] M. H. Amoozgar, A. Chamseddine, and Y. Zhang, "Fault-tolerant fuzzy gain-scheduled pid for a quadrotor helicopter testbed in the presence of actuator faults," in *IFAC Conference on Advances in PID Control, Brescia, Italy*, vol. 2830, 2012.

[117] J. D. J. Anderson, *Fundamentals of Aerodynamics (Chapter 1)*. McGraw-Hill Book Company, 2001.

[118] P. McKerrow, "Modelling the draganflyer four-rotor helicopter," in *Robotics and Automation, 2004. Proceedings. ICRA '04. 2004 IEEE International Conference on*, vol. 4, pp. 3596–3601 Vol.4, April 2004.

[119] P. Martin and E. Salaun, "The true role of accelerometer feedback in quadrotor control," in *Robotics and Automation (ICRA), 2010 IEEE International Conference on*, pp. 1623–1629, May 2010.

[120] I. Dikmen, A. Arisoy, and H. Temeltas, "Attitude control of a quadrotor," in *Recent Advances in Space Technologies, 2009. RAST '09. 4th International Conference on*, pp. 722–727, June 2009.

[121] A. Bramwell, G. Done, and D. Balmford, "9 - aeroelastic and aeromechanical behaviour," in *Bramwell's Helicopter Dynamics (Second Edition)* (A. Bramwell, G. Done, and D. Balmford, eds.), pp. 319 – 359, Oxford: Butterworth-Heinemann, second edition ed., 2000.

[122] Y.-C. Lai and S.-S. Jan, "Attitude estimation based on fusion of gyroscopes and single antenna gps for small uavs under the influence of vibration," *GPS Solutions*, vol. 15, no. 1, pp. 67–77, 2011.

[123] C. Reitsma, "A novel approach to vibration isolation in small, unmanned aerial vehicles," in *Technologies for Practical Robot Applications, 2009. TePRA 2009. IEEE International Conference on*, pp. 84–87, Nov 2009.

[124] S. Shevtsov, D. Tsahalis, M. Flek, and I. Samochenko, "Comparison of active and passive modes of piezoelectric patch actuators for scaled helicopter rotor blade vibration suppression," in *Proceedings of Int. Conf. on Noise and Vibration Engineering ISMA2010, Leuven, Belgium*, pp. 441–456, 2010.

[125] G. Hoffmann, D. Rajnarayan, S. Waslander, D. Dostal, J. S. Jang, and C. Tomlin, "The stanford testbed of autonomous rotorcraft for multi agent control (starmac)," in *Digital Avionics Systems Conference, 2004. DASC 04. The 23rd*, vol. 2, pp. 12.E.4–121–10 Vol.2, Oct 2004.

[126] R. Buchi, *Fascination Quadrocopter*. BoD–Books on Demand, 2011.

[127] J. D. J. Anderson, *Fundamentals of Aerodynamics (Chapter 5)*. McGraw-Hill Book Company, 2001.

[128] VehicleSim, *http://www.carsim.com/*. Last visited 28^{th} June 2015, 2015.

[129] C. M. Ramirez, M. Tomás-Rodríguez, and S. A. Evangelou, "Análisis dinámico y modelado de suspensiones hossack en motocicletas de competición," in *XXXIII Jornadas de Automática, Vigo*, 2012.

[130] S. Evangelou and M. Tomas-Rodriguez, "Influence of road camber on motorcycle stability," in *Communications, Control and Signal Processing, 2008. ISCCSP 2008. 3rd International Symposium on*, pp. 231–236, March 2008.

[131] S. Evangelou, D. Limebeer, and M. Tomas-Rodriguez, "Suppression of burst oscillations in racing motorcycles," in *Decision and Control (CDC), 2010 49th IEEE Conference on*, pp. 5578–5585, Dec 2010.

[132] R. Sharp, S. Evangelou, and D. J. Limebeer, "Advances in the modelling of motorcycle dynamics," *Multibody system dynamics*, vol. 12, no. 3, pp. 251–283, 2004.

[133] R. S. Sharp, S. Evangelou, and D. J. Limebeer, "Multibody aspects of motorcycle modelling with special reference to autosim," in *Advances in computational multibody systems*, pp. 45–68, Springer, 2005.

[134] G. N. M. Plasencia, M. T. Rodríguez, P. Campoy, A. H. Lopez, and S. C. Rivera, "Reducción de las vibraciones de un sistema de visión a bordo de un helicóptero mediante un controlador inteligente," in *XXXIII Jornadas de Automática, Vigo*, 2012.

[135] S. Estellés and M. Tomás-Rodríguez, "Control pva aplicado a un quadrotor validado a través de un modelo de simulación multicuerpo," in *XXXIII Jornadas de Automática, Vigo*, pp. 393–398, 2012.

[136] M. Tomas-Rodriguez and R. Sharp, "Automated modeling of rotorcraft dynamics with special reference to autosim," in *Automation Science and Engineering, 2007. CASE 2007. IEEE International Conference on*, pp. 974–979, Sept 2007.

[137] M. Tomás-Rodríguez, "Helicopter rotor dynamics modelling.," Master's thesis, Imperial College, 2008.

[138] T. R. Kane and D. A. Levinson, *Dynamics, theory and applications*. McGraw Hill, 1985.

[139] T. R. Kane, "Dynamics of nonholonomic systems," *Journal of Applied Mechanics*, vol. 28, pp. 574–578, 1961.

[140] A. Purushotham and M. J. Anjeneyulu, "Kane's method for robotic arm dynamics: a novel approach," *Journal of Mechanical and Civil Engineering*, pp. 7–13, 2013.

[141] K. Parsa, "The lagrangian derivation of kane's equations," *Trans. Canad. Soc. Mech. Engineering*, vol. 31, pp. 407–420, 2007.

[142] E. Smith, *Mechanical Engineer's Reference Book*. Elsevier Science, 2013.

[143] P. Paultre, *Dynamics of Structures*. Wiley, 2013.

[144] F. Orban, "Damping of materials and members in structures," in *Journal of Physics: Conference Series*, vol. 268, p. 012022, IOP Publishing, 2011.

[145] Simulink, *http://www.mathworks.co.uk/products/simulink*. Last visited 28^{th} June 2015, 2015.

[146] H. Le-Huy, "Modeling and simulation of electrical drives using matlab/simulink and power system blockset," in *Industrial Electronics Society, 2001. IECON '01. The 27th Annual Conference of the IEEE*, vol. 3, pp. 1603–1611 vol.3, 2001.

[147] S. Buller, E. Karden, D. Kok, and R. De Doncker, "Modeling the dynamic behavior of supercapacitors using impedance spectroscopy," *Industry Applications, IEEE Transactions on*, vol. 38, pp. 1622–1626, Nov 2002.

[148] M. Ropp and S. Gonzalez, "Development of a matlab/simulink model of a single-phase grid-connected photovoltaic system," *Energy Conversion, IEEE Transactions on*, vol. 24, pp. 195–202, March 2009.

[149] A. El Hajjaji and M. Ouladsine, "Modeling and nonlinear control of magnetic levitation systems," *Industrial Electronics, IEEE Transactions on*, vol. 48, pp. 831–838, Aug 2001.

[150] I. H. Altas and A. M. Sharaf, "A generalized direct approach for designing fuzzy logic controllers in matlab/simulink gui environment," *International*

Journal of Information Technology and Intelligent Computing, vol. 1, no. 4, pp. 1–27, 2007.

[151] P. Pivoňka and V. Mikšánek, "Real-time communication between matlab/simulink and plc via process visualization interface," in *Proc. of the 11th WSEAS International Conference on Systems*, pp. 28–32, 2007.

[152] A. Qiu, B. Wu, and H. Kojori, "Sensorless control of permanent magnet synchronous motor using extended kalman filter," in *Electrical and Computer Engineering, 2004. Canadian Conference on*, vol. 3, pp. 1557–1562 Vol.3, May 2004.

[153] B. Jakubczyk, "Introduction to geometric nonlinear control; controllability and lie bracket," *Mathematical control theory, Part*, vol. 1, no. 2, pp. 107–168, 2001.

[154] J. Levine, *Analysis and control of nonlinear systems: A flatness-based approach*. Springer Science & Business Media, 2009.

[155] S. Ning and G. Bone, "High steady-state accuracy pneumatic servo positioning system with pva/pv control and friction compensation," in *Robotics and Automation, 2002. Proceedings. ICRA '02. IEEE International Conference on*, vol. 3, pp. 2824–2829, 2002.

[156] J. Freedner, B. Kushnir, J. P. Rottinger, and D. T. Worts, "Autonomous quadcopter," degree thesis, The College of New Jersey, December 2004.

[157] A. R. Bramwell, D. Balmford, and G. Done, *Bramwell's helicopter dynamics*. Butterworth-Heinemann, 2001.

[158] M. Ashby, *Materials Selection in Mechanical Design*. Elsevier Science, 2004.

[159] M. A. Dundar, *Free vibration analyses of abs (acrylonitrile-butadiene-styrene) rectangular plates with completely free boundary conditions*. PhD thesis, Wayne State University, 2012.

[160] M. Ciornei, "Experimental investigations of wood damping and elastic modulus," *DOCT-US*, vol. 1, no. 1, p. 56, 2009.

[161] L. Cremer, M. Heckl, and E. Ungar, *Structure-borne sound, 1988*. Springer-Verlag, NY.

[162] *MIL-HDBK-17-2F Composite Materials Handbook Volume 2: Polymer Matrix Composites Material Properties*. U.S. Department of Defense, Washington 2002.

[163] J. Yang, J. Xiong, L. Ma, B. Wang, G. Zhang, and L. Wu, "Vibration and damping characteristics of hybrid carbon fiber composite pyramidal truss sandwich panels with viscoelastic layers," *Composite Structures*, vol. 106, pp. 570–580, 2013.

[164] C. Venkatesan, *Fundamentals of Helicopter Dynamics*. CRC Press, 2014.

[165] E. W. Swokowski, *Calculus with analytic geometry. Cálculo con geometría analítica.* México:. Grupo Editorial Iberoamérica, 1989.